DETECTION OF WEAK, BROADBAND SIGNALS UNDER DOPPLER-SCALED, MULTIPATH PROPAGATION

Henry S. Chang

COMMUNICATIONS & SIGNAL PROCESSING LABORATORY
Department of Electrical Engineering and Computer Science
The University of Michigan
Ann Arbor, Michigan 48109

September 1992

Technical Report No. 282
Approved for public release; distribution unlimited

To my parents,
Shu-Chi and Siu-Siang

ACKNOWLEDGEMENTS

I would like to express my appreciation to my thesis advisor, Professor Theodore G. Birdsall who introduced me to the study of self-clutter in ocean acoustic tomography. His guidance, encouragement and support throughout the course of this study was especially helpful during the crucial stages of this study. He always have time for my questions even during his busy schedules. I would like to thank Professors John R. Birge, Gregory H. Wakefield, and Andrew E. Yagle for serving on the committee, and for their valuable suggestions. I greatly appreciate their help.

I would also like to acknowledge the help of Dr. Kurt Metzger for providing me the Lake Seneca data and his computer programs which played an essential role in the development of this study. A special note of appreciation to Dr. Zhaohong Zhang for his invaluable help in the course of my doctoral work.

I would like to thank my friend Wen-Hsien Fang for his intellectual stimulation during the early years of my graduate studies. I would also like to thank Tsunglun Yu for providing me the moral support and humor necessary for keeping my life within proper perspective. His friendship will be greatly missed.

Finally, I am sincerely grateful to my parents for their persistent support and unconditional encouragement.

TABLE OF CONTENTS

LIST OF FIGURES

LIST OF APPENDICES

Appendix

CHAPTER I

Introduction

1.1 Background

The problem of weak signal detection in the presence of multipaths is an important problem in both radar and sonar. The problem of resolving signals in both time-delay and doppler has received wide attention in the past. However, much of the progress is due to Woodward who applied the radar ambiguity function as a tool for analyzing radar ambiguity. The narrowband ambiguity function allows the interpretation of multiple targets with significant radial velocities. The ambiguity function is basically a time-doppler autocorrelation function given by

$$\chi(f_d, \tau) = \int m(t)m^*(t-\tau)e^{j2\pi f_d t}dt \ , \tag{1.1}$$

where $m(t)$ is a narrowband radar waveform. The ambiguity function may be thought of as the output of the matched filter which is tuned in time delay and doppler to the received signal. The filter responses that are large but far away from the desired target parameters are known as the ambiguities of the target. These ambiguities are undesirable since other targets may appear at these locations. In other words, ambiguities from one target may interfere with the detection of other targets. An ideal ambiguity function would be a single spike at the origin of the range-doppler

plane and zero everywhere else. However, the fundamental properties of the ambiguity function prohibits this type of idealized behavior. Specifically, Woodward showed that the volume of the $| \chi(f_d, \tau) |^2$ function is a constant[1] regardless of the type of the transmitted waveform. Under this constraint, previous works in this area have concentrated on reducing ambiguities at critical regions of the range-doppler plane. Which regions are considered critical usually depends on the signal path and clutter environment. Usually a thorough and bounded description of the signal path and clutter environments is required for unique selection of appropriate waveforms [35],[36], [37],[39]. In the development of a radar theory, many attempts have been made to determine an optimum signal waveform only to find that a waveform suitable for one application have severe deficiencies for others. It is found that, in general, an optimum radar waveform for signal resolution cannot exist. Radar signal design for signal resolution consists of matching the waveform to the characteristics of the propagating medium, and a signal can be optimum only in the sense that the best match is achieved.

The problem of weak signal detection in the presence of other signals may be subdivided into two categories; signal detection under *uniform* clutter and signal detection under self-clutter. Uniform clutter usually implies that the clutter-causing scatterers are so dense that they cannot be resolved within a resolution cell. A typical example is the interference from raindrops or sea waves. In contrast, the term self-clutter is used to describe the presence of sidelobes in a pulse compression radar/sonar which cause mutual interference among desirable path arrivals.

There has been considerable effort in optimizing performance in *uniform* clutter. In many situations it is adequate to assume that the scatterers are randomly located,

[1] $\int\int | \chi(f_d, \tau) |^2 \, df_d d\tau = 1$ for $\int | m(t) |^2 \, dt = 1$.

independent, and so dense that they are unresolvable. This becomes a problem of signal detection in colored, gaussian noise. The general solution to this problem is to place a "pre-whitening" filter ahead of a basic matched filter. Both Urkowitz[48] and Rihaczek[34] have studied appropriate filters for signal detection in *uniform* clutter. Urkowitz utilized a clutter rejection filter of the form

$$\begin{aligned} H_c(f) &= \frac{aM^*(f)e^{-j2\pi f\tau}}{k \mid M(f) \mid^2} \\ &= \frac{ae^{-j2\pi f\tau}}{kM(f)} \end{aligned} \tag{1.2}$$

where $k \mid M(f) \mid^2$ is the power spectral density of the uniform clutter, and a, k are constants. Rihaczek suggested that the usual match filter of the form

$$H_m(f) = aM^*(f)e^{-j2\pi f\tau} \tag{1.3}$$

is superior to the clutter rejection filter under most practical situations. Others have concentrated their efforts in *uniform* clutter rejection by signal design [27], [1], [28], [36]. However, as pointed out earlier, the optimum signal exists only for a particular clutter enviroment. When there is known to be a significant "doppler shift" in the clutter (i.e. non-uniform clutter), the best known method is the MTI (Moving Target Indicator) processor which is the most widely used class of radar processors for detecting moving targets in a background of clutter [40], [29], [24], [14]. The simplest MTI processor uses a single delay-line canceler to subtract two successive periods of the reception. Therefore, signals from stationary sources would cancel, while those from moving sources produce fluctuating signals. It has been shown that MTI processors are useful in the case of narrowband clutter.

Although the problem of *uniform* clutter is an important issue, this entire dissertation will be devoted to the problem of self-clutter. Unlike the *uniform* clutter,

self-clutter assumes only a few path arrivals within the reception. Another important distinction between self-clutter and *uniform* clutter is that self-clutter assumes that the time-delay and doppler of the interfering path can be determined from the range-doppler plane whereas the individual scatterers of the *uniform* clutter are unresolvable. In the case when all path arrivals have approximately the same strengths, the individual paths are all resolvable, and self-clutter does not pose a problem. On the other hand, if the reception consists of both strong and weak paths, the sidelobes of the strong path may interfere with the detection of the weaker path.

Short pulses are transmitted in many radar systems. These pulsed radar systems which are commonly known as pulse doppler radar are utilized to extract the doppler frequency shift and time-delay associated with moving targets in both forms of clutter. In the case of low pulse repetition frequency and very short pulse duration (i.e. very large gaps between successive pulses), self-clutter does not pose a problem. This is due to the fact that the ambiguities (i.e. the 2-D sidelobes) associated with these short pulses do not occupy a significant region within a receiver surface; hence, multipaths with different time-delays and dopplers do not interfere with one another. However, in the case of *uniform* clutter, the application of MTI processors to remove the uniform clutter results in significant blind-spots for low pulse repetition frequencies [40]. These blind-spots reject any moving targets whose doppler frequency happens to be the same as multiples of the pulse repetition frequency. Therefore, for radar systems utilizing pulse doppler radar, the majority of past research was devoted to the problem of detecting moving targets under *uniform* clutter and not self-clutter. Previous efforts in removing self-clutter are focused primarily in the area of signal design. To the best of the author's knowledge, no previous references on self-clutter rejection are available once the type of radar/sonar signal

for transmission has been decided.

In ocean acoustic tomography, the problem of self-clutter cannot be ignored because the signal is transmitted continously. Under continous transmission of signal (e.g. m-sequence signaling), the ambiguities associated with a single path occupies the entire receiver surface; hence, the mutual interference among multipaths is significant and cannot be ignored if weak paths are to be detected. In this dissertation, two new approaches to eliminate self-clutter are proposed and analyzed. These computationally efficient methods have the advantage that self-clutter can be entirely removed for most radar and sonar signals.

1.2 Ambiguity, Resolution and Floor Level Under Self-Clutter

Under self-clutter, there are three aspects of the receiver output that need to be considered. Suppose the diagram in figure (1) is the response due to a single-path reception.

The true travel time and doppler are determined by the location of the major peak. In figure (1.1), the travel time of this signal is $\tau = 175$ and the true doppler bin is $\gamma = 5$. One aspect of importance is the "resolution" which is measured by the size of the major lobe of this true peak. The problem of "resolution" is a subject of the uncertainty principle. A second aspect of importance is the large "false peaks" or "ambiguities" associated with the signal (i.e. the two other large peaks in figure (1.1)). Due to these "ambiguities", the receiver output $A(\gamma, \tau)$ have come to be known as the "ambiguity function" of the signal. A third aspect, the proposed research, is the general "floor level" filling the diagram and under the peaks. The general "floor level" can be better understood by observing the magnitude of the

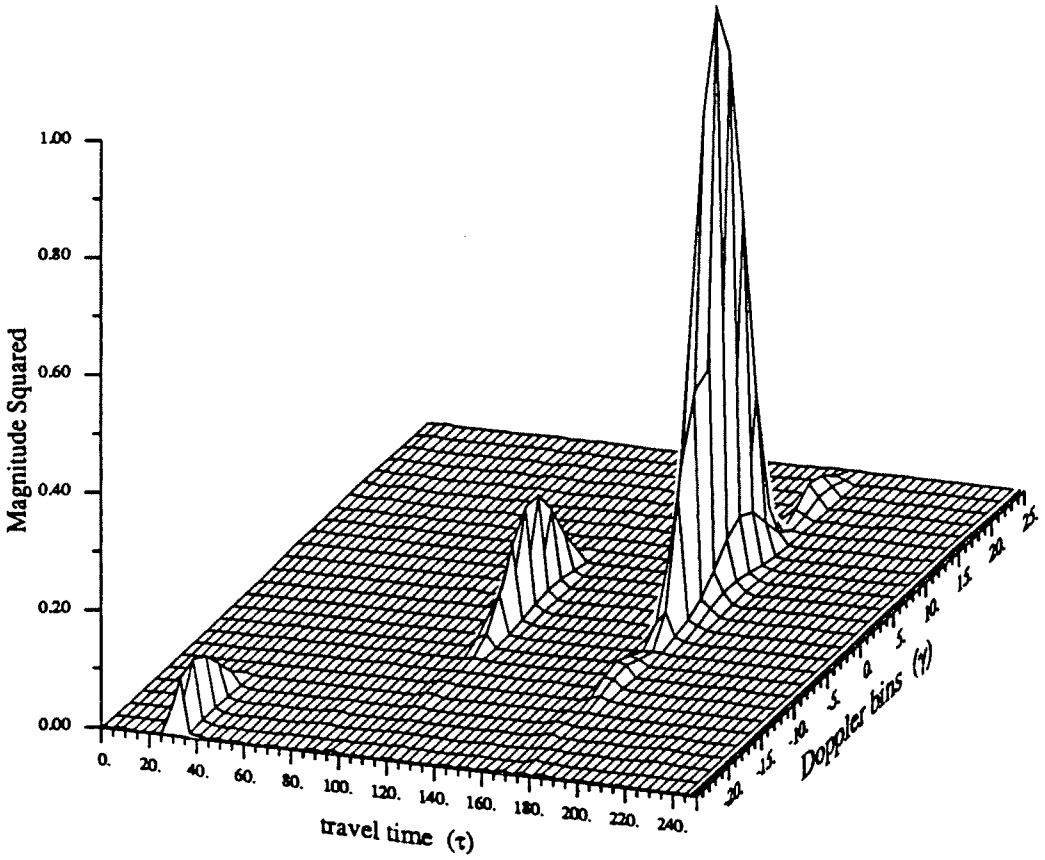

Figure 1.1: Magnitude-squared of the receiver output due to one signal plus noise, $| A(\gamma, \tau) |^2$; one doppler bin is equivalent to 0.58 knots.

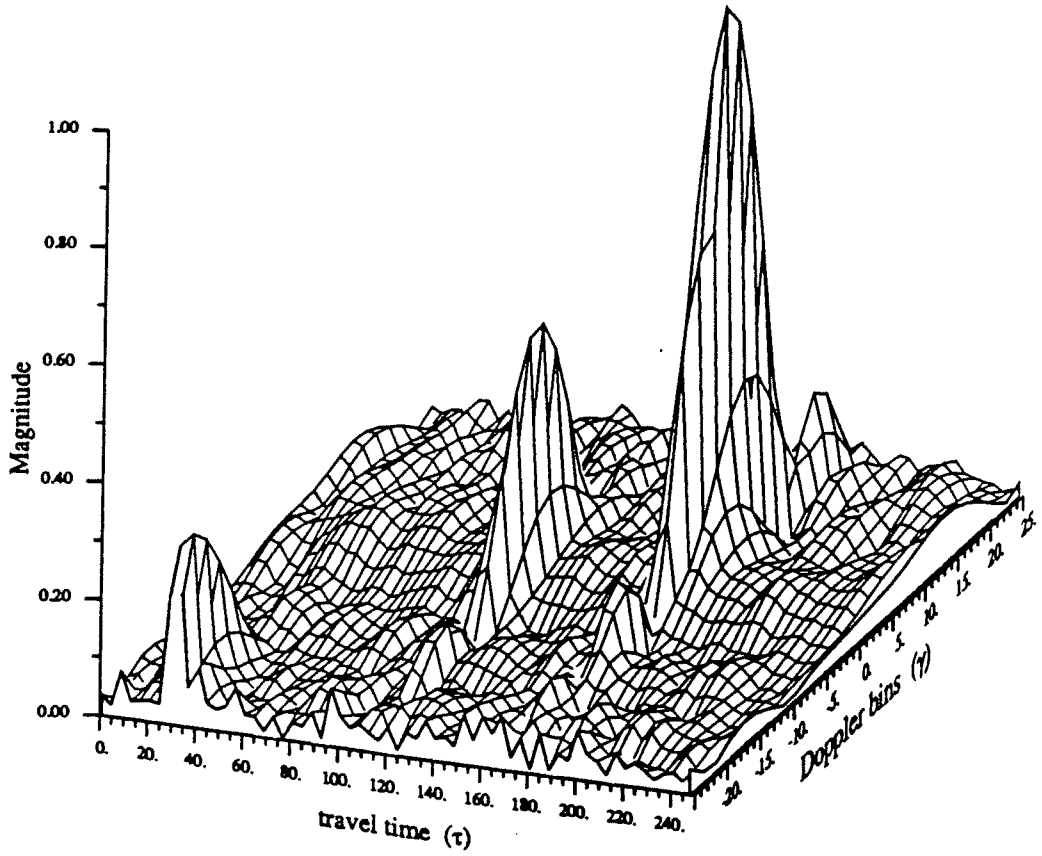

Figure 1.2: Magnitude of the receiver output due to one signal plus noise, $\mid A(\gamma, \tau) \mid$; one doppler bin is equivalent to 0.58 knots.

receiver output plotted in figure (1.2). The only difference between figures (1.1) and (1.2) is that figure (1.1) is the *magnitude-squared* response while figure (1.2) is the *magnitude* response. There are really two components that make up the "floor level"; the noise floor and the signal floor (i.e. the interference). In some cases, the signal floor is much higher than the noise floor. Under this circumstance, other signals (i.e. weak signals) with relatively high signal-to-noise ratio but low signal-to-interference ratio (SIR) cannot be detected at the output of the receiver. The purpose of this research is to somehow reduce the signal floor to the level of the noise floor so that weak signals may be detected.

1.3 Overview

Chapter II discusses some of the fundamentals of resolution in a radar/sonar system. In general, resolution is a measure of the width of the main lobe of a signal. And two pulses that are separated by this width are said to be resolvable. Chapter II begins with a discussion on single parameter resolution. For narrowband waveforms, it is shown that the resolution in travel time is inversely proportional to an equivalent bandwidth while the resolution in doppler is inversely proportional to an equivalent time duration. When the two parameters are jointly considered, the limit on the combined resolution is often associated with the "uncertainty principle" in quantum mechanics. Contrary to popular belief, the "uncertainty principle" does not play an important role in the combined resolution of radar/sonar systems. Instead the limit of the 2-D resolution is better understood through Woodward's narrowband ambiguity function. As mentioned previously, the volume of Woodward's ambiguity function is a constant. Therefore, a waveform designed to improve the 2-D resolution will exhibit higher "floor level" and increased ambiguity.

The difference between narrowband and broadband ambiguity functions is the main focus of chapter III. In order to analyze their differences, the true time-delay is approximated by a linear, time-varying model. This model assumes that the received signal is not only shifted in time by a constant delay but scaled in time by a doppler factor (i.e. compression). Essentially, the difference between narrowband and broadband ambiguity function lies in the way the baseband portion of the reception is treated. In the case of a narrowband transmission, it is assumed that the time-scaling of the baseband waveform is negligible so that the received signal is simply "doppler-shifted". In the case of a broadband transmission, the received signal consists of both a doppler shift and a time-scale of the baseband waveform. As a result the broadband receiver differs from the narrowband receiver. Chapter III discusses two types of receivers for narrowband and broadband processing: (1) Processing using transmission time scaling (PUTTS) and (2) processing using receiver time scaling (PURTS) [6]. If the signal is transmitted in one-period bursts, PUTTS utilizes the speed of FFT to implement the crosscorrelation. This may be implemented under narrowband and broadband receptions. However, when signals are transmitted continuously, the coherent averaging required for higher signal-to-noise ratio prohibits the use of PUTTS. Instead, the broadband receiver is implemented using PURTS. The advantage of PURTS is that the matched-filter is fixed since the received signal is rescaled in time prior to crosscorrelation. Additionally, PURTS may be implemented with either linear or cyclic crosscorrelation. Chapter III concludes with a discussion on the existence of a shift-invariant property for both narrowband and broadband receivers.

In Chapter IV, a new method for weak signal detection is presented. The Shift-Invariant Method for Strong Path Cancellation (SIMSPC) has the advantage that the

strong paths can be removed with very few computations due to the shift-invariance nature of a *modified*, broadband ambiguity surface. Since a strong path can be easily identified at the output of the receiver, a *reference* ambiguity surface having the same doppler and time-delay as the strong path may be subtracted from the output of the receiver to eliminate this strong path. This is based on the fact that the reference ambiguity surface exhibits all the properties associated with the strong path (i.e. the same ambiguities and floor level as the strong path). If the broadband ambiguity surface were truly shift-invariant, only one reference ambiguity surface would be required for memory storage. This is the basic principle behind the efficiency of the SIMSPC.

In order to obtain a shift-invariant broadband ambiguity surface, both the doppler and time-delay must be shift-invariant. In the doppler domain, the invariance is accomplished by an apt choice of variables. The doppler factor is moved to an exponent. Since the doppler factor is moved to an exponent, the time scaling and rescaling is merely a shift in the doppler plane. Unlike the doppler parameter, shift-invariance in time-delay cannot be accomplished with a simple choice of variables. Fortunately, with the exception of a constant phase shift, the output of a sliding processing receiver will be shift-invariant in time. In other words, the *envelope* of the broadband ambiguity surface is shift-invariant in time. The sliding processing receiver is simply a receiver that utilizes linear crosscorrelation. Although the storage requirement for the sliding processing receiver is at a minimun, the number of computations required for the linear crosscorrelation may be large. Alternately, a block processing receiver with efficient cyclic correlator may be utilized. Due to the nature of the cylic crosscorrelation, even the envelope of the broadband ambiguity surface cannot be shift-invariant in time. It is shown that the demodulate surface is shift-invariant

in both doppler and time-delay. Therefore, the SIMSPC under block processing is achieved by combining the speed of cyclic crosscorrelation along with the storage efficiency of the demodulate surface. Finally, the performance of the SIMSPC is evaluated through several simulations.

In chapter V, another new approach to strong signal cancellation operates to prevent the formation of the floor level from the strong paths. It implements the strong path cancellation through a preprocessing stage known as the Hyperslice Cancellation by Coordinate Zeroing (HCCO) preprocessing. This simple yet effective means for strong path cancellation has the advantage that removing the strong paths at a single doppler channel is equivalent to removing the entire floor level of associated with the strong paths. The basic principle behind HCCO preprocessing is as follows.

In "normal" processing, the reception is filtered, sampled and complex demodulated as if the paths had zero doppler. For pulse compressed signals such as m-sequences, if the strong path has zero doppler as its true doppler channel, the output of the strong path at zero doppler will be compressed into a very narrow pulse. Most of its energy is concentrated within this narrow pulse. Meanwhile, if a weak path were present in the reception but with a different true doppler, the energy of the weak path would be "uniformly" distributed across the entire period of the zero-doppler output. Therefore, the zero doppler output would consists of a narrow pulse due to the strong path and a "uniformly" distributed floor level due to the weak path. At this point, the strong path and the weak path are well separated in time. The idea is to remove the strong path contribution by replacing the narrow pulse with zeroes before processing for the full ambiguity surface. Hence, there would be no floor level due to the strong path. This is a *subtract before full analysis* concept as opposed to the *subtract after full analysis* concept described in chapter IV. Chapter V concludes

with the performance analysis of this method with m-sequences.

In previous chapters, the main focus is on the improvement of the signal-to-interference ratio (SIR) using path canceling techniques. The interference considered here is the signal floor associated with the strong paths. It is assumed that the SNR is much larger than the SIR. If this were not the case, no strong path canceling technique will be able to uncover a hidden weak path. Although the noise floor may be much lower than the signal floor, noise peaks may be present within the ambiguity surface which may be falsely identified as a path reception. The magnitude of these noise peaks and their effect on the detectability of the weak paths is the subject of chapter VI.

Chapter VI begins with a discussion on the noise peak of a single doppler channel. Two methods for calculating the probability of false alarm (P_F) are described. The first method approximates P_F by the distribution of the noise peak. It is assumed that the probability of false alarm P_F is equivalent to the probability that a single noise peak exceeds a threshold. This is a good approximation in the case of a high threshold. In the single doppler case, the noise-only reception may be modeled as an i.i.d. random sequence; hence, the P_F may be approximated by the distribution of the noise peak. It is shown that the extreme value distribution is a good approximation to the distribution of the noise peak. In the second approach, P_F is modeled as a problem in level crossing. In the problem of level crossing, P_F is determined by the frequency at which a noise peak crosses a specified threshold. It is assumed that the crossing rate of the noise peak is so small that the noise peaks exceeding the threshold can be considered independent. Therefore, the crossing rate may be described by the Poisson distribution. Using Rice's formula for the crossing rate, the P_F may be readily calculated. It is shown that both methods lead to similar result at small P_F

(or at high threshold); however, the first method provides a more accurate measure of P_F when it is extended to the entire ambiguity surface.

The second part of chapter VI discusses the noise peak for the entire ambiguity function. Unlike the i.i.d. assumption in the single doppler channel, every doppler channel in the ambiguity surface is a linear function of the single doppler channel. Under this circumstance, the problem is to characterize the noise peak for the ambiguity surface in relation to the noise peak of the single doppler. This would provide a simple generalization of P_F from a single doppler channel to the entire ambiguity surface. It is shown that the extreme value distribution is a valid approximation for the distribution of the noise peak even for correlated sequences. Chapter VI concludes with a discussion on the detectability of weak paths through the signal-to-noise peak ratio.

Chapter VII summarizes the study conducted in this dissertation and highlights some of the possibilities for future research.

CHAPTER II

Resolution and Ambiguity

Although detection, parameter estimation, resolution and ambiguity are all parts of the same measurement process in a reception, these terms have very different meaning. Detection refers to the possibility of recognizing a path arrival in the presence of noise, while parameter estimation refers to the precision of estimating a certain parameter in the presence of noise. On the other hand, resolution and ambiguity describes the possible interference from other signals. Although high signal-to-noise ratio ensures good detection performance and high measurement precision, it is merely a prerequisite for resolution and ambiguity.

To illustrate the differences between resolution and ambiguity, consider the reception of two pulses. If the two pulses do not merge, then the two arrivals can be easily distinguished and hence, the two arrivals are said to be resolved. If one arrival is weaker than the other and the arrivals overlap to some degree, they may or may not be resolvable. This is the problem of signal resolution. In most cases, the receiver's response to a pulse is never concentrated in a single pulse. There are usually sidelobes or tails associated with the pulse reception. If one arrival is much stronger than the other, the sidelobes or tails of the stronger arrival may mask the main peak of the weaker arrival. Alternatively, the sidelobes may be falsely iden-

tified as a weak arrival. This is the problem of ambiguity. As illustrated above, it is difficult to define resolution and ambiguity quantitatively even in the simplest situation. Basically, resolution is a measure of the width of the main lobe of a signal whereas ambiguity is a measure of tails and sidelobes due to a single arrival. In the case of moving targets, both travel time resolution and doppler resolution must be considered. These two types of resolutions are discussed separately in sections (2.1) and (2.2).

Whenever doppler and travel time resolution are jointly discussed, the "uncertainty principle" in quantum physics is sometimes used to describe the condition that doppler and travel time resolution may not be simultaneously improved without bound. The applicability of such a constraint in sonar/radar will be discussed in section (2.3). In the case of doppler and travel time measurement, the appropriate tool for the description of resolution and ambiguity is Woodward's narrowband ambiguity function.

2.1 Travel Time (Range) Resolution

Suppose the received signal differs from the transmitted signal m(t) only in amplitude and time-delay. The received signal is simply a delayed version of the transmitted signal written as $[a\ m(t - T_0)]$. In bistatic sonar, this corresponds to fixed transducer and receiver. For a matched filter receiver, the output of the receiver is proportional to

$$c(\tau) \ = \ \int_{-\infty}^{\infty} m(t - T_0) m^*(t - \tau) dt. \tag{2.1}$$

With no loss in generality we may assume that $T_0 = 0$ so that the maximum value of $\mid c(\tau) \mid$ occurs at $\tau = 0$. If $\mid c(\tau) \mid$ is equal to $\mid c(0) \mid$ for some $\tau \neq 0$ then two received signals differing by this delay are completely indistinguishable, and if $\mid c(\tau) \mid$ is close

to but not equal to $\mid c(0) \mid$ for some τ then the signals are somewhat distinguishable. This problem of near-indistinguishable receptions at different delays is known as the travel time or range resolution of the signal.

In order to quantify the range resolution of a given signal, the range resolution constant $\triangle\tau$, sometimes called the "nominal time uncertainty", as defined by Woodward [49]

$$\triangle\tau \triangleq \frac{\int_{-\infty}^{\infty} \mid c(\tau) \mid^2 d\tau}{c^2(0)} . \tag{2.2}$$

Due to the additive property of power, the square of the envelope is chosen rather than the envelope itself. The denominator in (2.2) is simply a normalizing factor. Since $c(\tau)$ is the autocorrelation of $m(t)$, its spectrum is

$$\mathcal{F}[c(\tau)] = \mid M(f) \mid^2 , \tag{2.3}$$

and so $c(\tau)$ can be expressed as the inverse Fourier transform

$$c(\tau) = \int_{-\infty}^{\infty} \mid M(f) \mid^2 e^{j2\pi f\tau} df ; \tag{2.4}$$

hence, the denominator of (2.2) is

$$c^2(0) = \left[\int_{-\infty}^{\infty} \mid M(f) \mid^2 df\right]^2 . \tag{2.5}$$

From Parseval's energy theorem, the numerator of (2.2) becomes

$$\begin{aligned} \int_{-\infty}^{\infty} \mid c(\tau) \mid^2 d\tau &= \int_{-\infty}^{\infty} \mid C(f) \mid^2 df \\ &= \int_{-\infty}^{\infty} \mid M(f) \mid^4 df , \end{aligned} \tag{2.6}$$

and the range resolution may be expressed as

$$\triangle\tau = \frac{\int_{-\infty}^{\infty} \mid M(f) \mid^4 df}{\left[\int_{-\infty}^{\infty} \mid M(f) \mid^2 df\right]^2} . \tag{2.7}$$

An effective bandwidth W_e may be defined as

$$W_e \triangleq \frac{\left[\int_{-\infty}^{\infty} \mid M(f) \mid^2 df\right]^2}{\int_{-\infty}^{\infty} \mid M(f) \mid^4 df} . \tag{2.8}$$

The form of this effective bandwidth is first proposed by Zakai[50] and has the general form given by

$$F_\nu \triangleq \left[\frac{\left(\int_{-\infty}^{\infty} \mid M(f) \mid^2 df\right)^{1/2}}{\left(\int_{-\infty}^{\infty} \mid M(f) \mid^\nu df\right)^{1/\nu}}\right]^{\frac{2\nu}{\nu-2}} . \tag{2.9}$$

The effective bandwidth in (2.8) corresponds to the general definition in (2.9) with $\nu = 4$. The above definition for the effective bandwidth is reasonable. Suppose the energy spectrum $\mid M(f) \mid^2$ is a rectangle with width b and height a, then the effective bandwidth defined above would be

$$W_e = \frac{(ab)^2}{a^2 b} = b , \tag{2.10}$$

which is intuitively satisfying. With this definition of effective bandwidth the range resolution constant is given by

$$\triangle\tau = \frac{1}{W_e} . \tag{2.11}$$

Therefore, range resolution is inversely proportional to the effective bandwidth of $c(\tau)$. If small range resolution constant is desired, one must utilize signals with broad bandwidth.

2.2 Doppler Resolution

When the transmitter and the receiver are in relative motion, the received signal will be frequency shifted or "doppler shifted"[1]. In order to discriminate between two

[1]In general, the received signal is actually frequency scaled or doppler scaled; however, due to the narrowband assumption of this section, the received signal can be viewed as a frequency shifted signal.

signals having the same travel time but with different doppler, a frequency correlation function $g(f_d)$ is defined as

$$g(f_d) \triangleq \int_{-\infty}^{\infty} m(t)m^*(t)e^{-j2\pi f_d t}\, dt \ . \tag{2.12}$$

where f_d denotes the doppler shift associated with the motion for a linear doppler model. This correlation function is essentially the output of the matched filter evaluated at $\tau = 0$. Using the Parseval's theorem the frequency correlation function can be written as

$$g(f_d) = \int_{-\infty}^{\infty} M^*(f)M(f - f_d)\, df \ . \tag{2.13}$$

Similar to the travel time case, a doppler resolution constant $\triangle f_d$ can be defined as the effective width of $\mid g(f_d) \mid^2$ by

$$\begin{aligned} \triangle f_d &\triangleq \frac{\int_{-\infty}^{\infty} \mid g(f_d) \mid^2 df_d}{g^2(0)} \\ &= \frac{\int_{-\infty}^{\infty} \mid m(t) \mid^4 dt}{\left[\int_{-\infty}^{\infty} \mid m(t) \mid^2 dt\right]} \end{aligned} \tag{2.14}$$

The effective duration T_e is given by

$$T_e \triangleq \frac{\left[\int_{-\infty}^{\infty} \mid m(t) \mid^2 dt\right]^2}{\int_{-\infty}^{\infty} \mid m(t) \mid^4 dt} \ , \tag{2.15}$$

which is obtained from the general form of effective duration proposed by Zakai[50]:

$$T_\mu \triangleq \left[\frac{\left(\int_{-\infty}^{\infty} \mid m(t) \mid^2 df\right)^{1/2}}{\left(\int_{-\infty}^{\infty} \mid m(t) \mid^\mu df\right)^{1/\mu}}\right]^{\frac{2\mu}{\mu-2}} \ . \tag{2.16}$$

Using the effective duration in (2.15),

$$\triangle f_d = \frac{1}{T_e} \ . \tag{2.17}$$

The doppler resolution is analogous to the travel time resolution in that the doppler resolution constant is inversely proportional to the effective duration of the signal.

If fine doppler resolution is desired, one must utilize signals with long duration in time.

It is worthwhile to point out that the definitions of travel-time resolution and doppler resolution were arbitrarily but thoughtfully chosen. They were selected because of their ease in quantifying widths of multi-humped as well as single-humped curves, and they provide a qualitative measure of the signal resolution. In principle, no matter how small the interval between two pulses is made, the resulting response differs from that of a single pulse and, consequently, it is possible, in principle, to distinguish whether one or two signals are present. However, this is only true in the absense of any random disturbance. In other words, the definition for the resolutions are meaningful only when noise and other interference are considered.

2.3 Uncertainty Principle

Whenever time and frequency (doppler) are jointly discussed, the uncertainty principle in quantum mechanics is often used to justify a certain limitation of the measurement of time and frequency variables. According to the Heisenberg uncertainty principle, an increase in the measurement accuracy of a particle can be achieved only at the expense of decreasing the measurement accuracy of its momentum, and vice versa. Specifically, the measurement accuracies of these two quantities have the following relationship:

$$\delta_x \delta_{\rho_x} \geq \frac{h}{4\pi}, \tag{2.18}$$

where δ_x, δ_{ρ_x} are the measurement accuracies of position and momentum respectively, and $h = 6.625\ x\ 10^{-34}$ joule-sec is the Planck's constant. There is a similar property in sonar/radar theory, but the interpretation for the uncertainty principle in quantum mechanics is quite different from that of the sonar/radar theory. In terms of time

and frequency, the uncertainty relationship in sonar/radar is the principle that the product of signal duration and its bandwidth cannot be arbitrarily decreased and that this product is always greater than a given constant:

$$\delta t \cdot \delta f \geq \mu \ , \tag{2.19}$$

where μ is approximately one. The actual value of μ will depend on the definition of signal duration and signal bandwidth along with different pulse forms.

For the class of definition proposed by Zakai[50] in (2.9), and (2.16),

$$T_\mu \cdot F_\nu \geq 1 \quad for \ \frac{1}{\mu} + \frac{1}{\nu} \geq 1 \ , \tag{2.20}$$

and

$$T_\mu \cdot F_\nu \geq 0 \quad for \ \frac{1}{\mu} + \frac{1}{\nu} < 1 \ . \tag{2.21}$$

As mentioned previously, effective duration and effective bandwidth can be defined in many ways. Aside from the definition given in sections (2.1) and (2.2), a well-known definition first proposed by Gabor [16] and later discussed by Woodward[49], Rihaczek[33], and Vakman[12] has the form

$$(\delta t)^2 \triangleq \int_{-\infty}^{\infty} t^2 \mid m(t) \mid^2 dt \tag{2.22}$$

$$(\delta f)^2 \triangleq \int_{-\infty}^{\infty} f^2 \mid M(f) \mid^2 df \ . \tag{2.23}$$

Assuming the origins of time and frequency are placed such that

$$\int_{-\infty}^{\infty} t \mid m(t) \mid^2 dt = 0$$

$$\int_{-\infty}^{\infty} f \mid M(f) \mid^2 df = 0 \ ,$$

the time-frequency product, derived in the above references, has the condition that

$$\delta t \cdot \delta f \geq \frac{1}{2} \tag{2.24}$$

Other forms of the uncertainty relationship for signals can be found in Vakman[12], and Helstrom[21].

Although the equations for the uncertainty principle in sonar/radar appears to have the same form as the uncertainty principle in quantum mechanics, the two principles have entirely different meanings. The expression in (2.18) is a probabilistic interpretation of the phenomena in the atomic scale, and it reflects the fundamental uncertainty in measuring the position and momentum simultaneously. However, the uncertainty principle in radar/sonar is not a relationship between measurement errors. As pointed out by Skolnik[40]: "The use of the word 'uncertainty' is a misnomer, for there is nothing uncertain about the 'uncertainty relation'... It states the well-known mathematical fact that a narrow waveform yields a wide spectrum and a wide waveform yields a narrow spectrum and both the time waveform and frequency spectrum cannot be made arbitrarily small simultaneously." In fact, the previous analysis of travel time resolution showed that sharp travel time resolution does not require a short pulse-like waveform, but a waveform with broad spectrum. Similarly, sharp doppler resolution does not require a narrowband waveform, but a waveform with long duration in time. These inverse relationships (i.e. travel time resolution increases with increasing bandwidth) are also pointed out by Woodward[49] for the effective duration and effective bandwidth defined in (2.22), (2.23).

Although there do not exist waveforms with very short durations in time and narrowband in frequency, there is no incompatibility between waveforms having both long durations in time and broadband in frequency. Therefore it might be assumed from the definition of travel time resolution constant T_e in (2.11) and the definition of doppler resolution constant W_e in (2.14) that both the travel time and the doppler resolution can be simultaneously improved without bound. One must be careful.

First of all, both the travel time resolution and the doppler resolution are derived assuming one unknown parameter. They do not express the resolution in the case when both parameters are unknown. For the case when both variables are unknown, the estimate of these variables are determined from a 2-D plane of size $T_e W_e$. The true peak is located within this 2-D plane and the size of its major lobe is $\frac{1}{T_e W_e}$. Therefore, increasing the time-bandwidth product reduces the size of the major lobe of the true peak. However, the uncertainty principle fails to describe the possibility of additional pulses within this 2-D plane away from the true peak. In other words, there may be ambiguities associated with a signal having a narrow major lobe. In order to describe the possible ambiguities associated with a given signal when both travel time and doppler are unknowns, one must make use of Woodward's ambiguity function described next.

2.4 Combined Travel Time and Doppler Ambiguity

When both the travel time and doppler are unknowns, one must use a correlation function in two variables (f_d, τ). Consider a modulated narrowband waveform given by its complex analytic form

$$v_1(t) = m(t)e^{j2\pi f_o t}, \tag{2.25}$$

where $m(t)$ is a real or complex baseband waveform and f_o is the carrier frequency. When this waveform is first delayed and then doppler-shifted, the waveform becomes

$$v_2(t) = m(t-\tau)e^{j2\pi(f_o - f_d)(t-\tau)}. \tag{2.26}$$

In (2.26), a narrowband waveform is assumed; the difference between narrowband and broadband waveforms will be made clear in chapter III. In order to have small delay and doppler ambiguities, and small delay and doppler resolutions, waveforms

differ in delay and/or doppler shift must be distinguishable at the receiver. In other words, a desirable signal waveform must have the property of being as different as possible from delayed and doppler shifted versions of itself. A convenient measure of the "distance" between these waveforms is to consider the squared departure of $v_1(t)$ from $v_2(t)$ given by

$$\Delta_{1,2}^2 = \int \mid v_1(t) - v_2(t) \mid^2 dt \ . \tag{2.27}$$

The distance $\Delta_{1,2}^2 = 0$ when $\tau = 0$ and $f_d = 0$. In order to minimize ambiguities and resolutions, $\Delta_{1,2}^2$ must be maximized when $\tau \neq 0$ and $f_d \neq 0$. Expanding (2.27) and using (2.25), (2.26) and the identity

$$\| v_1 - v_2 \|^2 = \| v_1 \|^2 + \| v_2 \|^2 - 2 \| v_1 v_2 \|, \tag{2.28}$$

$\Delta_{1,2}^2$ may be expressed as

$$\begin{aligned} \Delta_{1,2} &= 2\int \mid v_1(t) \mid^2 dt \ - \ 2Re \int v_1(t) v_2^*(t-\tau) dt \\ &= 2\int \mid v_1(t) \mid^2 dt \ - \ 2Re\{e^{j2\pi(f_o - f_d)\tau} \int m(t) m^*(t-\tau) e^{j2\pi f_d t} dt\} \end{aligned} \tag{2.29}$$

Therefore, maximizing the squared departure in (2.27) is equivalent to minimizing the second term of (2.29). Specifically, the narrowband ambiguity function (i.e. Woodward's ambiguity function) given by

$$\chi_N(\tau, f_d) = \int_{-\infty}^{\infty} m(t) m^*(t-\tau) e^{j2\pi f_d t} dt \tag{2.30}$$

is to be kept small for $\tau \neq 0$ and $f_d \neq 0$. The value of $\chi_N(f_d, \tau)$ for all values of τ and f_d is known as the narrowband ambiguity surface of the signal $m(t)$.

A note of terminology is in order. The complex envelope, $\chi_N(f_d, \tau)$, is frequently referred to as the matched-filter response, while the magnitude of the complex envelope, $\mid \chi_N(f_d, \tau) \mid$ is sometimes called the uncertainty function. And it is the

squared envelope, $\mid \chi_N(f_d,\tau) \mid^2$, that is often referred to as the ambiguity function [38]. However, any of these three forms may appear in the literature under the designation of ambiguity function. In this dissertation, the term ambiguity function is used synonymously with the matched-filter response in delay and doppler without being consistent as to which of the three forms is addressed. When necessary, the particular form of the ambiguity function will be specified.

A valuable constraint of the narrowband ambiguity function is obtained by considering the volume of the magnitude-squared ambiguity function

$$V_N = \int_{-\infty}^{\infty}\int_{-\infty}^{\infty} \mid \chi_N(\tau,f_d) \mid^2 d\tau df_d \ . \tag{2.31}$$

Expanding (2.31) yields

$$\begin{aligned} V_N &= \int_{-\infty}^{\infty}\int_{-\infty}^{\infty} \mid \chi_N(\tau,f_d) \mid^2 d\tau df_d & (2.32)\\ &= \int_{-\infty}^{\infty}\int_{-\infty}^{\infty}\int_{-\infty}^{\infty}\int_{-\infty}^{\infty} m(t_1)m^*(t_1-\tau)m^*(t_2)m(t_2-\tau) \\ &\quad \cdot e^{-j2\pi f_d(t_2-t_1)}\, dt_1 dt_2 d\tau df_d & (2.33)\\ &= \int_{-\infty}^{\infty}\int_{-\infty}^{\infty}\int_{-\infty}^{\infty} m(t_1)m^*(t_1-\tau)m^*(t_2)m(t_2-\tau) \\ &\quad \cdot \left[\int_{-\infty}^{\infty} e^{-j2\pi f_d(t_2-t_1)}\, df_d\right] dt_1 dt_2 d\tau \ . & (2.34) \end{aligned}$$

The inner integral of (2.34) is simply the Fourier transform of $e^{j2\pi f_d t_1}$ which results in the delta funtion $\delta(t_2 - t_1)$. Therefore, evaluating the remaining integrals for $t_1 = t_2 = t$,

$$\begin{aligned} V_N &= \int_{-\infty}^{\infty} \mid m(t) \mid^2 \left[\int_{-\infty}^{\infty} \mid m(t-\tau) \mid^2 d\tau\right] dt \\ &= \left[\int_{-\infty}^{\infty} \mid m(t) \mid^2 \ dt\right]^2 \\ &= \chi_N^2(0,0) \ = \ E_m^2 \ , & (2.35) \end{aligned}$$

where E_m is the total baseband signal energy.

If the volume V_N is equal to the peak value $\mid \chi(0,0) \mid^2$, the normalized volume is equal to unity. The ramification of this property is that the magnitude of the ambiguity surface cannot be reduced in some $\tau \cdot f_d$ area without increasing it elsewhere. If one designs a signal having really small ambiguities in a certain region of the ambiguity surface, then this signal must have significant volume elsewhere in the ambiguity surface in order to satisfy the unity property of the narrowband ambiguity. Furthermore, signals with sharp resolution must have non-zero "false peaks" or a "floor" in the ambiguity surface. Therefore, travel time and doppler resolutions can only be improved at the expense of increasing ambiguities. This property rules out the possibility of an ambiguity surface with only a spike at the origin and zero elsewhere.

The above analysis assumes continuous time processing. However, in practical systems, discrete-time processing is utilized. In particular, the discrete, periodic form of the narrowband ambiguity may be written as

$$\chi_N[n,\theta_d] = \sum_{l_1=0}^{P_n-1} m[l_1]m^*[l_1-n]e^{j\theta_d l_1} , \tag{2.36}$$

where integer arguments are modulo P_n,

$$m[n] = m(nt_s) \tag{2.37}$$

$$\theta_d = 2\pi f_d t_s , \tag{2.38}$$

and $t_s = 1/m_r f_o$ is the sampling interval. The appropriate volume in this case is

$$\begin{aligned} V_{(N,d)} &= \int_{-\pi}^{\pi} \sum_{n=0}^{P_n-1} \mid \chi_N[n,\theta_d] \mid^2 d\theta_d \\ &= \int_{-\pi}^{\pi} \sum_{n=0}^{P_n-1} \sum_{l_1=0}^{P_n-1} \sum_{l_2=0}^{P_n-1} m[l_1]m^*[l_1-n]m^*[l_2]m[l_2-n] \\ &\quad \cdot e^{-j\theta_d[l_2-l_1]}d\theta_d \end{aligned}$$

$$
\begin{aligned}
V_{(N,d)} &= \sum_{n=0}^{P_n-1} \sum_{l_1=0}^{P_n-1} \sum_{l_2=0}^{P_n-1} m[l_1] m^*[l_1-n] m^*[l_2] m[l_2-n] \\
&\quad \cdot \int_{-\pi}^{\pi} e^{-j\theta_d[l_2-l_1]} d\theta_d \\
&= \sum_{l_1=0}^{P_n-1} \mid m[l_1] \mid^2 \left[\sum_{n=0}^{P_n-1} \mid m[l_1-n] \mid^2 \right] \\
&= \chi_N^2[0,0] \;=\; E_m^2 \; . \qquad (2.39)
\end{aligned}
$$

Again, the total volume of the discrete ambiguity surface is a constant. The integration in (2.39) from $-\pi$ to π spans the principal or unaliased frequency domain. If one is interested in evaluating the ambiguity function for large frequency shifts, the sampling rate must be high enough so that aliasing will not occur.

Examples of the narrowband ambiguity surfaces can be found in many references such as [3], [13], [40], and [49]. Although (2.35) is the most well-known property of the narrowband ambiguity function, additional properties may be found in [33], [41], [42], and [43].

The connection between the ambiguity function and time-frequency distribution functions has been recognized since 1953 [10]. Specfically, the ambiguity function and the Wigner distribution are related through a double Fourier transform (i.e. the ambiguity function is the characteristic function of the Wigner distribution). Although the relationship between the two functions are clear, not all properties of the ambiguity function have been shown to have an obvious interpretation in terms of time-frequency distribution. For example, while the ambiguity function is generally complex, the Wigner distribution is real but not always positive. A detailed analysis of their differences may be found in [45].

Both the travel-time resolution and the doppler resolution are calculated under the assumption that only one variable is unknown. The attempt to define a time-

doppler resolution using the time-bandwidth product of section 2.4 is a gross approximation at best. The ambiguity function is calculated from the assumption that both variables are unknown, and the constraint on the volume of the ambiguity function replaces the looser concept that the time-bandwidth product must be greater than unity. Although travel-time resolution and doppler resolution may depend on many factors and interpreted in many different ways, the narrowband ambiguity function can be considered as dependent on only the signal form and interpreted in only a single way. With the narrowband ambiguity function in (2.30), it is possible to determine the extent of the ambiguity and resolution for any narrowband waveform. With modern computers it is not difficult to calculate the ambiguity function for a specific waveform; however, in general it is not possible to synthesize a waveform with a given ambiguity function. The question remains as to whether or not it is possible to obtain any arbitrary ambiguity function.

Recall that the objective of this research is to reduce the travel time-doppler "floor level" to the level of the noise. Although the ambiguity function differs from one signal to another, the significance of the "floor level" may be illustrated using the following example. This example uses the time-bandwidth product to describe the major peak[2] while the volume constraint of the ambiguity function describes the "floor level" associated with the signal. Suppose T_e and W_e are the effective duration and effective bandwidth associated with a given signal. If the signal energy is E_m^2 (i.e. $E_m^2 = V_n$), and the major peak of the signal[3] on the ambiguity surface has a

[2]Assuming the major peak is located at zero-doppler and at a time-delay of τ_o, the travel-time resolution is an accurate description the major peak at zero doppler and the doppler resolution is an accurate description of the major peak at a constant time-delay of τ_o. If the major peak is cone-shaped, the time-bandwidth product is a good approximation of the resolution of the major peak.

[3]In general, the volume occupied by the peak(s) is insignificant as compared to the volume occupied by the entire "floor level".

peak level of E_m^2 and volume $\frac{1}{T_e} \cdot \frac{1}{W_e} \cdot 1.0$, then the average "floor level" denoted by E_{floor}^2 is given by

$$\begin{aligned} E_{floor}^2 &= \left(E_m^2 - \frac{E_m^2}{T_e W_e} \right) \frac{1}{T_e W_e} \\ &\approx \frac{E_m^2}{T_e W_e} \, . \end{aligned} \tag{2.40}$$

Under this condition, it is often said that "the floor level is $T_e W_e$ below the peak value of the ambiguity surface". Furthermore, any weak signal with peak energy less than $\frac{E_m^2}{T_e W_e}$ cannot be detected at the output of the receiver. Under this circumstance, the average "floor level" must be reduced in order to detect weak signals[4].

[4]The above calculation for the average "floor level" is only true in the case of narrowband signaling. However, the "floor level" of broadband signals is usually well approximated by the "floor level" of the same signal under narrowband assumption.

CHAPTER III

Narrowband VS. Broadband

In chapter II, the doppler resolution and Woodward's ambiguity function were evaluated under the assumption that narrowband waveforms were transmitted. In radar, the narrowband assumption is usually acceptable since the speed of targets is a very small fraction of the speed of light. However, for the case of sonar, the narrowband assumption may not hold true due to the much slower speed of sound. The difference between narrowband and broadband waveforms will be analyzed in this chapter. Specifically, the broadband ambiguity function will be developed, which may be viewed as a generalized form of Woodward's narrowband ambiguity function.

Due to the added complexity of the broadband ambiguity function, broadband receivers will, generally, require many more computations than narrowband receivers. In addition to the increased complexity of broadband receivers, the basic form of broadband receivers do not offer the shift-invariant property of narrowband receivers.

3.1 Travel-Time Approximation

The basic difference between the narrowband and the broadband assumption is that the doppler scaled narrowband signal is modeled as a frequency shift of the original signal while the doppler scaled broadband signal is modeled as a time

compression or expansion of the original signal. To gain a better understanding of this difference a doppler scaled and time delayed version of the transmitted signal is described. Consider a transmission modeled as the analytic signal $a\ m(t)e^{j2\pi f_o t}$, and the signal reception written as

$$r(t) \ = \ m(t-\tau(t))e^{j2\pi f_o(t-\tau(t))} \ . \tag{3.1}$$

The transmitter to receiver delay $\tau(t)$ is generally a function of time for moving targets. In (3.1), $\tau(t)$ is the delay of a signal received at time t. For moving targets, the delay depends on the target position at the instant of signal reflection. In the case of monostatic radar, the signal reflection occurs at time $t-\tau(t)/2$ for a signal received at time t. Since target range R is also a function of time, the relationship between delay and target range is given by

$$\tau(t) \ = \ \frac{2}{c}R\left(t-\frac{\tau(t)}{2}\right) \ , \tag{3.2}$$

where c is the nominal velocity of the propagation. However, for the case of bistatic radar, the reflection occurs at time $t-\tau(t)$. Correspondingly,

$$\tau(t) \ = \ \frac{R(t-\tau(t))}{c} \ . \tag{3.3}$$

The question is how much this delay varies over the non-zero duration of $m(t)$. If the variation is negligible, the target may be assumed stationary so that the delay can be treated as a constant. On the other hand, for signals with very long duration and high-speed targets, $\tau(t)$ may be a very complicated function of time. Fortunately, under most situations, the delay and target range is a smooth funtion of time within the coherent signal processing time. Therefore, the delay can be expanded into a Taylor's series with the higher order terms dropped. Specifically, if $\tau(t)$ is analytic

at t_o, the Taylor series expansion for $\tau(t)$ about t_o is

$$\tau(t) = \sum_{k=0}^{\infty} \frac{\tau^{(k)}(t_o)}{k!}(t-t_o)^k \ . \tag{3.4}$$

With higher ordered terms dropped, the linear doppler model for $\tau(t)$ is given by

$$\tau(t) = \tau(t_o) + \dot{\tau}_{t_o}(t-t_o) \tag{3.5}$$

where

$$\dot{\tau}_{t_o} = \frac{d\tau(t)}{dt}\,|_{t=t_o} \ . \tag{3.6}$$

In general, the physical meanings of $\tau(t_o)$ and $\dot{\tau}(t_o)$ are difficult to describe. But for a special case of linear, single path reception, the parameters $\tau(t_o)$ and $\dot{\tau}_{t_o}$ do have some physical meaning. Consider the case of an isovelocity medium for a moving transmitter with constant radial velocity v_t and a moving receiver with constant radial velocity v_r. If the path of signal propagation between the transmitter and the receiver is assumed to be a line of sight, the range between the transmitter and the receiver can be written as

$$R(t) = R(t_o) - (v_t - v_r)(t-t_o) \ . \tag{3.7}$$

where t_o is any selected time. Differentiating the delay $\tau(t)$ in (3.3) with respect to t,

$$\begin{aligned} \dot{\tau}_{t_o} &= \frac{1}{c}\dot{R}(t_o)[1-\dot{\tau}_{t_o}] \\ &= \frac{\dot{R}(t_o)}{c}\left[1+\frac{\dot{R}(t_o)}{c}\right]^{-1} \\ &\approx \frac{\dot{R}(t_o)}{c} \ . \end{aligned} \tag{3.8}$$

Substituting the range function (3.7) into the time delay function in (3.3) and (3.8),

$$\tau(t_o) = \frac{R(t_o)}{c} \tag{3.9}$$

$$\dot{\tau}(t_o) = \frac{v_r - v_t}{c} \ . \tag{3.10}$$

Therefore, the linear doppler factor is determined by the ratio of the relative velocity of the target to the nominal speed of the propagation. In general, however, there is no simpler way to describe the parameters $\tau(t_o)$ and $\dot{\tau}(t_o)$ other than the travel time and its first derivative at time t_o.

3.2 Narrowband VS. Broadband Ambiguity Function

Using the travel time approximation of section (3.1), the received signal becomes

$$\begin{aligned} r(t) &= a\, m(t-\tau(t_o)-\dot{\tau}_{t_o}(t-t_o))e^{j2\pi f_o(t-\tau(t_o)-\dot{\tau}_{t_o}(t-t_o))} \\ &= a\, m((1-\dot{\tau}_{t_o})t-\tau(t_o)+\dot{\tau}_{t_o}t_o)e^{j2\pi f_o(1-\dot{\tau}_{t_o})t}e^{-j2\pi f_o(\tau(t_o)-\dot{\tau}_{t_o}t_o)}\ , \end{aligned} \quad (3.11)$$

where a is the attenuation constant. In the narrowband case, it is assumed that the target motion does not distort the complex envelope $m(t)$. The doppler factor affects only the carrier and only the constant delay term is retained for the complex envelope. Specifically, narrowband waveforms assumes

$$m((1-\dot{\tau}_{t_o})t-\tau(t_o)+\dot{\tau}_{t_o}t_o) \approx m(t-\tau(t_o))\ . \quad (3.12)$$

Whether or not the narrowband approximation is a legitimate assumption depends on the similarity between $m((1-\dot{\tau}_{t_o})t-\tau(t_o)+\dot{\tau}_{t_o}t_o)$ and $m(t-\tau(t_o))$. To gain a better understanting of the extent of this approximation, consider the case of a constant-carrier pulse reception followed by match filtering. The effect of the target motion will be to change the phase of the signal so that the received signal will not be matched to the filter. In a doppler-shifted, narrowband reception, if the total phase shift of the received signal is π over the duration of a period (i.e. $2\pi f_o(1-\dot{\tau}_{t_o})T_p = \pi$; where T_p is the period), a filter matched to the zero-doppler signal will have its output reduced by $2/\pi$. This corresponds to a drop of 4dB. For a broadband reception, if the received signal is first demodulated, then match-filtered, the peak of the resultant

complex envelope will drop by approximately 4dB for a phase shift of $\pi(\frac{f_o}{B})$ where B is the bandwidth of the complex envelope. This is due to the fact that the complex envelope is less motion-sensitive than the carrier by the factor $(\frac{B}{f_o})$. Therefore, a phase shift of $\triangle\theta_o$ in the carrier has the same affect as a phase shift of $\triangle\theta_o(\frac{f_o}{B})$ in the complex envelope. If the change in range over the signal duration T is $\triangle R$, then the phase change is

$$\triangle\theta \;=\; 2\pi(\triangle R/\lambda)\;. \tag{3.13}$$

Using the linear range model in (3.7),

$$\begin{aligned}\triangle R \;&=\; \dot{R}(t)T \\ &=\; (v_t - v_r)T\end{aligned} \tag{3.14}$$

Therefore the condition under which the effects of target motion can be neglected for the complex envelope is

$$\triangle\theta \;\ll\; \pi\frac{f_o}{B}\;. \tag{3.15}$$

or

$$(v_t - v_r)T\frac{2\pi}{\lambda} \;\ll\; \pi\frac{f_o}{B}\;. \tag{3.16}$$

which results in

$$TB \;\ll\; \frac{1}{2\dot{\tau}_{t_o}} \tag{3.17}$$

The inequality in (3.17) implies that the time-bandwidth product must be less than reciprocal of the doppler factor $\dot{\tau}_{t_o}$ for the narrowband assumption to hold. Alternatively, the inequality in (3.17) also implies that the amount of doppler time-compression within the time of observation must be less than the reciprocal of the bandwidth in order for the signal to be considered narrowband. This condition can be found in various papers as a general rule of thumb for the narrowband assumption

[46], [33], [2], [23]. When (3.17) is satisfied, the time scaling of the baseband signal $m(t)$ may be ignored so that the received signal may be written as

$$r(t) \;=\; a\; m(t-\tau(t_o))e^{j2\pi f_o(1-\dot{\tau}_{t_o})t}e^{-j2\pi f_o(\tau(t_o)-\dot{\tau}_{t_o}t_o)}\;. \tag{3.18}$$

which represents a frequency shift of $f_o\dot{\tau}_{t_o}$ (i.e. "doppler shift"). Therefore, the narrowband ambiguity function given by Woodward has the form

$$\chi_N(\tau(t_o),\dot{\tau}_{t_o})) \;=\; \int_{-\infty}^{\infty} m(t)m^*(t-\tau(t_o))e^{j2\pi f_o\dot{\tau}_{t_o}t}dt\;. \tag{3.19}$$

The narrowband criterion above is a mathematical description of the differences between narrowband and broadband signals. The mathematical description of broadband signals takes into account the time-bandwidth product of the transmitted signal as well as the doppler-scale incurred. It does not depend on the frequency at which the signal is modulated since the process of demodulation at the receiver would shift the modulated signal back to DC. However, from the standpoint of physical modeling of signal propagation, the terms broadband and narrowband take on different meanings. From the physical perspective, whether a signal is considered broadband or narrowband usually depends on the bandwidth of the signal in relation to the center frequency (i.e. frequency of modulation). A common measure of this relationship is known as the Q of the modulated signal which is simply the ratio between the center frequency and the bandwidth of the modulated signal. The higher the Q the narrower the pulse in the frequency domain. There are no set rule as to how high a Q must be before the modulated signal can be considered narrowband, but a conservative rule of thumb is to assume the modulated signal to be broadband if the signal spans an octave or more (i.e. $Q \geq 1.5$).

In underwater acoustics, the attenuation coefficient and the time-delay vary with frequency due to absorption. A complete model of the reception would take into

account this dispersive effect of the medium. However, since the Q utilized in underwater acoustics is relatively high (e.g. $f_o = 250$ Hz, Q = 4), the transmitted signal may be considered narrowband in the physical sense. Therefore, the effect of this dispersion is minimal and the attenuation coefficient and the time-delay may be assumed constant over the signal frequencies. This does not imply that the signal reception can be modeled as narrowband using the mathematical description. In fact, for continuous transmission of sonar signals, the condition in (3.17) is not satisfied. This is primarily due to the relatively low sound speed of the acoustic medium. Under these circumstances, the broadband model of the received signal in (3.11) must be utilized. In future discussions, the term broadband will be used solely in the context of the mathematical description.

At first, it would seem that the proper form of the broadband ambiguity function would involve the use of the first two terms of the Taylor series expansion in both the carrier and the complex envelope. This approximation suggests that the doppler effect merely compresses or stretches the time scale of the signal. In reality, the doppler effect causes a change in the signal amplitude as well. From the property of the Fourier Transform, if a signal is frequency scaled from $S(f)$ to $S(\frac{f}{1-\dot{\tau}_{t_o}})$ then the corresponding signal in the time domain is $(1-\dot{\tau}_{t_o})s((1-\dot{\tau}_{t_o})t)$. Therefore, the doppler effect changes the amplitude of the signal by an amount proportional to $(1-\dot{\tau}_{t_o})$. Correspondingly, the broadband ambiguity function can be derived as [17], [31], [44]

$$\chi_B(\tau(t_o),\dot{\tau}_{t_o}) \;=\; (1-\dot{\tau}_{t_o})\int_{-\infty}^{\infty} m(t)m^*((1-\dot{\tau}_{t_o})t-\tau(t_o)+\dot{\tau}_{t_o}t_o)e^{j2\pi f_o\dot{\tau}_{t_o}t}dt \;. \quad (3.20)$$

If the doppler factor in (3.20) is neglected, the narrowband ambiguity function in (3.19) is obtained.

For a 30 knot ship in water, $(1-\dot{\tau}_{t_o}) = 0.99$; a negligible amplitude change.

Unlike the narrowband ambiguity function, the volume of the broadband ambiguity function is not a constant. In fact, Purdy and Cooper [31] showed that the volume of the broadband ambiguity function will be infinite for any signal with a continuous spectrum that is not zero at zero frequency.

3.3 Narrowband Receivers with PUTTS

In section 2.4, the narrowband ambiguity function described the ambiguities for $\tau \neq 0$ and $f_d \neq 0$. This ambiguity function is useful from the signal designer's perspective. Once a particular signal waveform is chosen, the objective of a receiver is to estimate the doppler and time delay associated with the received signal. One approach to the design of an appropriate receiver is to utilize the ambiguity function as the basis for construction. The narrowband receiver is implemented with *processing using transmission time scaling* (PUTTS)[1]. With PUTTS, the crosscorrelation in the matched-filter may be efficiently computed using the FFT. For M_d doppler channels of interest, M_d frequency shifted versions of the reference signal are stored in memory. The demodulated samples of the reception is crosscorrelated with each of the reference signals, and the outputs, collectively, form the narrowband ambiguity surface. The steps for PUTTS are detailed below.

Let $r[n] \quad 0 \leq n \leq N_1 - 1$ represent samples of a one-period reception at a sampling rate of $r_s = m_r f_c$. The demodulated samples are obtained by multiplying the sampled reception by a complex rotator and is given by

$$\begin{aligned} z[n] &= r[n]e^{j2\pi n f_c/r_s} \\ &= r[n]e^{j2\pi n/m_r} \ . \end{aligned} \tag{3.21}$$

In order to utilize the efficiency of FFT, $z[n]$ is padded with N_2 zeroes ($N_2 > N_1$)

[1]For narrowband processing, the time scaling reduces to a simple frequency shift.

such that $N_1 + N_2$ is a power of 2. Let $Z[k]$ represent the DFT of the zero-padded $z[n]$ through FFT. The next step is to form the M_d reference signals for the M_d doppler channels of interest. In discrete time, the reference signals are

$$\begin{aligned} m_{\alpha'}[n] &= m\left(\frac{n}{r_s}\right) e^{j2\pi n(1-\alpha')f_c/r_s} \\ &= m[n]e^{j2\pi n(1-\alpha')/m_r} \qquad for \begin{cases} \alpha'_{min} \le \alpha' \le \alpha'_{max} \\ 0 \le n \le N_1 - 1 \end{cases} \end{aligned} \tag{3.22}$$

where α' is the search variable for doppler. In (3.22), it is assumed that α' are evaluated at discrete intervals. The total number of doppler channels M_d is detailed in Appendix C. Again, $m_{\alpha'}[n]$ is padded with N_2 zeros. Then, $M_{\alpha'}[k]$, the DFT of $m_{\alpha'}[n]$ through FFT, is stored in memory. The output of the crosscorrelation for the α^{th} doppler channel is given by

$$y_{\alpha'}[n] = IDFT\{Z[k]M^*_{\alpha'}[k]\} , \tag{3.23}$$

where IDFT is the inverse discrete Fourier Transform computed through FFT. The narrowband receiver with PUTTS is block diagrammed in figure (3.1).

3.4 Broadband Receivers

3.4.1 Broadband Receivers With PUTTS

In the case of a broadband signal reception, the signal will be doppler-shifted and time-scaled. The extent of this time-scale would depend on the magnitude of the doppler factor $\dot{\tau}_{t_o}$. If T_p represent the nominal period at 0-doppler, a one-period reception at the α^{th} doppler channel corresponds to the period $(1-\alpha')T_p$. For PUTTS, a one-period processing would require a minimum of $(1-\alpha'_{min})N_1$ 0-doppler samples [2]. This is to ensure that a full period of the signal is recorded regardless

[2] α'_{min} corresponds to the minimum compression or maximum expansion of signals among all doppler channels of interest. (i.e. $1-\alpha'_{min} \ge 1-\alpha'$ for all α')

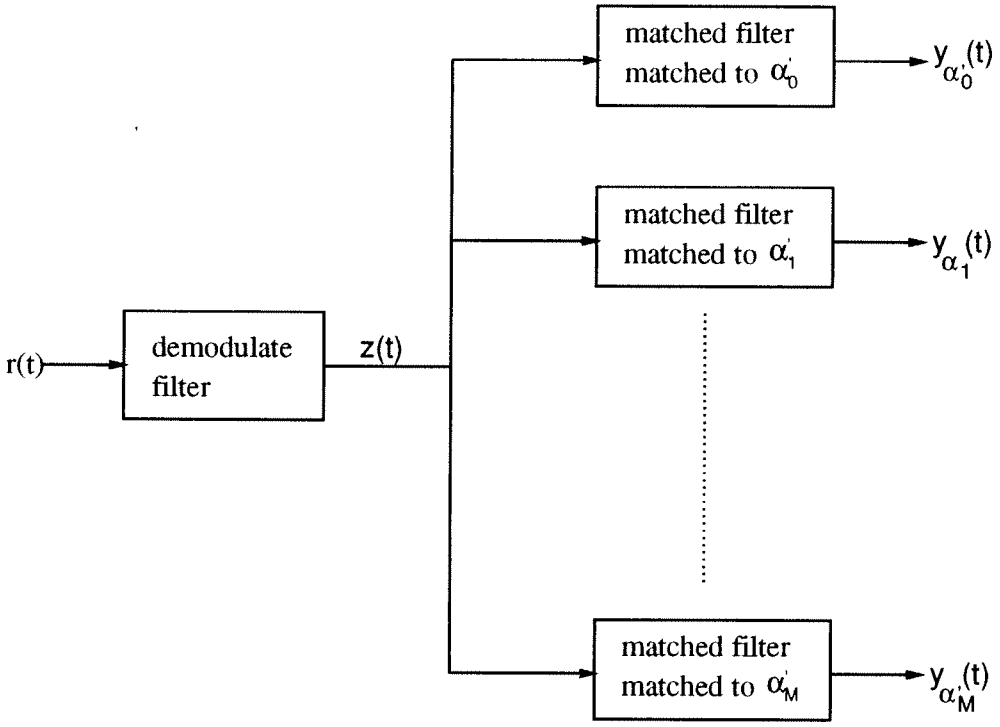

Figure 3.1: The narrowband receiver with PUTTS. The crosscorrelation in the matched filtering is implemented using FFT. The outputs $y_{\alpha_o}(t)$ to $y_{\alpha_M}(t)$ combines to form the narrowband ambiguity surface.

of the signal's doppler-scaling. Let $z[n]$ represent the $(1-\alpha'_{min})N_1$ demodulated samples of the 0-doppler reception. As in the case of narrowband processing, $z[n]$ must be padded with enough zeros such that the total number of samples is a power of 2. Unlike the narrowband case, the reference signal under broadband modeling must be scaled in time and shifted in frequency. The samples of the α^{th} reference signal is

$$m_{\alpha'}[n] \;=\; m\left(\frac{n(1-\alpha')}{r_s}\right) e^{j2\pi n(1-\alpha')f_c/r_s} \quad for \;\; 0 \le n \le \lfloor (1-\alpha')N_1 \rfloor \; . \qquad (3.24)$$

Similarly, $m_{\alpha'}[n]$ must be padded with enough zeros such that it has the same number of samples as the padded $z[n]$. The rest of the procedure is the same as in the narrowband case. The crosscorrelation is obtained by the inverse DFT of the product between $M_{\alpha'}[k]$ and $Z[k]$.

In the general case of K-period transmission, the demodulated samples $z[n]$ must contain all K periods of the reception prior to zero-padding. Similarly, the reference signal must also span K periods prior to zero-padding. In other words, if K periods are transmitted, K periods must be processed.

One of the main drawback of PUTTS is that the crosscorrelation must be a *linear* crosscorrelation. This is due to the fact that zero-padding removes the periodicity of the processed signal. If *cyclic* crosscorrelation is desired, the demodulated samples cannot be zero-padded; hence, FFT cannot be utilized[3]. Under this circumstance, a different method for broadband processing is proposed which utilizes *one* reference signal for all doppler channels (i.e. fixed matched-filter). This is known as the *processing using receiver time scaling* (PURTS) described next.

[3]Since the total number of samples in one period changes from one doppler channel to the next, it is impossible to calculate the DFT using one of the fast transform algorithms described in Blahut [8]

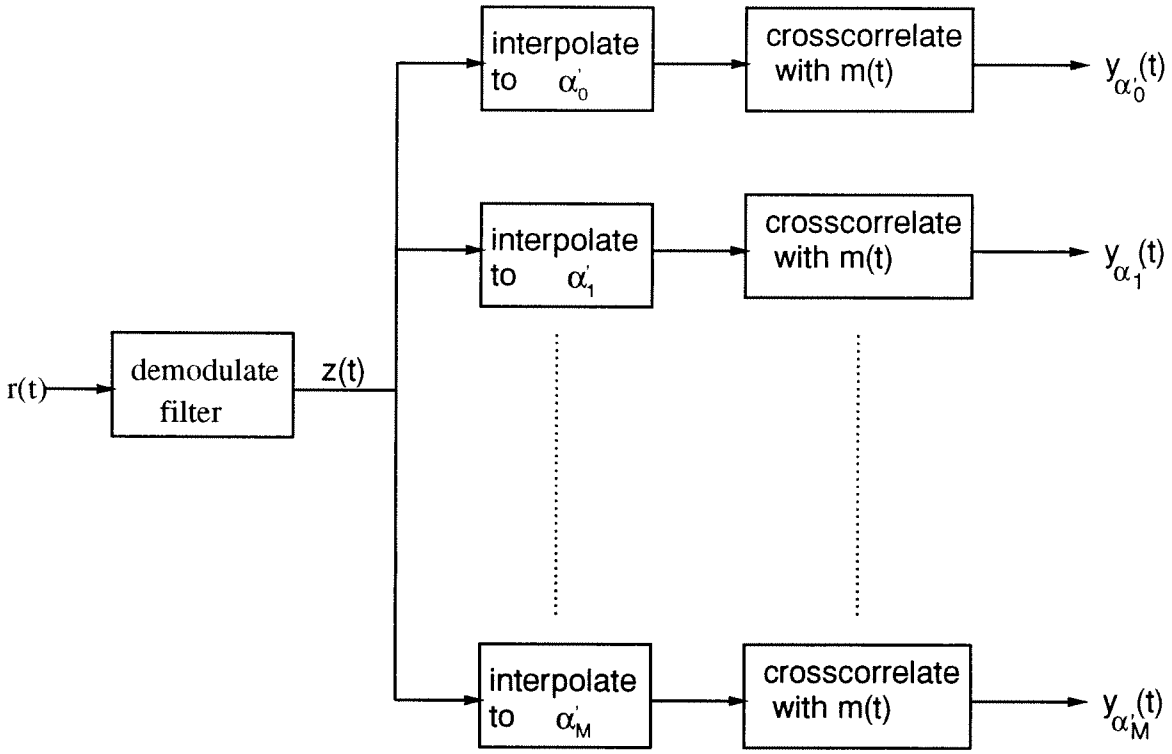

Figure 3.2: The broadband receiver with PURTS. The outputs $y_{\alpha_o}(t)$ to $y_{\alpha_M}(t)$ combines to form the broadband ambiguity surface.

3.4.2 Broadband Receivers With PURTS

The basic principle behind PURTS is to compensate for the time-scale prior to the crosscorrelation. As a result, each doppler channel would have the same number of samples per period. Therefore, only one reference signal is required for processing all doppler channels. It is much easier to design a fast algorithm for one reference signal than to design M fast algorithms for M doppler channels as in the case of PUTTS. In fact, for the case of m-sequences, the Fast Hadamard Transform described in Appendix A may be utilized under PURTS. A block diagram of the broadband receiver utilizing PURTS is shown in figure (3.2).

In continuous time, the demodulated response at 0-doppler is

$$z(t) \;=\; r(t)e^{-j2\pi f_o t}\;. \tag{3.25}$$

The compensation in time-scale (i.e. the linear interpolation) is implemented in two steps. The first step adjusts the phase of $z(t)$ for proper demodulation so that

$$z'_{\alpha'}(t) \;=\; z(t)e^{j2\pi f_o t}e^{-j2\pi f_o(1-\alpha')t} \;. \tag{3.26}$$

The second step is to time-compress the demodulate response to give

$$z_{\alpha'}(t) \;=\; z'_{\alpha'}\left(\frac{t}{1-\alpha'}\right) \;. \tag{3.27}$$

Finally, the output of the crosscorrelation is

$$A_B(\tau,\alpha') \;=\; \int z_{\alpha'}(t+\tau)m^*(t)dt \;. \tag{3.28}$$

Equation (3.28) represents the broadband processing with PURTS in continuous time.

In order to show the validity of equations (3.26) and (3.27) as a means for linear interpolation, consider the case of a single path reception given by

$$r(t) \;=\; a_o(t)(1-\beta')m((1-\beta')t-S)e^{j2\pi f_o(1-\beta')t}e^{-j2\pi f_o S} \;, \tag{3.29}$$

where

$$\beta' \;=\; \dot{\tau}_{t_o} \tag{3.30}$$

is the true doppler of the signal and

$$S \;=\; \tau(t_o) - \beta' t_o \tag{3.31}$$

is the remapped time delay. From (3.25), the demodulated response is

$$z(t) \;=\; a_o(t)(1-\beta')m((1-\beta')t-S)e^{-j2\pi f_o\beta' t}e^{-j2\pi f_o S} \;, \tag{3.32}$$

In (3.32), the 0-doppler demodulation did not compensate for the doppler-shift in the carrier (i.e. $e^{j2\pi f_o\beta' t}$); therefore, the purpose of the "two-step" interpolation

is to correct for this carrier mismatch and to rescale the baseband signal prior to crosscorrelation. From (3.26), the phase compensation results in

$$z'_{\alpha'}(t) \;=\; a_o(t)(1-\beta')m((1-\beta')t-S)e^{j2\pi f_o[(1-\beta')-(1-\alpha')]t}e^{-j2\pi f_o S}\;, \tag{3.33}$$

and the time-compressed response at the α^{th} doppler channel is

$$\begin{aligned} z_{\alpha'}(t) \;&=\; a_o(t)\left(\frac{1-\beta'}{1-\alpha'}\right)m\left(\frac{1-\beta'}{1-\alpha'}t-S\right) \\ &\quad\cdot exp\left\{j2\pi f_o\left[\left(\frac{1-\beta'}{1-\alpha'}-1\right)t-S\right]\right\}\;. \end{aligned} \tag{3.34}$$

Therefore, if the zero doppler response is interpolated to the true doppler channel of the signal (i.e. $\alpha' = \beta'$), then the time-compressed response in (3.34) would become

$$z_{\alpha'}(t) \;=\; a_o(t)m(t-S)e^{-j2\pi f_o S}\;, \tag{3.35}$$

which is just a time-shifted version of the baseband signal.

In discrete time analysis, K periods of the sampled reception will be coherently averaged to reveal the full potential of the PURTS. For K-period processing, the minimum number of samples required is $KN_1(1-\alpha'_{min})$. As in (3.26), the phase of $z[n]$ is adjusted so that

$$z'_{\alpha'}[n] \;=\; z[n]e^{j2\pi n f_o/r_s}e^{-j2\pi n f_o(1-\alpha')/r_s}\;. \tag{3.36}$$

To implement the linear interpolation in discrete time, let the desired but unattainable sample index be

$$x[n] \;=\; n(1-\alpha'), \tag{3.37}$$

and the integer on the left of desired index be $c[n]$, given by

$$c[n] \;=\; \lfloor x[n] \rfloor\;. \tag{3.38}$$

c[n] is the greatest integer less than or equal to $x[n]$. In addition, let

$$\lambda[n] \;=\; x[n] - c[n] \tag{3.39}$$

be a number between 0 and 1 such that $x[n] = c[n] + \lambda[n]$ is the integer plus fraction representation of $x[n]$. Then the time compressed samples at the α^{th} doppler channel are

$$z_{\alpha'}[n] \;=\; (1 - \lambda[n]) z'_{\alpha'}[c[n]] + \lambda[n] z'_{\alpha'}[c[n] + 1] \;, \tag{3.40}$$

where $z'_{\alpha'}[c[n]]$ is the actual sample immediately before the desired $z_{\alpha'}[n]$. An important point to keep in mind is that regardless of which doppler channel is being processed, the number of demodulated samples in one period is always the same. In this particular case, there are N_1 samples in a period for each doppler channel. The coherent average of K periods is given by

$$z_{\alpha',K}[n] \;=\; \frac{1}{K} \sum_{m=1}^{K} z_{\alpha'}[n + mN_1] \;; \quad 0 \leq n < N_1 \;, \tag{3.41}$$

and the crosscorrelation for the α^{th} doppler channel is $z_{\alpha',M}[n] \otimes m[n]$. In general, $\otimes$ may be a linear or cyclic crosscorrelation since zero-padding is not required. Again, the only reference signal required is the transmitted signal $m[n]$.

Due to the advantages of PURTS, it will be used exclusively in the analysis of weak signal detection in subsequent chapters. To simplify notations, the subscript B in (3.28) will be dropped.

3.5 Shift-Invariance Property of Receiver Output

In sections 3.3 and 3.4, PUTTS and PURTS were described in terms of their processing efficiency, capabilities for coherent averaging, and differences in the types of crosscorrelations. In this section, the existence of a shift-invariant property for narrowband and broadband receivers is discussed. Unlike the emphasis between

PUTTS and PURTS for narrowband and broadband receivers, the existence of a shift-invariant property depends on whether the reception is doppler-shifted or doppler-scaled (i.e. narrowband or broadband reception).

3.5.1 Narrowband Reception

In narrowband signal processing, the envelope of the receiver output with PUTTS is shift-invariant in both time-delay and doppler. Assuming a single path noiseless reception with attenuation constant a, the continuous time reception of a narrowband signal can be modeled as

$$\begin{aligned} r(t) &= a\, m(t-\tau(t))e^{j2\pi f_o(t-\tau(t))} \\ &= a\, m(t-\tau(t_o))e^{j2\pi f_o(1-\dot{\tau}_{t_o})t}e^{-j2\pi f_o(\tau(t_o)-\dot{\tau}_{t_o}t_o)}\ , \end{aligned} \tag{3.42}$$

Equation (3.42) may be written more compactly as

$$r(t) = a\, m(t-\tau(t_o))e^{j2\pi f_o(1-\beta')t}e^{-j2\pi f_o(\tau(t_o)-\beta' t_o)}\ , \tag{3.43}$$

Complex demodulating the reception in (3.43) gives,

$$\begin{aligned} z(t) &= r(t)e^{-j2\pi f_o t} \\ &= a\, m(t-\tau(t_o))e^{-j2\pi f_o\beta' t}e^{-j2\pi f_o(\tau(t_o)-\beta' t_o)}\ , \end{aligned} \tag{3.44}$$

When the output of the crosscorrelation is conditional on the parameters of the modeled reception, the output of the narrowband receiver may be written as[4]

$$\begin{aligned} A_N(\tau,\alpha' \mid T,\beta',a) &= a\, e^{j2\pi f_o(\beta' t_o-\tau(t_o))}\int m(t-\tau(t_o))m^*(t-\tau)e^{j2\pi f_o(\alpha'-\beta')t}dt \\ &= a\, e^{j2\pi f_o(\beta' t_o-\tau(t_o))}e^{j2\pi f_o(\alpha'-\beta')\tau(t_o)} \\ &\quad \cdot \int m(t)m^*(t'+\tau(t_o)-\tau)e^{j2\pi f_o(\alpha'-\beta')t'}dt'\ . \end{aligned} \tag{3.45}$$

[4]The limit of integration have been omitted intentionally to allow focusing on the integrand. Subsequent sections will focus on these limits, and its significance in the estimate of the time delay $\tau(t)$.

The significance of the narrowband ambiguity function is that the integral in (3.45) is only a function of the differences between search and true variables for both time-delay and doppler which means

$$\mid A_N(\tau, \alpha' \mid \tau(t_o), \beta', a) \mid = \mid a\ A_N(\tau - \tau(t_o), \alpha' - \beta') \mid 0, 0, 1) \mid \tag{3.46}$$

3.5.2 Broadband Reception

When the broadband processing with PURTS is conditional on the parameters of the single-path reception, the time-scaled, demodulated response may be obtained from equations (3.29)–(3.34). Therefore, the output of the crosscorrelation is given by

$$\begin{aligned} A_B(\tau, \alpha' \mid S, \beta', a) \;=\; & a\left(\frac{1-\beta'}{1-\alpha'}\right) exp\left\{j2\pi f_o\left[\left(\frac{1-\beta'}{1-\alpha'}-1\right)\tau - S\right]\right\} \\ & \cdot \int m\left[\frac{1-\beta'}{1-\alpha'}t + \tau - S\right] m^*(t) \\ & \cdot exp\left\{j2\pi f_o\left(\frac{1-\beta'}{1-\alpha'}-1\right)t\right\} dt\ . \end{aligned} \tag{3.47}$$

The integral on the right of (3.47) is not shift invariant with respect to τ and α'. In chapter IV, a variation of this broadband receiver is introduced with the advantage that its broadband receiver ambiguity function is approximately shift-invariant in both doppler and time-delay. This invariance property is the key to computation economy for weak signal detection under multipath propagation.

CHAPTER IV

Shift-Invariant Method for Strong Path Cancellation

As mentioned in the introduction, when both weak and strong paths are present at the reception, the floor level due to the strong paths may be higher than the peaks of the weak paths. Under this circumstance, the floor level of the strong paths must be removed in order to detect the presence of the weak paths. The Shift-Invariant Method for Strong Path Cancellation (SIMSPC) described in this chapter has the advantage that the strong paths can be removed without affecting the strength of the weak paths. More important, (SIMSPC) can be implemented with very few computations due to the absence of interpolation utilized in generating a broadband ambiguity surface. The basic principle behind (SIMSPC) is to pre-calculate a reference ambiguity surface consisting of a single-path reception and store it in memory. To remove the strong path interference, the reference surface may be shifted, rescaled, and subtracted from the observed ambiguity surface with minimal interference to the weak paths.

Two types of shift-invariant surfaces are introduced. The first type is formed using the sliding processing receiver whereby the crosscorrelation utilizes two periods of the reception to form a one-period output. It has the advantage that the broadband

ambiguity surface at the output of the receiver is shift-invariant in both doppler and time-delay. The second type of shift-invariant surface is formed using block processing. Due to the cyclic crosscorrelation in block processing, the broadband ambiguity surface is no longer shift-invariant in time-delay. However, the demodulate surface is shift-invariant in both time-delay and doppler; hence, a computational efficient method for weak signal detection may be constructed using this demodulate surface. The efficacy of these two shift-invariant surfaces is shown using m-sequence signals.

4.1 Strong Path Cancellation Without Shift-Invariant Ambiguity Surfaces

In all but the simplest situations, the received broadband signal is the sum of many delayed, doppler-scaled, and attenuated replicas of the transmitted signal. One application to the model of this reception is the transmission of sound in deep sea. The deep sound channel, sometimes known as the sofar channel, is a consequence of the characteristic velocity profile of the deep sea.

The velocity profile may be divided into several layers. The surface layer is affected by the daily changes of heating, cooling and wind action. Below the surface layer lies the seasonal thermocline where the velocity changes with depth as the temperature changes. This negative velocity gradient will vary with seasonal changes. Under the seansonal thermocline is the main thermocline where the velocity profile is only slightly affected by seasonal changes. In this layer the velocity will decrease with decreasing temperature until the water temperature reaches to about 4^{o} C. Underneath the main thermocline is the deep isothermal layer where the temperature decreases very slowly as the pressure becomes enormous. However, due to the

increase in pressure with depth, the sound velocity will also increase with depth due to the effect of pressure on sound velocity. Therefore, the depth at which the main thermocline layer and the deep isothermal layer meets is where the sound velocity reaches its minimum velocity which varies from near the surface to about 4000 feet [47]. The velocity profile causes the deep sea channel to act much like a lens. The negative velocity gradient in the main thermocline layer will cause sound rays to bend down toward the depth with minimum velocity. In the deep isothermal layer, sound rays will bend upward toward the depth of minimum velocity.

Sound rays from the source to the receiver may take on many different paths depending on the geometry of the source and receiver as well as the sound velocity profile. Some of the rays or paths from the source would experience surface or bottom reflections, but the majority of the paths will remain within the acoustic channel and experience no acoustic losses by scattering from either the surface or the bottom. Both the surface and bottom bounces produces a frequency-independent phase-shift as well as a loss due to scattering or absorption. The most significant cause for transmission loss within the acoustic channel is due to spherical and cylindrical spreading. Paths within the acoustic channel may also experience added loss due to absorption [47]. Regardless of the trajectories of these paths and the propagation medium, the path receptions may be accurately modeled as attenuated, time-delayed and doppler-scaled replicas of the transmitted signal. The goal is to identify each and every path.

Any bandlimited bandpass signal with period P_T can be modeled as the positive frequency "analytic signal"

$$s(t) \;=\; a\; m(t)e^{j2\pi f_o t}\;. \tag{4.1}$$

The noiseless multipath reception is

$$\begin{aligned} r(t) &= \sum_{p=1}^{N} a_p \; m(t-\tau_p(t)) e^{j2\pi f_o(t-\tau_p(t))} \\ &= \sum_{p=1}^{N} a_p \; m((1-\beta'_p)t - S_p) e^{j2\pi f_o(1-\beta'_p)t} e^{-j2\pi f_o S_p} \;, \end{aligned} \tag{4.2}$$

where

$$\beta'_p = \dot{\tau}_{(p,t_o)} \tag{4.3}$$

$$S_p = \tau_p(t_o) - \dot{\tau}_{(p,t_o)} t_o \;. \tag{4.4}$$

and a_p is the *complex* attenuation coefficient which takes into account of both geometric losses and possible phase-shifts. The index p in the summation indicates the different path receptions. In order to differentiate the strong signal receptions from the weak signal receptions, it is assumed that the first M paths in the summation correspond to the major paths (strong paths) and the remaining (N–M) paths correspond to the weak paths. Each path may be characterized by the parameters S_p, β'_p and the relative amplitude a_p.

A straight forward approach to strong signal cancellation would be to precalculate a receiver ambiguity surface with unity amplitude for each and every possible combinations of β' and S, and store these receiver ambiguity surfaces in memory. These stored receiver ambiguity surfaces are referred to as the "reference ambiguity surfaces" in order to distinguish them from the receiver ambiguity surface observed at the output of the receiver. Once the time-delays, doppler, and amplitude (S_p, β'_p, a_p) are obtained for each of the major paths, reference ambiguity surfaces corresponding to these major paths may be retrieved from memory and subtracted from the receiver ambiguity surface. The residue consisting of weak paths is

$$A_{-M}(\tau,\alpha) = A(\tau,\alpha \mid \boldsymbol{S},\boldsymbol{\beta}',\boldsymbol{a}) - \sum_{p=1}^{M} a_p \; A_r(\tau,\alpha \mid S_p,\beta'_p,1) \;, \tag{4.5}$$

where

$$\boldsymbol{S} = [S_1, S_2, ..., S_N] \tag{4.6}$$

$$\boldsymbol{\beta'} = [\beta'_1, \beta'_2, ..., \beta'_N] \tag{4.7}$$

$$\boldsymbol{a} = [a_1,\ a_2, ..., a_N]\ , \tag{4.8}$$

and $A_r(\tau, \alpha \mid S_p, \beta'_p, 1)$ is the reference ambiguity surface with unity gain. This method of strong signal cancellation has a drawback. It requires the storage of reference ambiguity surfaces for all possible values of S_p and β'_p. A typical *small* underwater acoustic measurement might use 50 search values for β'_p and 2000 search values for S_p, so each reference ambiguity surface would require 10^5 pixels (one pixel = one complex number). Due to the doppler invariance to be described in section 4.2, only 2000 of the 10^5 reference surfaces are required for storage. At 8 bytes/pixel, this corresponds to 1.6 gigabytes of memory. In 1992, 1.6 gigabytes of memory would cost approximately $1600 which is certainly within practical limitations. However, for transmission of signals with long periods and small sampling intervals (see Appendix C), the cost could easily rise to $250,000-$2 million. Therefore, the strong signal cancellation based on all precalculated surfaces is fast but very costly. If the reference function had been shift-invariant in time the required memory would be drastically reduced to 10^5 pixels—a practical PC memory in 1992. Hence, this current research searches for processing with time shift-invariant surfaces.

4.2 Shift-Invariant Ambiguity Surface With Sliding Processing

The primary objective of this section is to describe the sliding processing receiver and how its output may be expressed as a shift invariant function of both time-delay and doppler. Part of this invariance is done by an apt choice of variables.The doppler

parameters are moved to an exponent. In order to describe the signal processing of the sliding processing receiver, let

$$e^{-\alpha} \triangleq 1 - \alpha' , \tag{4.9}$$

where α' is the search variable for the doppler parameter β' defined in (3.30). Therefore,

$$e^{\alpha} t = \frac{t}{1 - \alpha'} . \tag{4.10}$$

To interpolate from the 0-doppler channel to the α^{th} doppler channel, the phase-compensated, demodulate response is

$$z'_{\alpha}(t) = z(t) e^{j2\pi f_o (1 - e^{-\alpha})t} . \tag{4.11}$$

where $z(t)$ is the demodulated reception in (3.25). The time-scaled, demodulated reception becomes

$$z_{\alpha}(t) = z'_{\alpha}(e^{\alpha} t) , \tag{4.12}$$

At this point the limits of integration for the crosscorrelation must be defined. The interval of integration corresponds to an integer number of periods of the signal at the search doppler, and is simply labeled P_T. For signal processing, the output of the crosscorrelation is expressed as

$$A_s(\tau, e^{\alpha}) = \int_0^{P_T} z_{\alpha}(t + \tau) m^*(t) dt , \tag{4.13}$$

where the subscript s denotes the use of a sliding processing receiver. The peaks of $A_s(\tau, e^{\alpha})$ will indicate the presence of individual paths in the reception. However, if one were to interpret the significance of the parameters corresponding to the peaks of the ambiguity surface, one would need to define the arrival time and provide a model for the reception. Let q_o be the arrival time of the first path detected,

and δ_o be the time difference between the first arrival and the last arrival. Assume that a single-period integration is over the interval from $t = t_o$ to $t = t_o + P_T$ where $t_o \geq q_o + \delta_o$. This would ensure that all the path arrivals are integrated for one period. Alternatively, it may be assumed that $r(t)$ is available for integration starting from $t = t_o$. For the integration in (4.13), the noiseless multipath reception may be modeled as

$$r(t) = \sum_{p=1}^{N} a_p \, m(t - \tau_p(t)) e^{j2\pi f_o (t - \tau_p(t))}; \qquad t \geq 0 \tag{4.14}$$

where

$$\tau_p(t) = \tau_p(t_o) + \dot{\tau}_{t_o}(t - t_o) \, . \tag{4.15}$$

Using the exponential form of doppler factor, β_p can be defined as

$$\begin{aligned} e^{-\beta_p} &\triangleq 1 - \beta'_p \\ e^{-\beta_p} &= 1 - \dot{\tau}_{(p,t_o)} \end{aligned} \tag{4.16}$$

so that

$$e^{(\alpha - \beta_p)t} = \frac{1 - \beta'_p}{1 - \alpha'} t, \tag{4.17}$$

and the noiseless multipath reception is written as

$$r(t) = \sum_{p=1}^{N} a_p \, m(e^{-\beta_p} t - S_p) e^{j2\pi f_o e^{-\beta_p} t} e^{-j2\pi f_o S_p} \, , \tag{4.18}$$

where

$$S'_p = \tau_p(t_o) - (1 - e^{-\beta}) t_o \, . \tag{4.19}$$

The demodulated reception is

$$z(t) = \sum_{p=1}^{N} a_p \, m(e^{-\beta_p} t - S_p) e^{j2\pi f_o (e^{-\beta_p} - 1) t} e^{-j2\pi f_o S_p} \, , \tag{4.20}$$

and the rescaled, demodulated reception becomes

$$\begin{aligned} z_\alpha(t) &= z'_\alpha(e^\alpha t) \\ &= \sum_{p=1}^{N} a_p \; m(e^{(\alpha-\beta_p)}t - S_p) e^{j2\pi f_o\left[(e^{(\alpha-\beta_p)}-1)t - S_p\right]} \; , \end{aligned} \tag{4.21}$$

where

$$z'_\alpha(t) \;=\; z(t) e^{j2\pi f_o(1-e^{-\alpha})t} \; . \tag{4.22}$$

In order to clarify that (4.13) is shift-invariant in time, define a new time-delay variable T_p as

$$\begin{aligned} T_p &\triangleq e^{(\beta_p-\alpha)} S_p \\ &= e^{(\beta_p-\alpha)} \left[\tau_p(t_o) - (1-e^{-\beta_p})t_o\right] \; , \end{aligned} \tag{4.23}$$

so that $z_\alpha(t)$ can be written as

$$z_\alpha(t) = \sum_{p=1}^{N} a_p \; m[e^{(\alpha-\beta_p)}(t-T_p)] e^{j2\pi f_o(e^{(\alpha-\beta_p)}-1)(t-T_p)} e^{-j2\pi f_o T_p} \; . \tag{4.24}$$

The output of the sliding processing receiver conditioned on the multipath parameters is given by

$$\begin{aligned} A_s(\tau, e^\alpha \mid \boldsymbol{T}, \boldsymbol{e^{-\beta}}, \boldsymbol{a}) &= \int_0^{P_T} z_\alpha(t+\tau) m^*(t) dt \\ &= \sum_{p=1}^{N} a_p e^{-j2\pi f_o T_p} \int_0^{P_T} m(e^{(\alpha-\beta_p)}(t+\tau-T_p)) m^*(t) \\ &\quad \cdot exp\{j2\pi f_o(e^{(\alpha-\beta_p)}-1)(t+\tau-T_p)\} dt \\ &= \sum_{p=1}^{N} A_s(e^\alpha, \tau \mid e^{-\beta_p}, T_p, a_p) \; , \end{aligned} \tag{4.25}$$

where the vector of remapped time delays is

$$\boldsymbol{T} \;=\; [T_1, \; T_2, ..., T_N] \; , \tag{4.26}$$

the vector of doppler compression for the N paths is

$$\boldsymbol{e^{-\beta}} \;=\; [e^{-\beta_1}, \; e^{-\beta_2}, ..., e^{-\beta_N}] \; , \tag{4.27}$$

and the vector of path amplitudes is

$$\boldsymbol{a} \;=\; [a_1,\; a_2, ..., a_N] \;. \tag{4.28}$$

In (4.25), the receiver ambiguity function of the p^{th} path is

$$\begin{aligned} A_s(\tau, e^{\alpha} \mid T_p', e^{-\beta_p}, a_p) \;&=\; a_p e^{-j2\pi f_o T_p} \int_0^{P_T} m[e^{(\alpha-\beta_p)}(t+\tau-T_p)] m^*(t) \\ &\quad \cdot exp\{j2\pi f_o (e^{(\alpha-\beta_p)}-1)(t+\tau-T_p)\} dt \;. \end{aligned} \tag{4.29}$$

This form of the receiver ambiguity function has the essential characteristic that

$$A_s(\tau, e^{\alpha} \mid T_p, e^{-\beta_p}, a_p) \;=\; a_p e^{-j2\pi f_o T_p} A_s(\tau - T_p, e^{(\alpha-\beta_p)} \mid 0, 1, 1) \;. \tag{4.30}$$

With the exception of a phase shift, the receiver ambiguity function is shift-invariant in both time-delay and doppler.

Through all this remapping of time-delays, it may be difficult to keep track the significance of each time-delay representation. In summary, the primary purpose for remapping time delays is to manipulate the parameters of the signal model in such a way that the ambiguity surface is seen to be shift-invariant in both time-delay and doppler. The exponential doppler factor suggests that if the doppler separations between successive doppler channels are exponentially spaced, the resultant ambiguity function will be shift-invariant in doppler and time-delay.

However, if *tracking* the various path arrivals is the primary objective, then the precise meaning of T_p becomes irrelevant. In other words, only the relative time-delays among the paths are essential. The absolute time-delays $\tau_p(t)$ of individual paths are of no concern.

In sonar targetting and in tomography, the knowledge of the absolute time-delay is crucial. In such cases, $\tau_p(t)$ may be calculated from T_p and β_p which are determined from the ambiguity surface. Since the constant time-delay determined from the

ambiguity surface is the true contant delay modulo T_p, one must add the constant t_o to the estimate of T_p from the ambiguity surface. The constant delay $\tau_p(t_o)$ is given by

$$\tau_p(t_o) = (T_p + t_o) + (1 - e^{-\beta_p})t_o \ . \tag{4.31}$$

This assumes that $\alpha = \beta_p$ at the peak of the path. Using (4.15), the absolute time-delay is

$$\begin{aligned} \tau_p(t) &= (T_p + t_o) + (1 - e^{-\beta_p})t_o + (1 - e^{-\beta_p})(t - t_o) \\ &= T_p + t_o + (1 - e^{-\beta_p})t \ . \end{aligned} \tag{4.32}$$

Recall that t_o on the right of (4.32) is the time-delay for all paths at the start of the integration in (4.25). In section 4.3, the shift-invariant property of this ambiguity function will be utilized to cancel strong paths within a reception.

4.2.1 Discrete Time Analysis of Shift-Invariant Surface

In practice, the demodulation and the doppler scaling are implemented through sampling. Both the time delay and doppler are calculated at discrete intervals. In order to avoid notational complexity, the discreteness of the doppler variables α will be implied through the use of brackets in the analysis. However, there will be times when a subscript for α is essential for the emphasis of an analysis at a particular doppler channel. When the nominal sampling interval t_1 is defined as

$$t_1 \triangleq \frac{1}{m_r f_o} \ , \tag{4.33}$$

where m_r is the "sampling multiplicity". For example, O. A. Tomography traditionally uses a sample rate of $4f_o$ samples per second. The discrete version of the demodulated reception is

$$z[n] = r(nt_1 + t_o)e^{-j2\pi f_o n t_1} \ . \tag{4.34}$$

Adjusting the phase for proper demodulation,

$$z'_\alpha[n] \;=\; z[n]e^{-j2\pi f_o(1-e^{-\alpha})nt_1} \;. \tag{4.35}$$

With the exception of the exponential doppler factor, the time-scaling is the same as in (3.37)-(3.40). To clarify the subtle differences, the equations are restated below. Let

$$\begin{aligned} x[n] &= ne^{\alpha} \\ c[n] &= \lfloor x[n] \rfloor \\ \lambda[n] &= x[n] - c[n] \;, \end{aligned} \tag{4.36}$$

then the time compressed samples at the α^{th} doppler channel is

$$z_\alpha[n] \;=\; (1-\lambda[n])z'_\alpha[c[n]] + \lambda[n]z'_\alpha[c[n]+1] \;. \tag{4.37}$$

The discrete version of the correlation output for signal processing is

$$A_s[\nu, e^{\alpha}] \;=\; e^{\alpha}t_1 \sum_{n=0}^{P_N-1} z_\alpha[n+\nu]m^*[n] \;, \tag{4.38}$$

where the discrete samples of the baseband reference is

$$m^*[n] \;=\; m^*(nt_1 + \delta_o) \;, \tag{4.39}$$

the number of samples in a period is

$$P_N \;=\; \frac{P_T}{t_1} \;, \tag{4.40}$$

and

$$\nu = \frac{\tau}{t_1} \;. \tag{4.41}$$

Conditional on the noiseless multipath parameters, the discrete version of the correlation output becomes

$$\begin{aligned} A_s[\nu, e^{\alpha} \mid \boldsymbol{S}, \boldsymbol{e^{-\beta}}, \boldsymbol{a}] \;=\; & e^{\alpha}t_1 \sum_{p=1}^{N} a_p \sum_{n=0}^{P_N-1} m(e^{(\alpha-\beta_p)}((n+\nu)t_1 - S_p)m^*[n] \\ & \cdot exp\left\{ j2\pi f_o \left[\left(e^{(\alpha-\beta_p)} - 1 \right) ((n+\nu)t_1 - S_p) \right] \right\} . \end{aligned} \tag{4.42}$$

In order to write the discrete version of the output in a time shift-invariant form, define

$$\tilde{T}_p \;=\; e^{(\beta_p-\alpha)}\frac{S_p}{t_1} \tag{4.43}$$

and the receiver ambiguity function becomes

$$\begin{aligned} A_s[\nu, e^{\alpha} \mid \tilde{\boldsymbol{T}}', \boldsymbol{e}^{-\beta}, \boldsymbol{a}] \;&=\; e^{\alpha}t_1 e^{-j2\pi f_o \tilde{T}_p t_1}\sum_{p=1}^{N} a_p \sum_{n=0}^{P_N-1} m(e^{(\alpha-\beta_p)}(n+\nu-\tilde{T}_p)t_1) \\ &\quad \cdot exp\left\{j2\pi f_o\left(e^{(\alpha-\beta_p)}-1\right)(n+\nu-\tilde{T}_p)t_1\right\}\;, \end{aligned} \tag{4.44}$$

where the vector of re-remapped time delays is

$$\tilde{\boldsymbol{T}} \;=\; [\tilde{T}_1,\ \tilde{T}_2, ..., \tilde{T}_N]\;. \tag{4.45}$$

Therefore, the second summation on the right of (4.44) is also shift invariant with respect to both time-delay and doppler.

4.3 Strong Signal Cancellation with Sliding Processing

This section describes the cancellation of strong paths utilizing the invariance property of the broadband ambiguity function in section 4.2. The invarinace property in (4.30) implies that only one reference ambiguity surface is required for storage. All reference ambiguity surfaces may be obtained by shifting the stored reference ambiguity surface to the desired point in the time-doppler plane along with the appropriate phase shift.

The reference ambiguity surface may be obtained from the reception consisting of only one path. Suppose the noise-free model of the single-path reception is

$$r_r(t) \;=\; a_r\; m(t-\tau(t)+t_r)exp\{j2\pi f_o(t-\tau(t)+t_r)\}\;, \tag{4.46}$$

where

$$\tau(t) \;=\; \tau_r(t_r) \;+\; \dot{\tau}_{t_r}(t-t_r)\;. \tag{4.47}$$

Following the same broadband processing as in section 3.4, the reference ambiguity function is[1]

$$\begin{aligned} A_{r,s}(\tau, e^{\alpha} \mid T_r, e^{\beta_r}, a_r) &= \int_0^{P_T} z_{r,\alpha}(t+\tau+q_r)m^*(t)dt \\ &= \int_0^{P_T} a_r e^{-j2\pi f_o T_r} m(e^{(\alpha-\beta_r)}(t+\tau-T_r))m^*(t) \\ &\quad \cdot exp\{j2\pi f_o(e^{(\alpha-\beta_r)}-1)(t+\tau-T_r)\}dt, \end{aligned} \tag{4.48}$$

where

$$T_r = e^{(\beta_r-\alpha)}\left[\tau_r(t_r) - (1-e^{-\beta_r})t_r\right] . \tag{4.49}$$

Recall in section 4.1 that a direct method for strong signal cancellation is to subtract the sum of the ambiguity functions of the strong paths from the receiver ambiguity function of the reception (i.e. the reception containing both strong and weak paths).

$$A_{s,-M}(\tau, e^{\alpha}) = A_s(\tau, e^{\alpha} \mid \boldsymbol{T}, \boldsymbol{e}^{-\beta}, \boldsymbol{a}) - \sum_{p=1}^{M} a_p \, A_s(\tau, e^{\alpha} \mid T_p, e^{-\beta_p}, 1) . \tag{4.50}$$

It is assumed that the parameters T_p, e^{β_p} and a_p can be accurately obtained[2] from the receiver ambiguity function $A_s(\tau, e^{\alpha} \mid \boldsymbol{T}, \boldsymbol{e}^{-\beta}, \boldsymbol{a})$. Without this knowledge, it would be impossible to determine the second summation on the right of (4.50). The advantage of the (SIMSPC) with sliding processing is that $A_s(e^{\alpha}, \tau \mid e^{-\beta_p}, T_p, 1)$ can be obtained from the shifted versions of the reference ambiguity surface since

$$A_s(\tau, e^{\alpha} \mid T_p, e^{\beta_p}, 1) = e^{-j2\pi f_o(T_p-T_r)} \frac{1}{a_r} A_{r,s}(\tau+T_r-T_p, e^{\alpha+\beta_r-\beta_p}, \mid e^{-\beta_r}, T_r, a_r). \tag{4.51}$$

Therefore, (SIMSPC) requires the storage space of only one reference ambiguity surface.

[1]Since the reception consists of only one path, the last arrival and the first arrival are the same so that δ_r will equal zero.

[2]The estimate of the amplitudes a_p is discussed in further detail in section 4.5.

Although the equivalence in (4.51) appears to have the desired shift-invariance in both time-delay and doppler, only the magnitude of the ambiguity function is shift-invariant. Fortunately, the phase difference between the left and right side of (4.51) is a constant for each doppler channel and may be easily calculated so that the phase-corrected, broadband ambiguity function will be truly shift-invariant in both magnitude and phase.

The (SIMSPC) with sliding processing is block diagrammed in figure 4.1.

4.4 Broadband Receiver Using Block Processing

For the sliding processing receiver the correlation between $z_\alpha(t)$ and $m(t)$ is calculated using a linear correlator. For block processing, the correlation is cyclic, and is given by

$$\begin{aligned} A_b[\nu, e^\alpha \mid \tilde{\boldsymbol{T}}', \boldsymbol{e}^{-\beta}, \boldsymbol{a}] &= \sum_{n=0}^{P_N-1} z_\alpha[n] m^*[n+\nu \bmod P_N] \\ &= \sum_{n=0}^{P_N-1} z_\alpha[n] m^*[[n+\nu]] \,, \end{aligned} \tag{4.52}$$

where [[ ]] denotes the mod P_N operation, and the subscript b denotes the use of a block processing receiver. Recall that $z_\alpha[n]$ is made up of two factors; $m(e^{(\alpha-\beta_p)}(n+\nu-\tilde{T}_p)t_1)$ and $exp\left\{j2\pi f_o\left[\left(e^{(\alpha-\beta_p)}-1\right)(n+\nu-\tilde{T}_p)t_1\right]\right\}$. The first factor is a doppler scaled and time delayed version of $m(t)$. It has periodicity $e^{(\beta_p-\alpha)}P_T$. The samples used in the crosscorrelation are taken from $n=0$ to $n=P_N-1$ which corresponds to one period of the zero doppler signal $m(t)$. In general, $z_\alpha[n]$ is non-periodic for two reasons. When $\alpha \neq \beta_p$, the P_N samples of $z_\alpha[n]$ do not represent one period of the baseband signal within $z_\alpha[n]$ since $m(e^{(\alpha-\beta_p)}(n+\nu-\tilde{T}_p)t_1)$ has periodicity of $e^{(\alpha-\beta_p)}P_T$ and not P_T. Second, the period of the phase term is $[f_o(e^{(\alpha-\beta_p)}-1)]^{-1}$ which also differs from P_T. Taking a cyclic correlation of a non-periodic signal is not

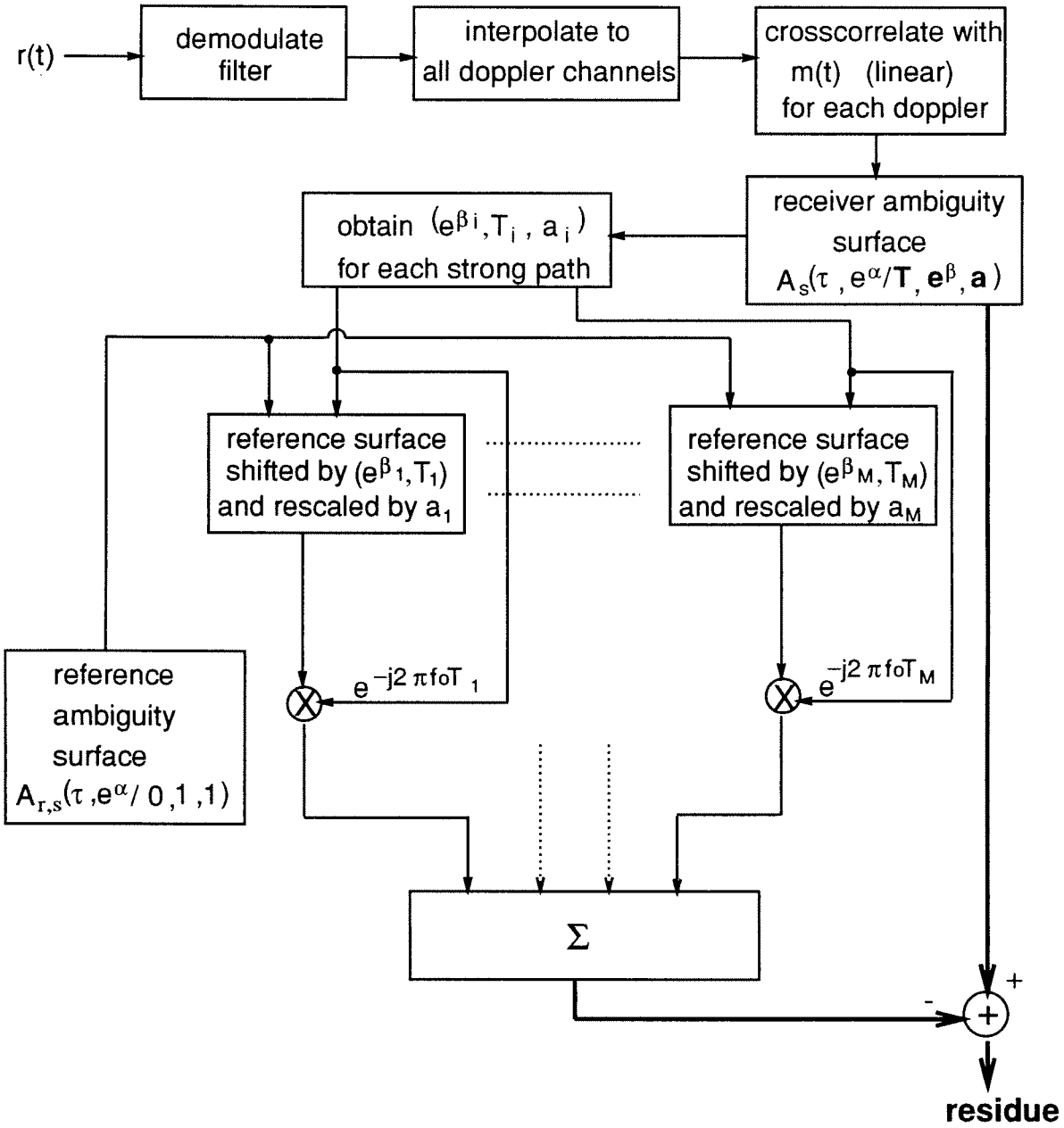

Figure 4.1: The (SIMSPC) with sliding processing receiver. The total number of strong paths is M. The "residue" is the ambiguity surface with strong paths removed. It is utilized for weak path detection.

equivalent to a linear correlation of a non-periodic signal. In fact, as long as $z_\alpha[n]$ does not have periodicity P_T, cyclic correlation is different from linear correlation. As a result,

$$A_b[\nu, e^\alpha \mid \tilde{T}_p, e^{-\beta_p}, 1] \neq e^{-j2\pi f_o T_p} A_b[\nu - \tilde{T}_p, e^{(\alpha-\beta_p)} \mid 0, 1, 1] \; . \tag{4.53}$$

The inequality in (4.53) states that the ambiguity function under block processing is not shift-invariant in *both* time-delay and doppler. However, the doppler invariance still hold [3]. Specifically, for $\tilde{T}_j = \tilde{T}_i$,

$$A_b[\nu, e^\alpha \mid \tilde{T}_j, e^{\beta_j}, a_j] = \frac{a_j}{a_i} A_b[\nu, e^{(\alpha+\beta_i-\beta_j)} \mid \tilde{T}_i, e^{\beta_i}, a_i] \; , \tag{4.54}$$

which implies that for a constant time-delay, the block ambiguity surface is invariant in the doppler variable e^α. This result is not surprising since cyclic correlation affects the time-delay $\tilde{T}_p$ and not the doppler scaling. As previously mentioned, if the ambiguity surface is only shift-invariant in doppler, the problem of memory storage arises. To circumvent this problem, an alternate method for strong path cancellation with block processing is proposed which utilizes the time shift-invariant property of the demodulate response as well as the speed of cyclic crosscorrelations.

4.4.1 Strong Signal Cancellation With Block Processing

Although the receiver ambiguity surface for block processing does not have the time shift-invariant property as the receiver ambiguity surface for sliding processing, the rescaled, demodulated reception $z_\alpha(t)$ is shift invariant in both time-delay and doppler. Conditional on the multipaths, the rescaled, demodulated surface may be

[3] Since the time-delay variable T_p is coupled to the doppler factor, one must be careful when comparing two paths with same time-delay but different doppler. In particular, in order for two paths with different doppler to have the same time-delay, the parameter $\tau_p(t_o)$ defined in (4.15) must differ for the two paths.

defined as

$$D_b(t, e^{\alpha} \mid \boldsymbol{T}, \boldsymbol{e}^{-\beta}, \boldsymbol{a}) \triangleq z_{\alpha}(t) , \tag{4.55}$$

where

$$D_b(t, e^{\alpha} \mid \boldsymbol{T}, \boldsymbol{e}^{-\beta}, \boldsymbol{a}) = \sum_{p=1}^{N} a_p \, D_b(t, e^{\alpha} \mid T_p, e^{-\beta_p}, 1) . \tag{4.56}$$

$D_b(t, e^{\alpha} \mid \boldsymbol{T'}, \boldsymbol{e}^{-\beta}, \boldsymbol{a})$ and $z_{\alpha}(t)$ differ mainly in their notation. $z_{\alpha}(t)$ is usually referred to as the output of the α^{th} doppler-time compressor whereas $D_b(t, e^{\alpha} \mid \boldsymbol{T'}, \boldsymbol{e}^{-\beta}, \boldsymbol{a})$ is referred to as the surface generated by all the doppler-time compressors. Since $z_{\alpha}(t)$ is shift-invariant in both time-delay and doppler, the demodulate surface is also shift-invariant in both variables; hence,

$$D_b(t, e^{\alpha} \mid T_p, e^{-\beta_p}, 1) = e^{-j2\pi f_o T_p} D_b(t - T_p, e^{\alpha-\beta_p} \mid 0, 1, 1) , \tag{4.57}$$

Therefore, the shift-invariance of a reference demodulated surface

$$D_{r,b}(t, e^{\alpha} \mid T_r, e^{-\beta_r}, a_r) \triangleq z_{r,\alpha}(t) \tag{4.58}$$

may be utilized for efficient cancellation of strong paths.

The block processing method for strong path cancellation may be implemented as follows. First, T_p, e^{β_p} and a_p are obtained from the observed receiver ambiguity function for each of the M strong paths. For each strong signal, a shifted version of the reference demodulate surface is constructed. Then the sum of the M shifted version of the reference demodulate surface is formed and is given by

$$\begin{aligned} D_{r,b,M}(t, e^{\alpha}) &\triangleq \sum_{p=1}^{M} \frac{a_p}{a_r} e^{-j2\pi f_o (T_p - T_r)} D_{r,b}(t + T_r - T_p, e^{\alpha+\beta_r-\beta_p} \mid T_r, e^{-\beta_r}, a_r) \\ &= \sum_{p=1}^{M} D_b(t, e^{\alpha} \mid T_p, e^{-\beta_p}, a_p) . \end{aligned} \tag{4.59}$$

Each doppler channel of the demodulate surface $D_{r,b,M}(t, e^{\alpha})$ must be crosscorrelated with the baseband signal $m(t)$ to produce the desired output. The resultant ambiguity surface $A_{r,b,M}(\tau, e^{\alpha})$ is constructed from the output of all the crosscorrelations.

Since all required shifts are pre-computed at the demodulate stage,

$$A_{r,b,M}(\tau, e^{\alpha}) \;=\; \sum_{p=1}^{M} A_b(\tau, e^{\alpha} \mid T_p, e^{-\beta_p}, a_p) \;, \tag{4.60}$$

and the reference ambiguity surface $A_{r,b,M}(\tau, e^{\alpha})$ equals the sum of the ambiguity surfaces of the M strong paths. Finally, the reference ambiguity surface is subtracted from the receiver ambiguity surface and the residual surface given by

$$\begin{aligned} A_{b,-M}(\tau, e^{\alpha}) &= A_b(\tau, e^{\alpha} \mid \boldsymbol{T}, \boldsymbol{e}^{-\beta}, \boldsymbol{a}) - A_{r,b,M}(\tau, e^{\alpha}) \\ &= \sum_{p=M+1}^{N} A_b(\tau, e^{\alpha} \mid T_p, e^{-\beta_p}, a_p) \;, \end{aligned} \tag{4.61}$$

consists of only weak paths; hence, weak paths may be identified by the peaks of this residual surface.

A block diagram of (SIMSPC) for the block processing receiver is provided in figure 4.2

4.5 Amplitude Estimation

In previous sections, it is assumed that the parameters of the strong paths may be readily obtained from the receiver ambiguity surface. This is true in the case of the doppler and time-delay variables, but the complex amplitudes a_p's are not readily available without additional calculations. For the case of a single-path reception, the peak of the receiver ambiguity surface is equal to the amplitude associated with the path. However, for multipath reception, each peak has components from all path arrivals. Specifically, if $\hat{A}_p$ is the peak of the p^{th} path at the point $(e^{-\beta_p}, T_p)$, then $\hat{A}_p$ may be expressed as

$$\begin{aligned} \hat{A}_p &= A_s(\tau, e^{\alpha} \mid \boldsymbol{T}, \boldsymbol{e}^{-\beta}, \boldsymbol{a}) \mid_{\substack{\tau=T_p \\ e^{\alpha}=e^{\beta_p}}} \\ &= \sum_{i=1}^{N} a_i \; A_s(\tau, e^{\alpha} \mid T_i, e^{-\beta_i}, 1) \mid_{\substack{\tau=T_p \\ e^{\alpha}=e^{\beta_p}}} \end{aligned}$$

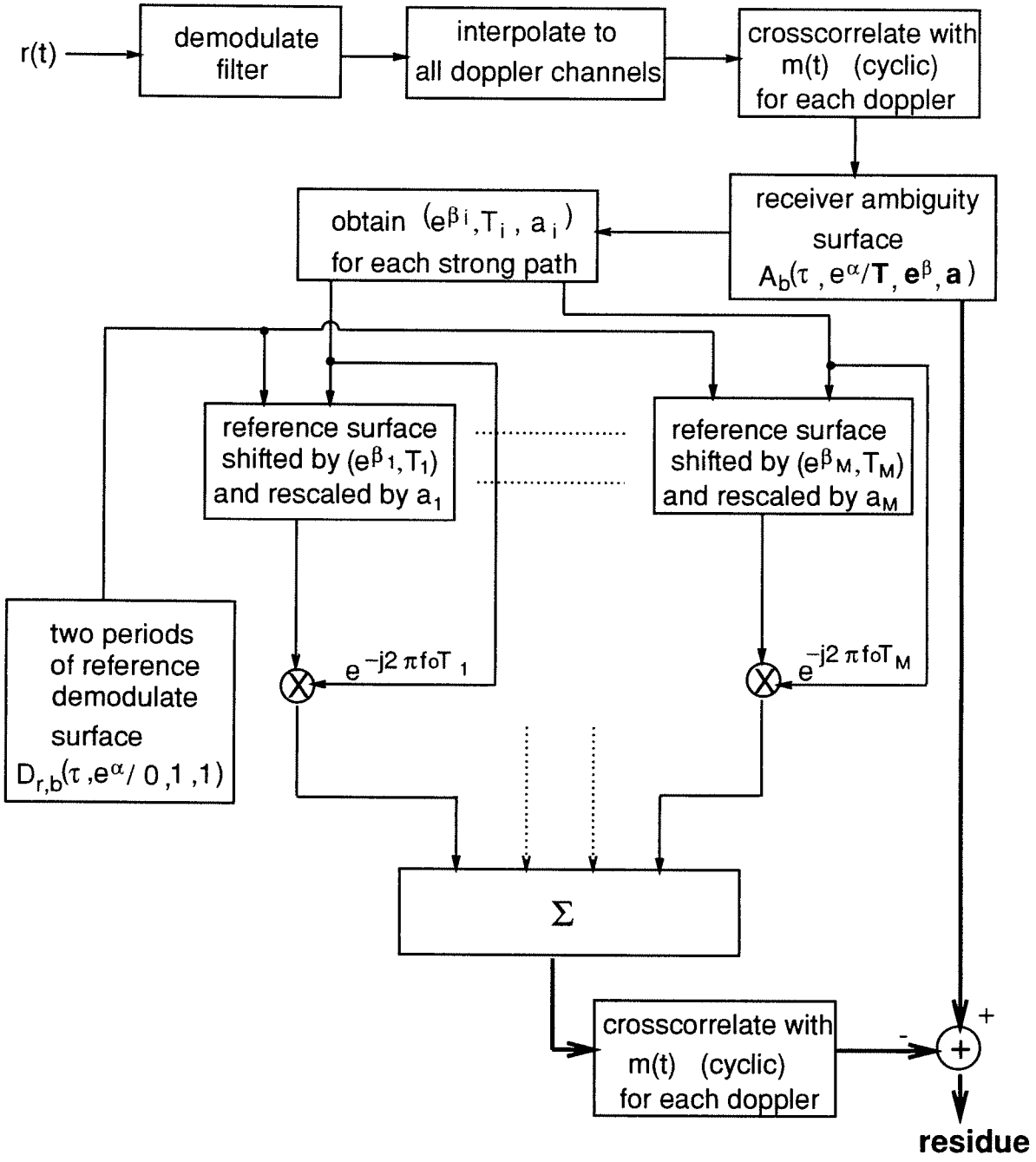

Figure 4.2: The (SIMSPC) with block processing receiver. The total number of strong paths is M. Unlike the (SIMSPC) with sliding processing receiver, the demodulate surface is shifted in both time and doppler. The "residue" is the ambiguity surface with strong paths removed. It is utilized for weak path detection.

$$\hat{A}_p = a_p e^{-j2\pi f_o T_p} + \sum_{\substack{i=1 \\ i\neq p}}^{N} a_i \; A_s(\tau, e^{\alpha} \mid T_i, e^{-\beta_i}, 1) \mid_{\substack{\tau=T_p \\ e^{\alpha}=e^{\beta_p}}}$$

$$= A_p + \sum_{\substack{i=1 \\ i\neq p}}^{N} a_i \; A_s(\tau, e^{\alpha} \mid T_i, e^{-\beta_i}, 1) \mid_{\substack{\tau=T_p \\ e^{\alpha}=e^{\beta_p}}} , \tag{4.62}$$

where

$$A_p \triangleq a_p e^{-j2\pi f_o T_p} \qquad for \;\; 1 \leq p \leq N \tag{4.63}$$

is the true peak associated with the p^{th} path. Assuming the contribution from the weak signals are negligible,

$$\hat{A}_p = A_p + \sum_{\substack{i=1 \\ i\neq p}}^{M} a_i \; A_s(\tau, e^{\alpha} \mid T_i, e^{-\beta_i}, 1) \mid_{\substack{\tau=T_p \\ e^{\alpha}=e^{\beta_p}}} . \tag{4.64}$$

The estimate of A_p's may be obtained by solving a set of linear equations given by

$$\boldsymbol{C}\boldsymbol{A} = \hat{\boldsymbol{A}} , \tag{4.65}$$

where

$$\boldsymbol{A} = [A_1, A_2, ..., A_M]^T \tag{4.66}$$

$$\hat{\boldsymbol{A}} = [\hat{A}_1, \hat{A}_2, ..., \hat{A}_M]^T \tag{4.67}$$

$$\boldsymbol{C} = \begin{bmatrix} c_{11} & c_{12} & \cdots & c_{1M} \\ c_{21} & c_{22} & \cdots & c_{2M} \\ \vdots & & \ddots & \vdots \\ c_{M1} & \cdots & \cdots & c_{MM} \end{bmatrix} \tag{4.68}$$

Therefore, if the coefficients c_{ip}'s were available, then a_p can be easily computed. In general, these coefficients cannot be determined from the receiver ambiguity surface of a multipath reception. However, since

$$A_s(\tau, e^{\alpha} \mid T_p, e^{-\beta_p}, 1) = \frac{a_p}{a_r} e^{-j2\pi f_o (T_p - T_r)} A_{r,s}(\tau + T_r - T_p, e^{(\alpha+\beta_r-\beta_p)} \mid T_r, e^{-\beta_r}, a_r) , \tag{4.69}$$

the coefficients can be obtained from shifted versions of the reference ambiguity surface as follows. Let

$$A_{p,r,s}(\tau,\alpha) \;=\; \frac{e^{-j2\pi f_o(T_p-T_r)}}{a_r} A_{r,s}(\tau+T_r-T_p, e^{(\alpha+\beta_r-\beta_p)}, \mid T_r, e^{-\beta_r}, a_r) \qquad (4.70)$$

be the shifted version of reference surface for the p^{th} path. Except for a scaled factor, $A_{p,r,s}(\tau,\alpha)$ is the same ambiguity function as the ambiguity function of the p^{th} path. Then the c_{ip} coefficient may be determined by evaluating $A_{p,r,s}(\tau,\alpha)$ at the point (T_i, e^{β_i}). Specifically,

$$c_{ip} \;=\; A_{p,r,s}(\tau,\alpha) \mid_{\substack{e^{\alpha}=e^{\beta_i} \\ \tau=T_i}} \;. \qquad (4.71)$$

Therefore, each column of $\boldsymbol{C}$ may be calculated from one shifted-version of the reference ambiguity surface. Once the A_p's are determined, a_p's can be readily obtained using equation (4.63).

For the block processing receiver, the procedure for estimating the amplitudes requires additional computation since the reference ambiguity surface is not shift-invariant in time-delay and doppler. In order to calculate c_{ip} for the p^{th} path, the reference *demodulate* surface is shifted to the point (T_p, e^{β_p}). Let

$$D_{r,b,p}(\tau,\alpha) \;\triangleq\; \frac{1}{a_r} e^{-j2\pi f_o(T_p-T_r} D_b(t+T_r-T_p, e^{\alpha+\beta_r-\beta_p} \mid T_r, e^{\beta_r}, a_r) \qquad (4.72)$$

represent the shifted version of the reference demoduate surface for the p^{th} path. Additionally, for each path p, let

$$z_{r,i,p}(t) \;\triangleq\; D_{r,b,p}(\tau,\alpha) \mid_{e^{\alpha}=e^{\beta_i}} \qquad for\ 1 \le i \le M;\ \ i \ne p \qquad (4.73)$$

represent the demodulate response of the β_i^{th} doppler channel. Then the coefficient c_{ip} is determined from the output of the cyclic crosscorrelation between $z_{r,i,p}(t)$ and $m(t)$ and is given by

$$c_{ip} \;=\; z_{r,i,p}(t) \otimes m(t) \mid_{t=T_i} \;. \qquad (4.74)$$

Equations (4.72) $\longrightarrow$ (4.74) is repeated for each and every strong path until all coefficients are obtained. Although amplitude estimation under block processing requires the additional complexity of crosscorrelations, it does avoid the necessity for interpolations.

4.5.1 Amplitude Approximation With M-Sequence Ambiguity Surface

In section 4.5, the coefficients c_{ip} are required for the calculation of the complex amplitudes a_p. However, if the coefficient matrix $\boldsymbol{C}$ in (4.68) were the identity matrix I, the reduction in computations may be substantial. For ambiguity surfaces with very low floor level, approximating the off-diagonal elements of $\boldsymbol{C}$ with zeros may be suitable. Consider the case of m-sequence transmission. The ambiguity surface is shaped like a thumbtack. It consists of a spike at the center and a plateau region surrounding the spike. The magnitude of the off-diagonal elements in $\boldsymbol{C}$ depends on the variations in this plateau region. To a good approximation, this plateau region may be assumed to have uniform distribution of energy. Specifically, it is assumed that each doppler channel has equal energy, and that this energy is evenly distributed within the doppler channel on the time-delay axis. The equal energy assumption for each doppler channel is based on the narrowband argument that for small differences in doppler

$$\begin{aligned} \int_0^{P_T} \mid A(t,F) \mid^2 dt &= \int_{-\infty}^{\infty} \mid M(f) \mid^2 \mid M(f-F) \mid^2 df \\ &\approx \int_{-\infty}^{\infty} \mid M(f) \mid^4, \end{aligned} \tag{4.75}$$

where

$$F = e^{\alpha-\alpha_o} f_o \, . \tag{4.76}$$

For m-sequence signals with L digits, the off-diagonal coefficients are 10 $log(L)$ dB below the peak of the ambiguity surface. Hence, if L is 1023 digits, the off-diagonal coefficients are 30 dB down from this peak. Recall that the purpose for calculating these coefficients is to eliminate the contribution of the strong paths at the peaks of the weak path. Ideally, if the strong paths are completely eliminated, the peak-to-floor level of the weak path would be infinite. However, when the off-diagonal coefficient of $\boldsymbol{C}$ are assumed to be zero this is no longer true. To evaluate the significance of the off-diagonal coefficients, define an error vector by

$$\boldsymbol{\varepsilon} \triangleq \tilde{\boldsymbol{C}}\,\tilde{\boldsymbol{A}}\,, \tag{4.77}$$

where

$$\tilde{\boldsymbol{C}} = \begin{bmatrix} 0 & \frac{1}{L} & \cdots & \frac{1}{L} \\ \frac{1}{L} & 0 & \cdots & \frac{1}{L} \\ \vdots & & \ddots & \vdots \\ \frac{1}{L} & \cdots & \cdots & 0 \end{bmatrix}. \tag{4.78}$$

is the matrix of the squares of the off-diagonal coefficients of $\boldsymbol{C}$ and

$$\tilde{\boldsymbol{A}} = [A_1^2, A_2^2, ..., A_M^2]^T \tag{4.79}$$

is the vector of the squares of the true amplitudes. Therefore, the error vector

$$\boldsymbol{\varepsilon} = [\varepsilon_1, \varepsilon_2, ..., \varepsilon_M]^T \tag{4.80}$$

represents the energy of the interference among the peaks of the strong paths. Each ε_p generates its own floor level which affects the detectability of the peaks of the weak path. The floor level due to ε_p is

$$\begin{aligned} F_p^2 &= \frac{1}{L}\varepsilon_p \\ &= \frac{1}{L^2}\sum_{\substack{i=1 \\ i\neq p}}^{M} A_i^2\,. \end{aligned} \tag{4.81}$$

Therefore, the sum of M floor levels due to interference is

$$F_T^2 = \sum_{i=1}^{M} F_i^2 . \tag{4.82}$$

Assuming A_1^2 is the largest among all strong paths,

$$F_T^2 \leq M(M-1)\frac{A_1^2}{L^2} . \tag{4.83}$$

From (4.78) to (4.83) it is assumed that the interference is coherently summed at the signal peaks. A measure of the total interference is the floor-to-signal ratio given by

$$\left(\frac{F_T^2}{A_1^2}\right)_{dB} \leq 10\ log\left(\frac{[M(M-1)]}{L^2}\right) . \tag{4.84}$$

For M=10 (10 strong paths), L=1023, the cost of neglecting the off diagonal terms in (4.68) is the presence of a floor level that is 40 dB down from the peak of the strong signal. Prior to strong path cancellation, the floor level due to the ten paths is 20 dB down from the peak. Therefore, if the peaks of the weak path is approximately 20dB down from the peak of the strong path, approximating $\boldsymbol{C}$ by the identity matrix will not affect the detectability of the weak paths.

4.6 Simulation Results

In this section, simulation results of (SIMSPC) are provided. Except for differences in computational complexities, the results are valid for both the sliding processing receiver and the block processing receiver. To carry out the simulation, a reference surface is created and stored in memory. To test the validity of doppler invariance, receiver ambiguity surfaces with various true dopplers are subtracted from the shifted versions of the reference surface. In other words, the reference ambiguity surface and the receiver ambiguity surface differ only in doppler. Similarly, for time-delay invariance, the receiver ambiguity surfaces with various true time-delays

are subtrated from the time-shifted versions of the reference surface. A detailed discussion of this simulation is provided in appendix D. The primary purpose of this simulation is to show the extent of the floor reduction after surface subtraction. It is not designed to provide a detailed analysis of the ripples in figures (4.3) $\longrightarrow$ (4.8). For example, the simulation for doppler invariance does not show why there are small variations in the performance of surface subtraction for various degrees of surface shifts. It does indicate that greater than 40 dB of improvement in floor reduction can be expected. Since it is assumed that the noise floor is much lower than the signal floor, the simulation consists of signal only and provides a set of examples for signal floor reduction. In order to analyze the performance of the different cancellation schemes, two different performance criteria are considered. The mean-square error criterion (m.s.e.) is a simple yet effective performance indicator utilized in many situations. The median criterion has the advantage that it is insensitive to outliers in the ambiguity surface. Therefore, the median is a useful criterion in cases where the ambiguity surface contains large narrow peak(s). In order to reduce the effect of outliers, the large peak(s) in the m-sequence ambiguity function is left out in the calculation for the (m.s.e.).

Figures (4.3) and (4.4) plot the results of strong signal cancellation for the case when the reference ambiguity surface and the strong signal ambiguity surface differ in doppler. The figures show improvement with increasing sampling rate. This is due to the effect of linear interpolation when a single processor is utilized. Similarly, for the case of strong signal cancellation in the direction of time-delay, figures (4.5) to (4.8) also indicate an improvement with increasing sampling rate. In both cases, the improvement is greater than 30dB. Figures (4.7) and (4.8) compares the cancellation of the ambiguity surface between transducer filtered reception and non-filtered

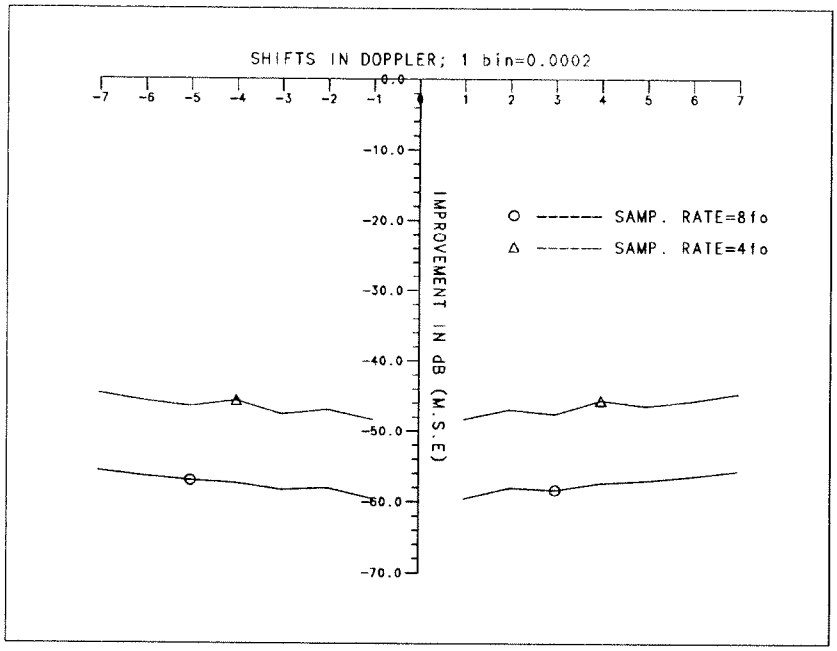

Figure 4.3: Floor level reduction after cancellation with different sampling rates. Shifts in doppler. (m.s.e. criterion)

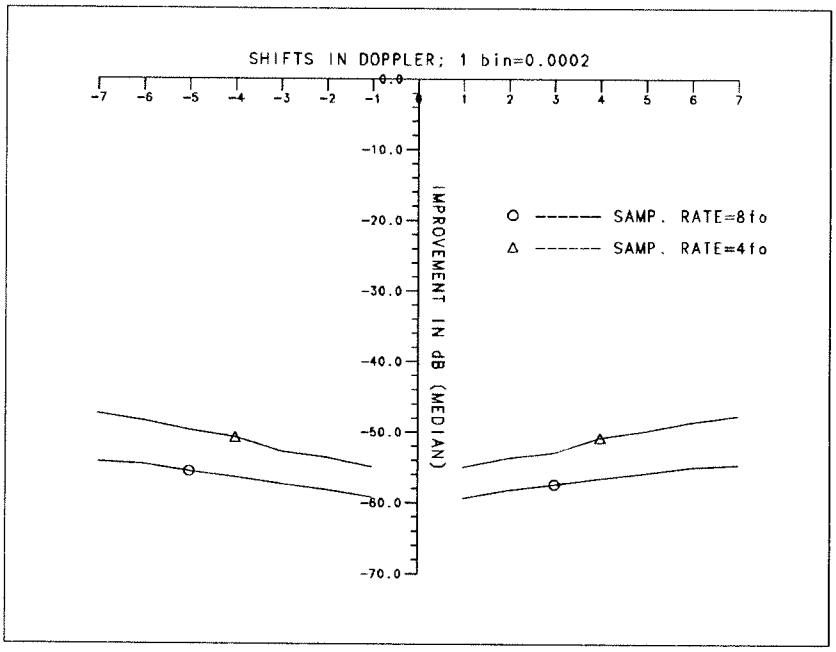

Figure 4.4: Floor level reduction after cancellation with different sampling rates. Shifts in doppler. (median criterion)

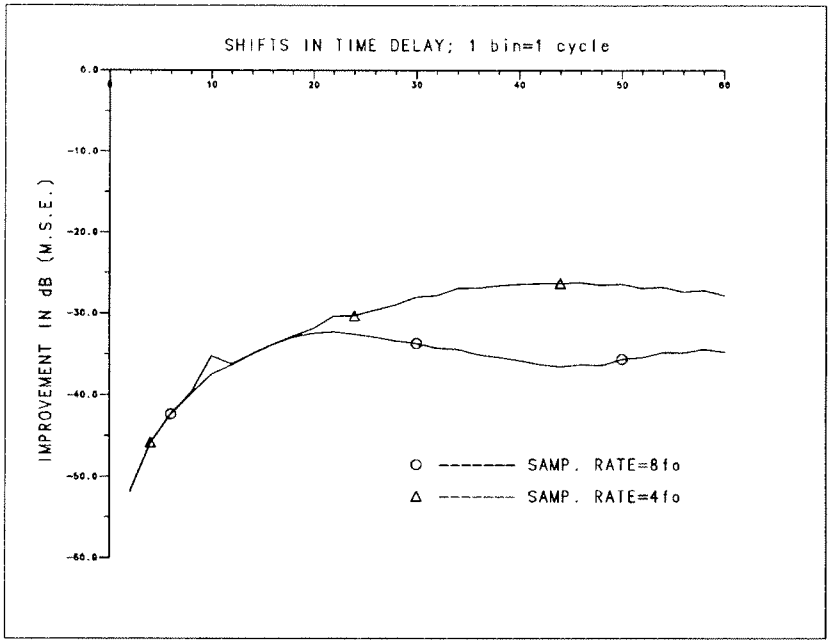

Figure 4.5: Floor level reduction after cancellation with different sampling rates. Shifts in time-delay. (m.s.e. criterion)

reception. It is interesting to note that the performance criteria does influence the outcome of this comparison.

4.7 Constructing the Reference Ambiguity Surface

Unlike the receiver ambiguity surface, the reference ambiguity surface must consists of only one path. At first, it may seem that the reference ambiguity surface may be constructed by calculating the ambiguity function in (3.28) for the transmitted signal. The problem with this form of construction is that the ambiguity function in (3.28) does not include the effect of filtering (i.e. transducer filtering, demodulate filtering, etc.) Therefore, the reference ambiguity surface must be constructed from a *single-path* reception. Ideally, the single-path reception would undergo the same filtering processes as the multipath reception. In most cases a single-path reception may be obtained by positioning the transducer and the receiver in close proximity.

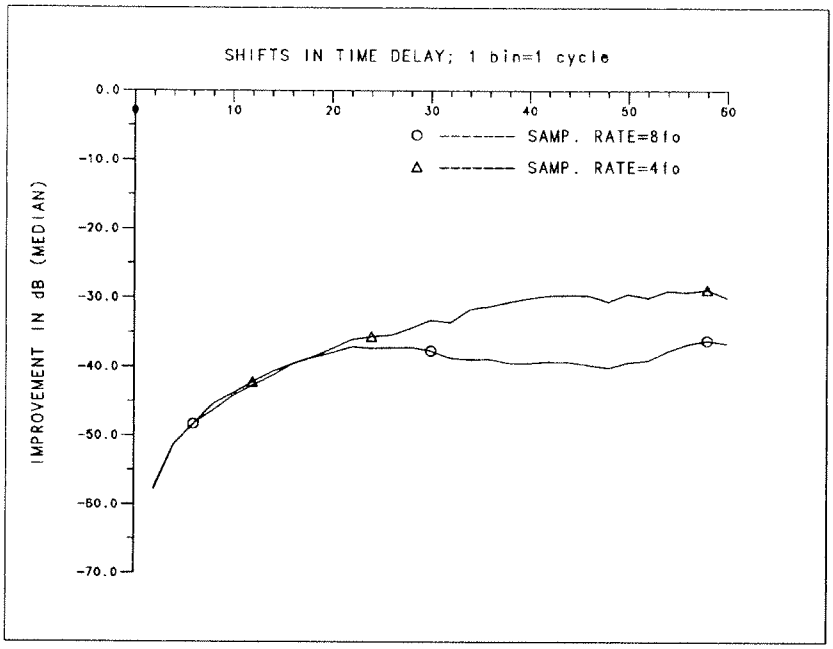

Figure 4.6: Floor level reduction after cancellation with different sampling rates. Shifts in time-delay. (median criterion)

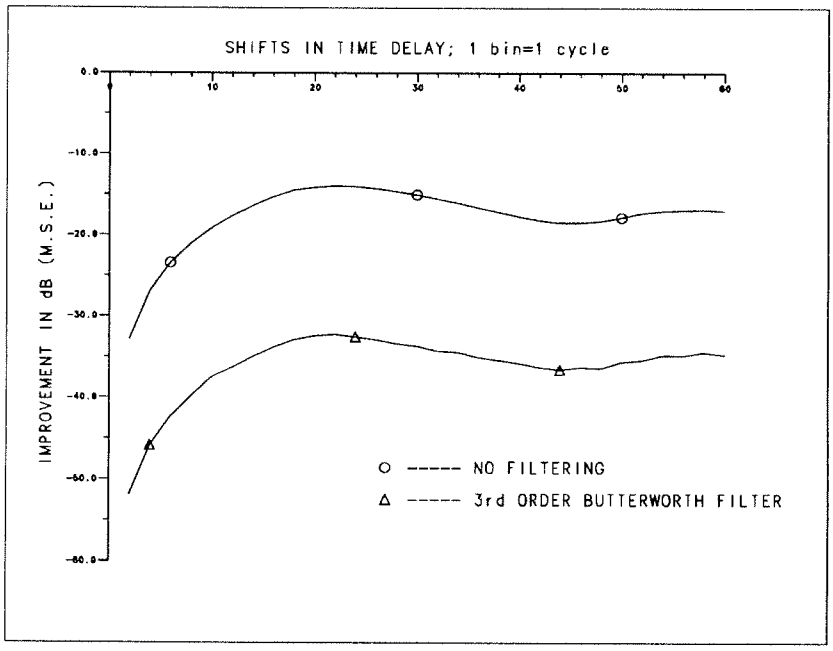

Figure 4.7: Floor level reduction after cancellation with different sampling rates. Filtering vs. no filtering. (m.s.e. criterion; sampling rate=8fo)

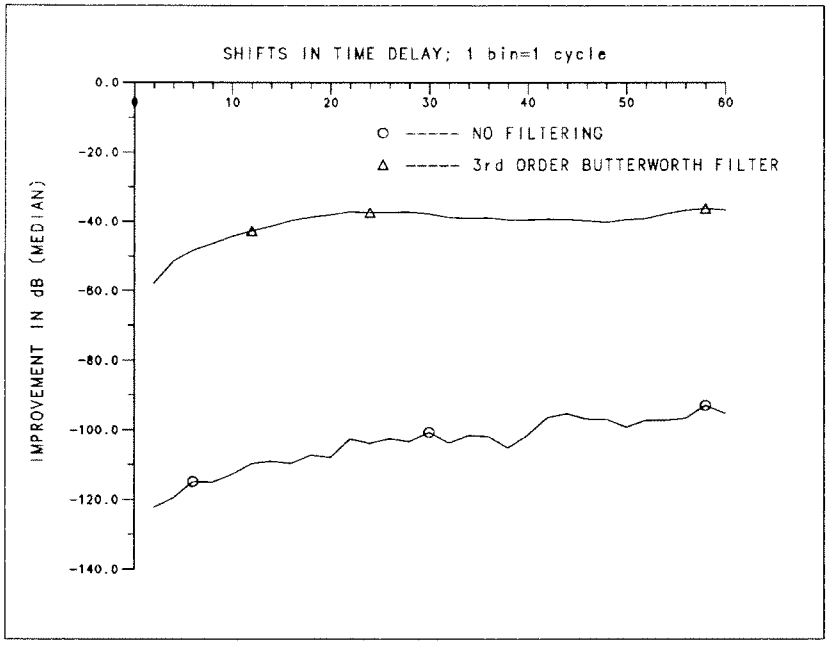

Figure 4.8: Floor level reduction after cancellation with different sampling rates. Filtering vs. no filtering. (m.s.e. criterion; sampling rate=8fo)

Alternatively, the reference ambiguity surface may be constructed using the receiver ambiguity surface for signals with good autocorrelation function. In principle, this method of construction is similar to the strong signal cancellation to be described in chapter V. Due to their similarity, detailed analysis of this construction is appended to the end of chapter V.

Signals with good autocorrelation function have the property that the main lobe of the autocorrelation is narrow, and the sidelobes are negligible. For this type of signal, the peaks of the strong paths are well isolated from one another in the receiver ambiguity surface. Therefore, it is possible to extract the p^{th} path from the receiver ambiguity surface by zeroing the output of the crosscorrelation at the p^{th} doppler channel except for the position of the p^{th} peak. The purpose for zeroing the p^{th} doppler channel is to eliminate the contribution from all other paths within the reception. Since all the energy of the p^{th} path is concentrated at the p^{th} peak, the

zeros would not significantly affect the p^{th} path. To create the reference surface, the "cleansed" version of the p^{th} doppler channel is crosscorrelated with $m^*(t)$ to form the modified demodulated output. This modified demodulated output is interpolated to all doppler channels to form the reference demodulate surface. For sliding processing, the reference demodulate surface may be crosscorrelated with $m(t)$ to form the reference ambiguity surface.

CHAPTER V

Hyperslice Cancellation by Coordinate Zeroing (HCCO)

The HCCO preprocessing is a simple yet effective means for eliminating the floor level associated with the strong paths (i.e. the strong paths) without significantly affecting the reception from the weak paths. The simplicity of the HCCO preprocessing stems from the fact that only a single doppler channel is required to perform the floor reduction as opposed to the previous technique which involved the subtraction of the entire ambiguity surface. Furthermore, HCCO preprocessing does not require the shift-invariant properties described in chapter IV. It does increase the number of computations at reduced complexity as compared to (SIMSPC).

The basic idea behind HCCO preprocessing is quite simple. Consider a hypothetical situation where one has two sources of light impinging on a distant surface. The light sources are red and blue. Suppose only the contribution from the red light source is desired. A straight forward method would be to construct a filter (i.e. a red filter) at the location of the surface to eliminate the contribution from the blue light source. More advanced filters may require knowledge of both the magnitude and phase of the blue light at the surface. A better approach to blue light cancellation would be to block off the blue light at its source so that it does not spread to the

entire surface; hence no filtering is required at the surface. This is the basic idea behind HCCO preprocessing. The two light sources are the weak and strong paths. The ambiguity surface is analogous to the spread of the light sources onto the distant surface. One does not need to eliminate the strong path from the entire ambiguity surface. Instead, the strong path may be canceled at a single doppler channel (i.e. the source) before the strong path is interpolated to all the doppler channels of the entire ambiguity surface. For signals with good autocorrelations (i.e. radar/sonar signals), the strong path and the weak path are "well" isolated at the true doppler of the strong path. This enables one to eliminate the strong path without disturbing the weak path (i.e. the red light and the blue light are isolated from each other at the source).

In section (5.1) HCCO preprocessing is described using the ideal, analytic model for reception. Section 5.1.1 describes the extent of floor reduction and the corruption of weak paths. The special case of HCCO preprocessing utilizing m-sequence signaling is described in section (5.2). Under this special case, the number of components zeroed is directly proportional to the extent of floor reduction and weak path corruption may be approximated quantitatively.

5.1 Strong Signal Cancellation Through HCCO Preprocessing

One of keys to HCCO preprocessing is the projection of the demdoulated sequence in the data space onto the arrival space and the projection of the processed sequence in the arrival space back to the data space. Both the forward projection and the back projection may be thought of as matrix transformations from one space to the other.

The data space is the space occupied by the demodulated sequence of the reception at a particular doppler channel. The number of coordinates N in the data space will depend on the sampling rate of the receiver. For pulse compressed signals, the data space is characterized by an even distribution of path energy among all the coordinates. As a result, the time-delay of a path reception cannot be estimated from the sequence in the data space. Figure 5.1 is a plot of the m-sequence signal in the data space.

In contrast, the arrival space is the space occupied by the pulse-compressed form of the path reception. Specifically, the energy of the strong path is concentrated within very few coordinates in the arrival space. The word Hyperslice in HCCO refers to the "slice" or subspace spanned by these few coordinates. The HCCO is used to describe the cancellation of the energy within these few coordinates in the arrival space by zeroing. The process of zeroing affects the arrival space only within these few coordinates where the energy of the strong path is concentrated; hence, the rest of the coordinates in the arrival space remains undistorted. However, when the zeroed sequence in the arrival space in projected back to the data space, the zeroing affects the values of all the coordinates in the data space. In figure 5.2, the arrival space of the m-sequence signal is plotted. Due to pulse-compression (i.e. the projection from the data space to the arrival space), the energy of the m-sequence signal is concentrated in very few coordinates indicated by T_s in figure 5.2. The two other small pulses in figure 5.2 are multipaths from bottom bounces. The number of coordinates occupied by T_s (i.e. the Hyperslice) will vary depending on the impulse response of the strong path.

HCCO preprocessing may be divided into four major steps. The first step is to rescale and demodulate the reception according to the true doppler of the strong

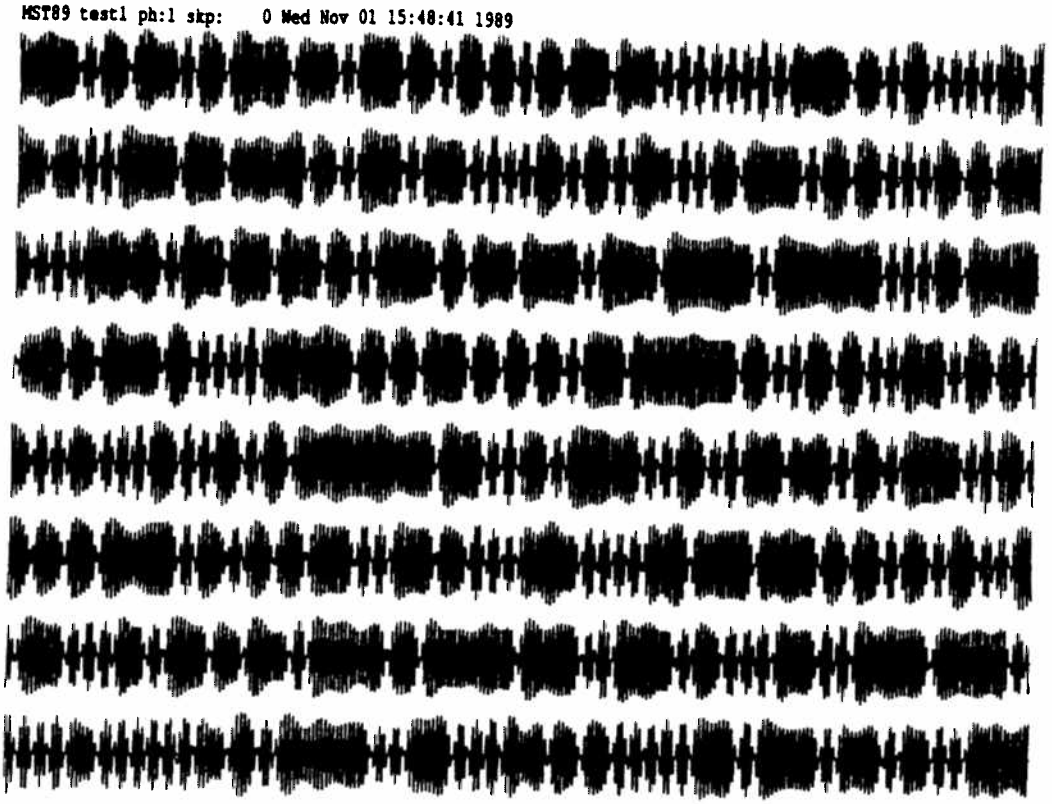

Figure 5.1: The demodulated sequence of the m-sequence signal in the data space. The energy of the m-sequence signal is spread evenly among all data space coordinates. The 8 lines are meant to be read as a single line (i.e. the beginning of the second line continues from the end of the first line and so on). A total of 512 digits of the 511-digit m-sequence are plotted (the first digit of line one is repeated in the last digit of line eight).

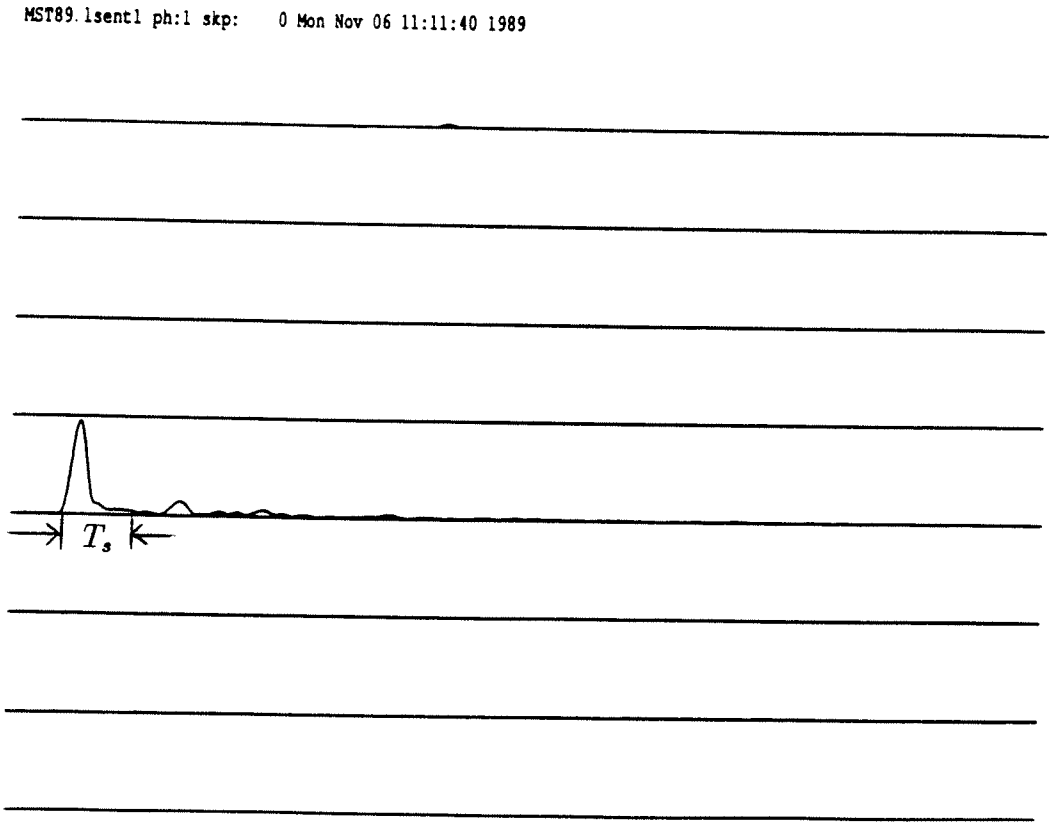

Figure 5.2: The pulse-compressed m-sequence signal in the arrival space. The energy of the pulse compressed m-sequence signal is concentrated in very few coordinates in the arrival space. T_s indicates the number of coordinates occupied by the strong path. The 8 lines are meant to be read as a single line (i.e. the beginning of the second line continues from the end of the first line and so on).

paths[1]. The second step is to project the rescaled, demodulate samples from the data space to the arrival space (forward projection). This is accomplished by cross-correlating the rescaled, demodulated reception with a replica of the transmission. The third step is to replace the major peaks in the arrival space by zeros in order to eliminate the strong paths. Unfortunately, this will also eliminate parts of the weak paths as well. Finally, the "cleansed" response from the arrival space is projected back to the data space (inverse projection). This is accomplished by correlating the "cleansed" response with the *conjugate* of the transmitted signal. Further processing will be required to detect the presence of weak paths. This involves the standard process of interpolation and crosscorrelation utilizing the modified, demodulated sequence in the data space. To analyze HCCO preprocessing in further detail, consider the simple case of a two-path reception given by[2]

$$\begin{aligned} r(t) &= r_s(t) + r_w(t) \\ &= a_s(t)(1-\beta'_s)s((1-\beta'_s)t - S_s) \\ &\qquad \cdot e^{j2\pi f_o[(1-\beta'_s)t - S_s]} \\ &\qquad + a_w(t)(1-\beta'_w)s((1-\beta'_w)t - S_w) \\ &\qquad \cdot e^{j2\pi f_o[(1-\beta'_w)t - S_w]}, \end{aligned} \tag{5.1}$$

where the subscript s and w denote the parameters of the strong path and the weak path respectively. S and β' are the constant delays and doppler factor defined in (3.31) and (3.30), respecitvely. The relative strength of the strong path and the weak path is determined by $a_s(t)$ and $a_w(t)$. Complex demodulating the two-path

[1]The true doppler is assumed to be known prior to preprocessing. The true doppler of the strong paths may be obtained from the ambiguity surface without the preprocessing, or in the case of a fixed-fixed bistatic sonar the true doppler would be zero-doppler. It is assumed that the strong paths all have the same doppler. The search for the true doppler of strong paths under relative motion of the transducer and the receiver is discussed in section (5.2.7).

[2]The exponential form of the doppler variable is purposely left out to emphasize the fact that shift-invariance is not required with HCCO preprocessing.

reception at zero doppler gives

$$\begin{aligned} z(t) &= r(t)e^{-j2\pi f_o t} \\ &= z_s(t) + z_w(t) . \end{aligned} \tag{5.2}$$

Instead of trying to eliminate the floor level of the strong path from the 2-D ambiguity surface, HCCO preprocessing eliminates the strong signal at a single doppler channel prior to the calculation of the ambiguity surface. This method of strong signal cancellation is best described using periodic, pulse compressed signals [40], [33].

Pulse compressed signals are long, modulated pulses that have most of the benefits of a short pulse while keeping within the practical constraints of the peak-power limitation of transducers. At the true doppler of a path reception, the crosscorrelation compresses the long pulse to a duration of 1/B, where B is the bandwidth of the modulated pulse. For the two-path reception above, $z_s(t)$ and $z_w(t)$ cannot be both compressed at the output of a single doppler channel due to their differences in doppler.

The basic principle behind HCCO preprocessing is to compress the reception of the strong signal into a short pulse while leaving the weak path uncompressed. The compressed pulse will be "well isolated" from the weak path; hence, the strong path can be easily separated from the weak path. Specifically, the demodulated reception is interpolated to the true doppler of the strong signal with $\alpha' = \beta'_s$ such that [3]

$$z_{\alpha'_s}(t) = z_{s,\alpha'_s}(t) + z_{w,\alpha'_s}(t) , \tag{5.3}$$

where

$$z_{s,\alpha'_s}(t) = a_s(t)s(t - S_s) , \tag{5.4}$$

[3]The true doppler of the strong path can be easily obtained by calculating the frequency shift in the carrier if the transmission uses an exalted carrier.

is simply a scaled and time-shifted version of the baseband signal in the tranmission and

$$\begin{aligned} z_{w,\alpha'_s}(t) &= a_w(t)\left(\frac{1-\beta'_w}{1-\alpha'}\right) s\left(\frac{1-\beta'_w}{1-\alpha'}t - S_w\right) \cdot \\ &\quad exp\left\{j2\pi f_o\left[\left(\frac{1-\beta'_w}{1-\alpha'} - 1\right)t - S_w\right]\right\} \end{aligned} \tag{5.5}$$

is a scaled, time-shifted and doppler-scaled version of the baseband signal. The next step is to project the rescaled, demodulated response in the data space to the arrival space. The output of this forward projection is given by

$$\begin{aligned} y_{\alpha'}(\tau) &= \int z_{\alpha'}(t)m^*(t-\tau)dt \\ &= y_{\alpha',s}(\tau) + y_{\alpha',w}(\tau)\ , \end{aligned} \tag{5.6}$$

where

$$y_{\alpha',s}(\tau) = a_s(t)\int_{T_P} s(t-T)s^*(t-\tau)dt \tag{5.7}$$

is the pulse compressed output of the strong path, and

$$y_{\alpha',w}(\tau) = \int_{T_P} z_{w,\beta'_s}(t)s^*(t-\tau)dt \tag{5.8}$$

is the doppler-mismatched output of the weak path. The energy of the strong path is concentrated within a very short duration whereas the energy of the weak path represented by $\mid y_{\alpha',w}(\tau) \mid^2$ is spread evenly over the entire period T_P. At this stage of the HCCO preprocessing, the strong path is "well isolated" from the weak path.

The next crucial step in the HCCO preprocessing is to replace the peak pulse and its impulse response of the strong path in $y_\alpha(\tau)$ with zeros. Since the zeros are placed within a very short time interval, the weak path is not affected significantly. However, the strong signal is mostly, if not totally, eliminated by this zeroing. Although the strong path has been identified and largely eliminated due to pulse compression,

the *uncompressed* weak path remains undetected. Therefore, the remaining task of the HCCO preprocessing is to detect the presence of the weak path by generating a broadband ambiguity surface from this "cleansed" output.

Let $\tilde{y}_{\alpha',w}(\tau)$ represent the modified form of $y_{\alpha',w}(\tau)$. In addition, let $S(f)$ and $\tilde{Y}_{\alpha',w}(f)$ represent the Fourier Transform of $s(t)$ and $\tilde{y}_{\alpha',w}(\tau)$ respectively. The next step in the preprocessing is to project the "cleansed" output back to the data space which may be implemented in the frequency domain by inverse filtering

$$\tilde{Z}_{\alpha'}(f) = \frac{\tilde{Y}_{\alpha',w}(f)}{S^*(f)} . \tag{5.9}$$

Let $\tilde{z}_{\alpha'}(t)$ be the inverse Fourier Transform of $\tilde{Z}_{\alpha'}(f)$. Then, $\tilde{z}_{\alpha'}(t)$ represents the modified, demodulated reception at the α^{th} doppler channel. With the strong path removed, $\tilde{z}_{\alpha'}(t)$ is interpolated to all doppler channels of interest using (3.26) and (3.27) with $z(t)$ replaced by $\tilde{z}_{\alpha'}(t)$. This is followed by calculating the crosscorrelation in (3.28) for each doppler channel to form the modified, broadband ambiguity surface $A_{hcco}(\tau, \alpha')$ where the weak path can now be detected.

Figure 5.3 summarizes the major steps for HCCO preprocessing.

5.1.1 Floor Reduction and Weak Path Corruption

In this section, a qualitative analysis of signal floor reduction will be discussed. In order to simplify notations, the exponential doppler factor discussed in chapter IV will be utilized. Futhermore, whenever a tilde (~) is used above a variable, it will denote the response after HCCO preprocessing.

In the analysis to follow, it is assumed that the reception consists of only a single strong path (i.e. $r(t) = r_s(t)$). Let α_i be the true doppler of this path. Then the response at the arrival space of this reception is denoted by $y_{\alpha_i}(t)$. Under HCCO

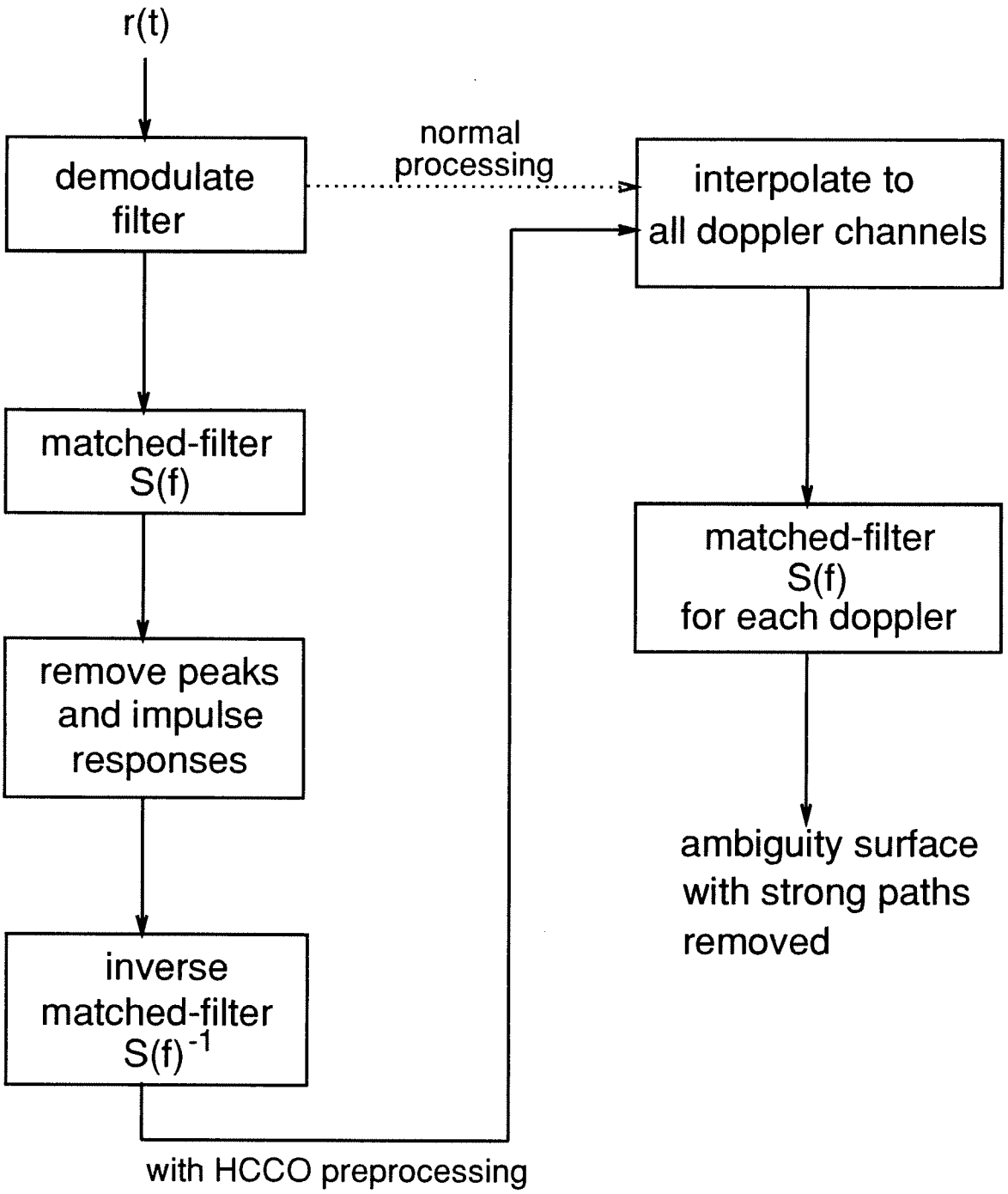

Figure 5.3: Block diagram of HCCO preprocessing. With the strong path removed, the residual ambiguity surface may be utilized for weak path detection.

preprocessing, this output is "cleansed" of its peaks in order to remove the strong signal. Let

$$\tilde{y}_{\alpha_i}(t) \;=\; y_{\alpha_i}(t) - y'_{\alpha_i}(t) \tag{5.10}$$

represent this "cleansed" output, where $y'_{\alpha_i}(t)$ is the component of the output that is zeroed. To analyze the extent of the floor reduction after the zeroing, the outputs at all doppler channels must be analyzed. Let $\tilde{y}_{\alpha_j}(t)$ be the output at the α_j^{th} doppler channel after HCCO preprocessing. In other words, $\tilde{y}_{\alpha_j}(t)$ represents the "residue" or floor level at the α_j^{th} doppler channel after HCCO preprocessing. In particular, $\tilde{y}_{\alpha_j}(t)$ will be a function of the "cleansed" output $\tilde{y}_{\alpha_i}(t)$. The objective, therefore, is to establish the functional relationship between $\tilde{y}_{\alpha_j}(t)$ and $\tilde{y}_{\alpha_i}(t)$ for all $j \neq i$.

In order to evaluate the relationship between $\tilde{y}_{\alpha_j}(t)$ and $\tilde{y}_{\alpha_i}(t)$, the general form for interpolating from one doppler channel to another is provided. First let $z_{\alpha_i}(t)$ be the demodulated response of the α_i^{th} doppler channel. To interpolate from $\alpha_i th$ doppler channel to α_j^{th} doppler channel, the phase-adjusted response is

$$z'_{\alpha_i,\alpha_j}(t) \;=\; z_{\alpha_i}(t)e^{j2\pi f_o(e^{\alpha_i}-e^{\alpha_j})t}\;, \tag{5.11}$$

where the subscript α_i, α_j in $z'_{\alpha_i,\alpha_j}(t)$ means the interpolation is from the α_i^{th} doppler channel to the α_j^{th} doppler channel. Time scaling $z'_{\alpha_i,\alpha_j}(t)$, the demodulated response at the α_j^{th} doppler channel is

$$z_{\alpha_j}(t) \;=\; z'_{\alpha_i,\alpha_j}(e^{\alpha_j-\alpha_i}t)\;. \tag{5.12}$$

The relationship between $\tilde{y}_{\alpha_j}(t)$ and $\tilde{y}_{\alpha_i}(t)$ is more easily obtained in the frequency domain. Let $\tilde{Y}_{\alpha_j}(f)$ and $\tilde{Y}_{\alpha_i}(f)$ denote the Fourier Transforms of $\tilde{y}_{\alpha_j}(t)$ and $\tilde{y}_{\alpha_i}(t)$, respectively. Then the output at the α_j^{th} doppler channel after HCCO preprocessing is

$$\tilde{Y}_{\alpha_j}(f) \;=\; S^*(f)\tilde{Z}_{\alpha_j}(f)\;, \tag{5.13}$$

where $\tilde{Z}_{\alpha_j}(f)$ is the spectrum of the "cleansed" demodulated response $\tilde{z}_{\alpha_j}(t)$. From (5.11) and (5.12), the demoulated response at the α_j^{th} doppler channel may be written as

$$\begin{aligned} \tilde{z}_{\alpha_j}(t) &= \tilde{z}_{\alpha_i}(e^{\alpha_j-\alpha_i}t)e^{j2\pi f_o(e^{\alpha_i}-e^{\alpha_j})t} \\ &= \tilde{z}_{\alpha_i}(e^{\alpha_j-\alpha_i}t)e^{j2\pi F_{ij}t} , \end{aligned} \tag{5.14}$$

where

$$F_{ij} \triangleq f_o(e^{\alpha_i} - e^{\alpha_j}) . \tag{5.15}$$

Using the time-scale and phase shift properties of the Fourier Transform, the "cleansed" demodulated response at the α_j^{th} doppler channel is

$$\tilde{Z}_{\alpha_j}(f) = e^{\alpha_i-\alpha_j}\tilde{Z}_{\alpha_i}(e^{\alpha_i-\alpha_j}(f - F_{ij})) . \tag{5.16}$$

From the inverse filtering in (5.9), the "cleansed" demodulated response at the α_i^{th} doppler channel is given by

$$\tilde{Z}_{\alpha_i}(f) = \frac{\tilde{Y}_{\alpha_i}(f)}{S^*(f)}; \tag{5.17}$$

hence, the output in (5.13) becomes

$$\tilde{Y}_{\alpha_j}(f) = S^*(f)\left[e^{\alpha_i-\alpha_j}\frac{\tilde{Y}_{\alpha_i}(e^{\alpha_i-\alpha_j}(f - F_{ij}))}{S^*(e^{\alpha_i-\alpha_j}(f - F_{ij}))}\right] \tag{5.18}$$

$$= S^*(f)\left[Z_{\alpha_j}(f) - e^{\alpha_i-\alpha_j}\frac{Y'_{\alpha_i}(e^{\alpha_i-\alpha_j}(f - F_{ij}))}{S^*(e^{\alpha_i-\alpha_j}(f - F_{ij}))}\right] \tag{5.19}$$

$$= Y_{\alpha_j}(f) - Y'_{\alpha_j}(f) \tag{5.20}$$

where $\tilde{Y}'_{\alpha_i}(f)$ is the transform of $y'_{\alpha_i}(t)$ in (5.10), and

$$Y'_{\alpha_j}(f) = S^*(f)\left[e^{\alpha_i-\alpha_j}\frac{Y'_{\alpha_i}(e^{\alpha_i-\alpha_j}(f - F_{ij}))}{S^*(e^{\alpha_i-\alpha_j}(f - F_{ij}))}\right] \tag{5.21}$$

is the component utilized to cancel the floor level at the α_j^{th} doppler channel.

Ideally, if the HCCO preprocessing is successful at eliminating all the contributions from the strong signal at the α_i^{th} doppler channel, then $Y_{\alpha_j}(f) = Y'_{\alpha_j}(f)$ for all $\alpha'_j s$ and the entire floor level of the ambiguity surface would be eliminated. In practice, it may not always be possible to eliminate all the sidelobes associated with the transducer response of the peak pulse during the process of zeroing. Under this circumstance the inverse filtering in (5.9) may magnify the remaining sidelobes to the point where the floor level is actually higher than it is before the HCCO preprocessing.

The degree of floor reduction may be measured by the amount of energy remained in each doppler channel. From Parseval's theorem

$$\int \mid \tilde{y}_{\alpha_j}(t) \mid^2 dt = \int \mid \tilde{Y}_{\alpha_j}(f) \mid^2 df; \tag{5.22}$$

therefore, using the relationship in (5.18), the total energy in the α_j^{th} doppler channel is

$$\int \mid \tilde{Y}_{\alpha_j}(f) \mid^2 df = e^{2(\alpha_i - \alpha_j)} \int \mid \frac{S^*(f)}{S^*((e^{\alpha_i - \alpha_j}(f - F_{ij}))} \tilde{Y}_{\alpha_i}(e^{\alpha_i - \alpha_j}(f - F_{ij})) \mid^2 df \ . \tag{5.23}$$

Applying Schwarz's Inequality [20] to the energy in (5.23),

$$\begin{aligned} \int \mid \tilde{Y}_{\alpha_j}(f) \mid^2 df &\leq e^{2(\alpha_i - \alpha_j)} \int \mid \frac{S^*(f)}{S^*((e^{\alpha_i - \alpha_j}(f - F_{ij}))} \mid^2 df \int \mid \tilde{Y}_{\alpha_i}(e^{\alpha_i - \alpha_j}(f - F_{ij})) \mid^2 df \\ &= C_{ij}(f) \int \mid \tilde{Y}_{\alpha_i}(e^{\alpha_i - \alpha_j}(f - F_{ij})) \mid^2 df \ , \end{aligned} \tag{5.24}$$

where the inter-channel energy coefficient is given by

$$C_{ij}(f) = e^{2(\alpha_i - \alpha_j)} \int \mid \frac{S^*(f)}{S^*((e^{\alpha_i - \alpha_j}(f - F_{ij}))} \mid^2 df \ . \tag{5.25}$$

Due to $C_{ij}(f)$ in (5.24), the amount of energy removed in the α_i^{th} doppler channel is not necessarily equal to the amount of energy removed in the α_j^{th} doppler channel.

Therefore, the extent of floor reduction through HCCO preprocessing will depend on both the autocorrelation of the signal and its inter-channel energy coefficient $C_{ij}(f)$.

In general, when the reception consists of both strong and weak paths, the zeroing implemented during HCCO preprocessing may affect the detectability of the weak signal. This results in an inherent tradeoff between the degree of floor reduction of the strong signal and the degree of weak signal corruption. Due to the linearity in the processing, the degree of weak signal corruption may be analyzed separately from the degree of floor reduction of the strong signal. To analyze the effect of the zeroing on weak paths, the above analysis for floor reduction is repeated with the exception that it is assumed the reception consists of a single, *weak* path instead of a single, *strong* path (i.e. $r(t) = r_w(t)$). Again, the degree of weak signal corruption will depend on the floor characteristics of the signal transmitted as well as the inter-channel coefficient.

In the following section, the m-sequence signal described has the advantage that its autocorrelation is "two-valued" and the total energy of each doppler channel is bounded above by a constant. Furthermore, due to the "uniformity" of the its signal floor level, weak signal corruption may be analyzed quantitatively.

5.2 HCCO Preprocessing With M-Sequences

As mentioned in the previous section, the inverse filtering may lead to undesired response within the HCCO preprocessing. In 1986, Birdsall and Metzger [5] described a unique way of m-sequence processing known as the Factor Inverse Filtering (FIF). Due to the special characteristics of FIF, a straightforward m-sequence crosscorrelation may be substituted for the inverse filtering; hence, none of the problems of inverse filtering exist under m-sequence processing. In section 5.2.1, FIF for

m-sequences will be described in further detail. Section 5.2.2 will discuss the floor reduction of strong signal and section 5.2.3 utilizes the properities of the ambiguity surface to better approximate weak signal corruption. Finally, HCCO preprocessing under m-sequence signaling is laid out step-by-step.

5.2.1 Factor Inverse Filtering (FIF)

M-sequence signals are a special class of signals used in pulse compression. An m-sequence signal is a continuous signal, phase modulated by a periodic binary control signal known as an m-sequence [26]. Its two-level autocorrelation function is ideal for separating the strong path from the weak path in a reception. In general, an m-sequence signal may be represented by

$$m[n] \;=\; u + vb_n \qquad n = 0, 1, 2, ..., L-1 \;, \tag{5.26}$$

where b_k take on interger values of +1 or -1, and L is the number of digits in a period of the m-sequence signal. In many publications [51], [26], $u = 0$ and $v = 1$ so that $m[n]$ takes on values of ± 1. The disadvantge of such an assignment is that the autocorrelation function of $m[n]$ has a non-zero off-peak value. In [7], it is shown that when $m[n]$ is expressed as

$$m[n] \;=\; e^{jb_n\theta} \;, \tag{5.27}$$

where $u \;=\; cos(\theta)$ and $v \;=\; jsin(\theta)$, and θ is chosen as the "period-matched angle" (i.e. $\theta = tan^{-1}(\sqrt{L})$) [7], the resultant autocorrelation function will have zero off-peak values.

$$\sum_{i=0}^{L-1} m[i]m^*[i+n] \;=\; 0 \qquad for\ n \;\neq\; 0, \pm L, \pm 2L, ... \tag{5.28}$$

$$\sum_{i=0}^{L-1} m[i]m^*[i+n] \;=\; L \qquad for\ n \;=\; 0, \pm L, \pm 2L, ... \tag{5.29}$$

In other words, each period of the discrete sequence autocorrelation function contains a single peak and zero everywhere else.

The complex form of the m-sequence transmission is

$$s_{mod}(t) = Ae^{j(2\pi f_o t + b_n\theta)} \quad , nT_d < t < (n+1)T_d \ , \tag{5.30}$$

where T_d is the duration of one digit. The single digit spectrum is given in [7] by

$$\begin{aligned} S_n(f) &= AT_d e^{jb_n\theta} e^{j2\pi(f_o-f)(n+0.5)T_d} sinc((f_o-f)T_d) \\ &= (-1)^{f_oT_d} AT_d e^{-j\pi fT_d} e^{-j2\pi fT_d n} sinc((f_o-f)T_d) \ . \end{aligned} \tag{5.31}$$

where f_oT_d is the integer number of cycles in a digit. Since the spectrum of L digits in one period is the sum of the spectra of each of the L digits

$$S_{mod}(f) = \sum_{n=1}^{L} S_n(f) \ , \tag{5.32}$$

the spectrum for a one-period m-sequence transmission is

$$S_{mod}(f) = (-1)^{f_oT_d} AT_d e^{-j\pi fT_d} sinc((f_o-f)T_d) \sum_{n=1}^{L} e^{jb_n\theta} e^{-j2\pi fT_d n} \ . \tag{5.33}$$

The demodulated or downshifted version of this transmission is given by

$$S(f) = (-1)^{f_oT_d} AT_d e^{-j\pi(f+f_o)T_d} sinc(fT_d) \sum_{n=1}^{L} e^{jb_n\theta} e^{-j2\pi fT_d n}. \tag{5.34}$$

It is much easier to think of $S(f)$ as a product of two factors; a pulse factor and a modulation factor.

$$S(f) = P(f)M(f) \tag{5.35}$$

The pulse factor

$$P(f) = (-1)^{f_oT_d} AT_d e^{-j\pi(f+f_o)T_d} sinc(fT_d) \tag{5.36}$$

has most of its energy concentrated around DC. The modulation factor

$$M(f) = \sum_{n=1}^{L} e^{jb_n\theta} e^{-j2\pi fT_d n} \tag{5.37}$$

is the discrete-time Fourier Transform of the complex modulation sequence. Due to the zero off-peak values of the autocorrelation function in (5.28), the discrete Fourier Transform (DFT) of the autocorrelation function $\mid M(k) \mid^2$ will be a constant for all k. In other words, if $M(f)$ in (5.37) is evaluated at the eigenfrequencies (i.e. $f = k/LT_d$) such that

$$M[k] = \sum_{n=1}^{L} e^{jb_n\theta} e^{-j2\pi kn/L} , \tag{5.38}$$

then $\mid M[k] \mid$ will be a constant.

Usually the output of a matched-filtered receiver is given by the product between the demodulated reception $Z[k]$ and the matched-filter $S^*[k] = P^*[k]M^*[k]$. Since $S(f)$ can be factored into two terms, the idea of FIF is to multiply $Z[k]$ by the modulation factor $M^*[k]$ only, so that the output of the receiver is

$$Y[k] = Z[k]M^*[k] \tag{5.39}$$

Since $\mid M[k] \mid$ is a constant, multiplying $Z[k]$ by $M^*[k]$ is the same as dividing $Z[k]$ by $M[k]$ except for a scale factor. Essentially, what FIF does is to divide the spectrum of the demodulated reception by $M[k]$ in order to recover the pulse spectrum $P[k]$. In practice, FIF is implemented in the time domain by crosscorrelating $z[n]$ with $m^*[n]$.

In (5.9), the inverse filtering corresponds to dividing the output $Y[k]$ in (5.39) by $S^*[k]$. However, under FIF, the inverse filtering corresponds to dividing $Y[k]$ by $M^*[k]$. Again, due to the constant magnitude of $M^*[k]$, dividing $Y[k]$ by $M^*[k]$ is the same as multiplying $Y[k]$ by $M[k]$ except for a scale factor. And in the time domain, this corresponds to the crosscorrelation between $y[n]$ and $m[n]$. Therefore, the problems associated with inverse filtering is no longer present under m-sequences with FIF. A block diagram of HCCO preprocessing using m-sequence signaling is

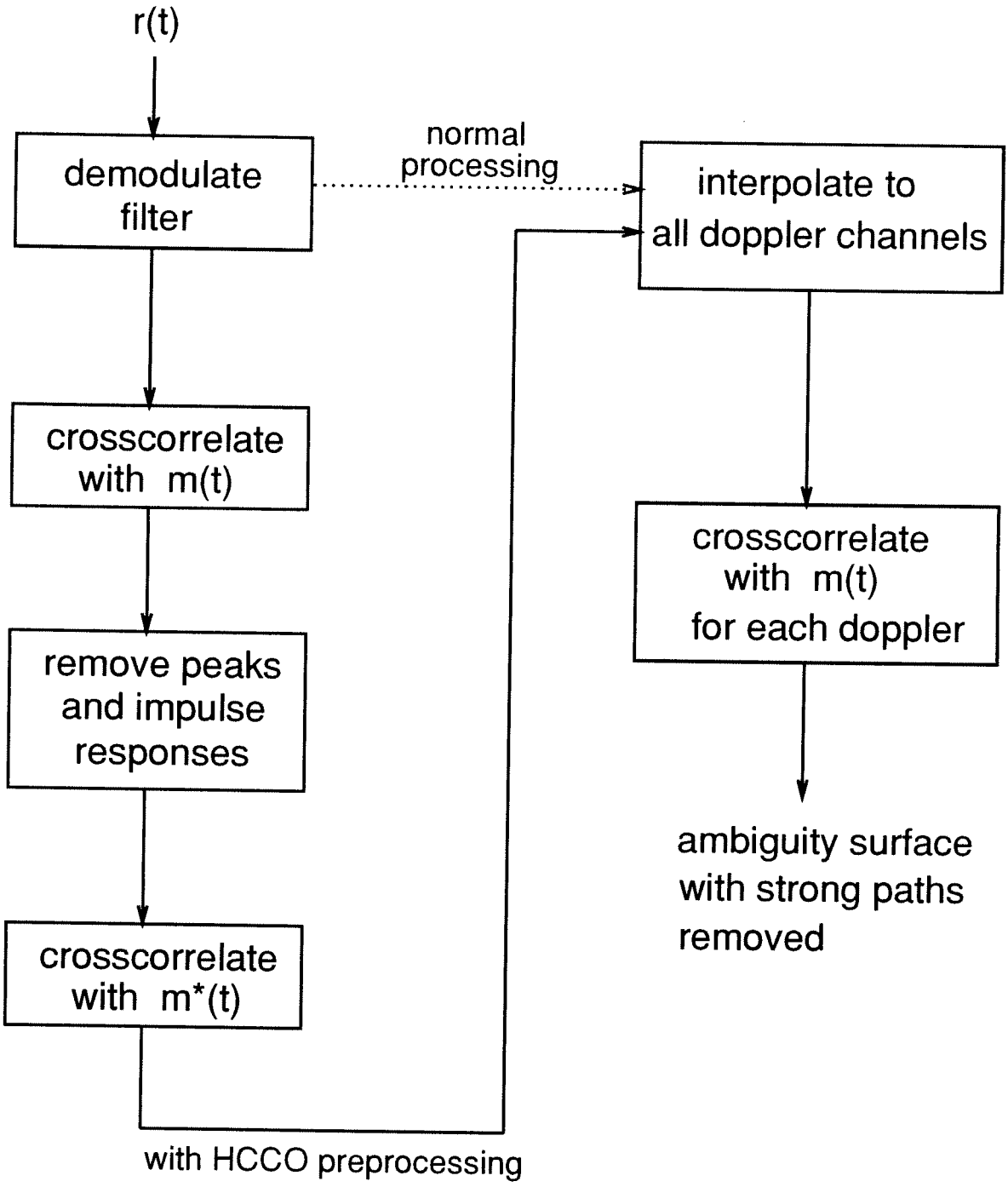

Figure 5.4: HCCO preprocessing with m-sequence signaling. With m-sequences, the inverse filtering in the frequency domain is the same as crosscorrelation with the complex conjugate of $m(t)$ in time except for a scale factor.

provided in figure 5.4.

In the analysis above, it is assumed that the reception is sampled at a rate of one sample per digit. The primary reason for this assumption is that FIF is a crosscorrelation with the m-sequence m[n] (one sample per digit). In section 5.2.7, the general case of multiple samples per digit will be analyzed in detail. Although the sampled reception consists of many samples per digit, the FIF crosscorrelation is still implemented as though the reception were sampled at one sample per digit. In order to perform FIF crosscorrelation at one sample per digit when the sampled reception consists of many samples per digit, the sampled reception is demultiplexed at the input and multiplexed at the output of the FIF crosscorrelation.

5.2.2 Floor Reduction

Narrowband Assumption

To approximate the degree of floor reduction, consider the case of narrowband processing. The narrowband processing with PURTS is similar to the broadband processing with the exception that time-scaling in (5.12) is omitted. In contrast to the frequency analysis of the floor reduction discussed in section 5.1.1, this section will analyze the floor reduction in the time domain. Due to the constant magnitude of $M[k]$, inverse filtering is replaced by the crosscorrelation with the complex conjugate of the sharp signal. This inverse projection onto the data space may be expressed as

$$\tilde{z}_{\alpha_i}[n] \;=\; \tilde{y}_{\alpha_i}[n] \otimes \frac{1}{L} m^*[n] \;, \tag{5.40}$$

where α_i is the doppler channel selected for HCCO preprocessing. Using matrix computations, the cyclic crosscorrelation in (5.40) becomes

$$\tilde{\boldsymbol{z}}_{\alpha_i} \;=\; \frac{1}{L} \boldsymbol{M} \tilde{\boldsymbol{y}}_{\alpha_i} \;, \tag{5.41}$$

where

$$\tilde{\boldsymbol{z}}_{\alpha_i} = [\tilde{z}_{\alpha_i}[0], \tilde{z}_{\alpha_i}[1], ..., \tilde{z}_{\alpha_i}[L-1]]^T \tag{5.42}$$

is one of the vector of the one-sample-per-digit "cleansed" demodulates in the data space,

$$\tilde{\boldsymbol{y}}_{\alpha_i} = [\tilde{y}_{\alpha_i}[0], \tilde{y}_{\alpha_i}[1], ..., \tilde{y}_{\alpha_i}[L-1]]^T \tag{5.43}$$

is the vector of the "cleansed" outputs in the arrival space, and

$$\boldsymbol{M} = \begin{bmatrix} m[0] & m[1] & \cdots & \cdots & m[L-1] \\ m[L-1] & m[0] & \cdots & \cdots & m[L-2] \\ \vdots & & \ddots & & \vdots \\ \vdots & & & \ddots & \vdots \\ m[1] & m[2] & \cdots & \cdots & m[0] \end{bmatrix} . \tag{5.44}$$

is the cyclic matrix of m-sequences (i.e. the inverse projection matrix from the arrival space to the data space) used in the crosscorrelation. The matrix $\boldsymbol{M}$ in (5.44) has the essential property that

$$\frac{1}{L}\boldsymbol{M}^H\boldsymbol{M} = \frac{1}{L}\boldsymbol{M}\boldsymbol{M}^H = I . \tag{5.45}$$

In other words, $\frac{1}{\sqrt{L}}\boldsymbol{M}$ is a unitary matrix. Using the property in (5.45), the total energy in $\tilde{\boldsymbol{z}}_{\alpha_i}$ in (5.41) is

$$\begin{aligned} \tilde{\boldsymbol{z}}_{\alpha_i}^H\tilde{\boldsymbol{z}}_{\alpha_i} &= \frac{1}{L^2}\tilde{\boldsymbol{y}}_{\alpha_i}^H\boldsymbol{M}^H\boldsymbol{M}\tilde{\boldsymbol{y}}_{\alpha_i} \\ &= \frac{1}{L}\tilde{\boldsymbol{y}}_{\alpha_i}^H\tilde{\boldsymbol{y}}_{\alpha_i} . \end{aligned} \tag{5.46}$$

Therefore, the total energy in $\tilde{\boldsymbol{z}}_{\alpha_i}$ is directly proportional to the total energy in $\tilde{\boldsymbol{y}}_{\alpha_i}$.

One way of evaluating the degree of floor reduction is to calculate the total volume of the ambiguity surface associated with the residue. A simple way to calculate this

volume is to consider cross-ambiguity function between $\tilde{z}_{\alpha_i}[n]$ and $m[n]$ given by

$$\chi_{m,z}[n, f_d] = \sum_{l_1=0}^{L-1} \tilde{z}_{\alpha_i}[n] m^*[l_1 - n] e^{jf_d l_1} , \tag{5.47}$$

where

$$f_d = 2\pi(e^{\alpha_j} - e^{\alpha_i}) f_o t_1 , \tag{5.48}$$

and $t_1 = 1/m_r f_o$ is the sampling interval. Using the volume constraint of (2.39), the total volume of this cross-ambiguity surface is

$$\begin{aligned} V_{m,z} &= \int_{-\pi}^{\pi} \sum_{n=0}^{L-1} \mid \chi_{m,z}[n, \theta_d] \mid^2 df_d \\ &= \sum_{l_1=0}^{L-1} \mid m[l_1] \mid^2 \left[\sum_{n=0}^{L-1} \mid \tilde{z}_{\alpha_i}[n] \mid^2 \right] \\ &= L \sum_{n=0}^{L-1} \mid \tilde{z}_{\alpha_i}[n] \mid^2 , \end{aligned} \tag{5.49}$$

where the integer arguments are modulo L. Substituting the total energy from (5.46) into (5.49),

$$V_{m,z} = \sum_{n=0}^{L-1} \mid \tilde{y}_{\alpha_i}[n] \mid^2 . \tag{5.50}$$

Equation (5.50) states that the total volume of the residue surface (i.e. the floor level) is directly proportional to the energy contained after the process of zeroing in the α_i^{th} doppler channel. If $1/L$ is the width of the resolution cell in the doppler domain, then the contribution of the α_i^{th} doppler channel to the total volume of the ambiguity surface is

$$\text{volume in } \alpha_i^{th} \text{ channel} = \frac{1}{L} \sum_{n=0}^{L-1} \mid \tilde{y}_{\alpha_i}[n] \mid^2 . \tag{5.51}$$

Zeroing the peaks associated with the strong signal will directly result in the cancellation of its floor. Although (5.50) provides a simple relationship between peak-zeroing and floor reduction, it cannot be easily generalized to the broadband case due to interpolation. However, for small differences in doppler, the narrowband results may be used to approximate the results in broadband signaling.

Broadband Assumption

Under the broadband assumption, the output at the α_j^{th} doppler channel is

$$\tilde{\boldsymbol{y}}_{\alpha_j} = \boldsymbol{M}^H \tilde{\boldsymbol{z}}_{\alpha_j} , \tag{5.52}$$

where $\tilde{\boldsymbol{y}}_{\alpha_j}$ and $\tilde{\boldsymbol{z}}_{\alpha_j}$ are equivalent to (5.43) and (5.42) with α_i replaced by α_j. Using the property in (5.45), the total residual energy in the α_j^{th} doppler channel is

$$\begin{aligned} \tilde{\boldsymbol{y}}_{\alpha_j}^H \tilde{\boldsymbol{y}}_{\alpha_j} &= \tilde{\boldsymbol{z}}_{\alpha_j}^H \boldsymbol{M}\boldsymbol{M}^H \tilde{\boldsymbol{z}}_{\alpha_j} \\ &= L\tilde{\boldsymbol{z}}_{\alpha_j}^H \tilde{\boldsymbol{z}}_{\alpha_j} . \end{aligned} \tag{5.53}$$

In broadband processing, the demodulates at the α_j^{th} doppler channel must be interpolated from the demodulates in the α_i^{th} doppler channel. First the demodulates at the α_i^{th} doppler channel is adjusted for proper demodulation.

$$\tilde{z}'_{\alpha_i,\alpha_j}[n] = \tilde{z}_{\alpha_i}[n] e^{j2\pi(1-e^{\alpha_i-\alpha_j})n/m_r} . \tag{5.54}$$

The time-scaling in discrete time is described from (3.37) to (3.40) and repeated here for the general case of interpolating from an off-doppler channel to another off-doppler channel.

$$\begin{aligned} x[n] &= ne^{\alpha_j-\alpha_i} \\ c[n] &= \lfloor x[n] \rfloor \\ \lambda[n] &= x[n] - c[n] . \end{aligned} \tag{5.55}$$

After linear interpolation, the demodulates at the α_j^{th} doppler channel is

$$\tilde{z}_{\alpha_j}[n] = (1-\lambda[n])\tilde{z}'_{\alpha_i,\alpha_j}[c[n]] + \lambda[n]\tilde{z}'_{\alpha_i,\alpha_j}[c[n]+1] . \tag{5.56}$$

The linear interpolation from (5.54) to (5.56) may also be expressed in matrix form by

$$\tilde{\boldsymbol{z}}_{\alpha_j} = \boldsymbol{T}\tilde{\boldsymbol{z}}_{\alpha_i} , \tag{5.57}$$

where $\boldsymbol{T}$ is the interpolating matrix whose elements are functions of α_i and α_j. Each row of $\boldsymbol{T}$ consist of only two non-zero elements. Specifically, the n^{th} row will have the non-zero components $(1-\lambda[n])$ and $\lambda[n]$ in columns $c[n]$ and $c[n]+1$, respectively. The interpolating matrix $\boldsymbol{T}$ may be easily computed with any desktop computer. The total energy in $\tilde{\boldsymbol{z}}_{\alpha_j}$ is given by

$$\tilde{\boldsymbol{z}}_{\alpha_j}^H \tilde{\boldsymbol{z}}_{\alpha_j} = \tilde{\boldsymbol{z}}_{\alpha_i}^H \boldsymbol{T}^H \boldsymbol{T} \tilde{\boldsymbol{z}}_{\alpha_i} . \tag{5.58}$$

In the narrowband case, $\boldsymbol{T}$ is the identity matrix and the relationship between any two doppler channels can be easily determined. In the broadband case, $\boldsymbol{T}^H\boldsymbol{T}$ is not diagonal; hence, the total energy in the α_j^{th} doppler channel cannot be easily related to the total energy in the α_i^{th} doppler channel. However, since the rows of $\boldsymbol{T}$ are properly normalized (i.e. $(1-\lambda[n])+\lambda[n] = 1$), an upper bound of $\mid \tilde{z}_{\alpha_j}[n] \mid^2$ is given by

$$\mid \tilde{z}_{\alpha_j}[n] \mid^2 \leq \mid \tilde{z}_{\alpha_i,max} \mid^2 , \tag{5.59}$$

where

$$\mid \tilde{z}_{\alpha_i,max} \mid = max[\mid \tilde{z}_{\alpha_i}[0] \mid, \mid \tilde{z}_{\alpha_i}[1] \mid, ..., \mid \tilde{z}_{\alpha_i}[L] \mid] \tag{5.60}$$

is the maximum of the α_i^{th} demodulates. Recall in (5.46) that

$$\tilde{\boldsymbol{z}}_{\alpha_i}^H \tilde{\boldsymbol{z}}_{\alpha_i} = \frac{1}{L} \tilde{\boldsymbol{y}}_{\alpha_i}^H \tilde{\boldsymbol{y}}_{\alpha_i} , \tag{5.61}$$

then the maximum componenet $\mid \tilde{z}_{\alpha_i,max} \mid^2$ may be further upper bounded by

$$\begin{aligned} \mid \tilde{z}_{\alpha_i,max} \mid^2 &\leq \tilde{\boldsymbol{z}}_{\alpha_i}^H \tilde{\boldsymbol{z}}_{\alpha_i} \\ &= \frac{1}{L} \tilde{\boldsymbol{y}}_{\alpha_i}^H \tilde{\boldsymbol{y}}_{\alpha_i} . \end{aligned} \tag{5.62}$$

Substituting the upper bounds in (5.59) and (5.62) into (5.53), the total energy in the α_j^{th} doppler channel becomes

$$\tilde{\boldsymbol{y}}_{\alpha_j}^H \tilde{\boldsymbol{y}}_{\alpha_j} \leq L \sum_{n=0}^{L-1} \mid \tilde{z}_{\alpha_i,max} \mid^2$$

$$\begin{aligned} \tilde{\boldsymbol{y}}_{\alpha_j}^H \tilde{\boldsymbol{y}}_{\alpha_j} &\leq L \sum_{n=0}^{L-1} \frac{1}{L} \tilde{\boldsymbol{y}}_{\alpha_i}^H \tilde{\boldsymbol{y}}_{\alpha_i} \\ &= L \tilde{\boldsymbol{y}}_{\alpha_i}^H \tilde{\boldsymbol{y}}_{\alpha_i} \ . \end{aligned} \tag{5.63}$$

Although (5.63) is a "loose" upper bound, it does indicate that the zeroing implemented during HCCO preprocessing will reduce the floor level associated with the strong path. In fact, if the energy of the strong path were totally eliminated at the α_i^{th} doppler channel, then the floor level associated with the strong path will be completely removed. Again, if the doppler search is within a small interval, the results in section 5.2.2 with narrowband assumption will provide a better approximation to the degree of floor reduction.

5.2.3 Weak Path Corruption

Unlike the analyses in previous sections, the detectabilily of the weak path will be determined by the ratio between the corrupted peaks of the weak paths and the floor level of these weak paths. In this section, it is assumed that the reception consists of a total of N paths; M strong paths and (N-M) weak paths. To determine the degree of weak path distortion, it is further assumed that the floor level of the strong paths are totally eliminated. Following the same notations used in previous sections, α_i will denote the doppler channel selected for preprocessing (i.e. the doppler channel of the strong paths [4]). In addition, the true dopplers of the weak paths are assumed to be different from α_i. If this were not so, the weak paths may be easily detected without HCCO preprocessing.

With the assumption that the energy is uniformly distributed within a doppler channel, a simple measure of weak path corruption may be derived. Specifically, it

[4]It is assumed that all strong paths have the same true doppler.

is assumed that

$$| \tilde{y}_{\alpha_i}[n] | \approx \sum_{p=M+1}^{N} \frac{| A_p |}{\sqrt{L}} , \tag{5.64}$$

where A_p is the complex amplitude of the p^{th} path arrival and L is the number of digits in a period. Note that the path amplitude A_p refers to the peak of a weak path when $M+1 \leq p \leq N$. Similarly,

$$| A[n, e^{\alpha}] | \approx \frac{1}{\sqrt{L}} . \tag{5.65}$$

Equation (5.65) says that each sampled residue at the α_i^{th} doppler channel creates its own floor level, and that the floor level is $1/\sqrt{L}$ below the magnitude of the sampled residue. Both assumptions (5.64) and (5.65) are based on the narrowband assumptions in (4.75) that for small differences in doppler the total energy is the same for each doppler channel. Furthermore, the uniformity of the energy does not come from mathematical proofs; it comes from limited experience with laboratory and field signals and computer simulations.

Due to the zeroing implemented during the preprocessing, the peaks of the weak paths are reduced. Since the number of digits removed during preprocessing is D; $L - D$ is the remaining digits that can be compressed to form the peak of the p^{th} weak path[5]. Therefore, the energy contained in the peak of the p^{th} weak path is approximately

$$| \tilde{A}_p |^2 = | A_p |^2 \left(1 - \frac{D}{L}\right)^2 , \tag{5.66}$$

where $\left(1 - \frac{D}{L}\right)^2$ represents the fraction of the total energy remained. Equations (5.66) implies that removing portions of a signal, then correctly doppler compensating and crosscorrelating, reduces the peak-magnitude-squared proportional to the

[5]In order to simplify the calculation of the peak level, it is assumed that interpolation among doppler channels are negligible. In other words, one digit removed "off-doppler" is equivalent to one digit removed "on-doppler". This is simply a narrowband argument.

fraction of time removed. Although $\tilde{A}_p$ represents the corruption of the p^{th} weak path due to preprocessing, it does not represent the actual peak that is *observed.* This is due to the fact that the (N-M) weak paths create their own mutual interference. Prior to preprocessing, the energy of the p^{th} weak path due to mutual interference is

$$| A_{p,obs} |^2 \approx | A_p |^2 - \sum_{\substack{j=M+1 \\ j \neq p}}^{N} \frac{| A_j |^2}{L} , \tag{5.67}$$

where $A_{p,obs}$ is the observed peak of the p^{th} path. From equations (5.66) and (5.67), the magnitude-squared peak after preprocessing becomes

$$\begin{aligned} | \tilde{A}_{p,obs} |^2 &\approx | \tilde{A}_p |^2 - \sum_{\substack{j=M+1 \\ j \neq p}}^{N} \frac{| \tilde{A}_j |^2}{L} \\ &= | A_p |^2 \left(1 - \frac{D}{L}\right)^2 - \frac{L-D}{L^2} \sum_{\substack{j=M+1 \\ j \neq p}}^{N} | A_j |^2 . \end{aligned} \tag{5.68}$$

In order to analyze the detectability of the weak paths, it is necessary to determine both the corruption of the peaks of the weak path as well as the floor level of the ambiguity surface after preprocessing. Prior to preprocessing, the mean-square floor of the ambiguity surface due to the weak paths is

$$M_s^2 = \frac{1}{L} \sum_{p=M+1}^{N} | A_p |^2 . \tag{5.69}$$

This simply states that the mean-square floor of the ambiguity surface is sum of the median level of the individual weak paths. At first, it would seem that an appropriate measure of the mean-square floor of the ambiguity surface after preprocessing would be

$$\begin{aligned} \hat{M}_s^2 &= \sum_{p=M+1}^{N} | \tilde{A}_p |^2 \\ &= \frac{1}{L} \sum_{p=M+1}^{N} | A_p |^2 \left(1 - \frac{D}{L}\right)^2 . \end{aligned} \tag{5.70}$$

This implies that the magnitude of each weak path is reduced by a factor of $\left(1-\frac{D}{L}\right)$, and the mean-square floor is simply $\frac{1}{L}$ times the sum of the combined peaks of the weak paths. One must be careful. The problem with the above statement is that although the peak is reduced by a factor of $\left(1-\frac{D}{L}\right)$, the sidelobe of the p^{th} weak path at the α_p^{th} doppler channel is no longer zero[6]. The non-zero sidelobe is one of the artifacts of partial crosscorrelation of m-sequences. These sidelobes must also be included in the calculations for the mean-square floor of the ambiguity surface. An easier way to measure the mean-square floor of the ambiguity surface is to determine the total available energy in any doppler channel.

Using the equal-energy assumption, the total energy at the α_j^{th} doppler channel is

$$\sum_{n=0}^{L-1} \mid \tilde{y}_{\alpha_j}[n] \mid^2 = \sum_{n=0}^{L-1} \mid \tilde{y}_{\alpha_i}[n] \mid^2 \ . \tag{5.71}$$

Since D components in the α_i^{th} doppler channel are zeroed, (5.71) becomes

$$\sum_{n=0}^{L-1} \mid \tilde{y}_{\alpha_j}[n] \mid^2 = \sum_{n=0}^{L-D-1} \mid \tilde{y}_{\alpha_i}[n] \mid^2 \ . \tag{5.72}$$

Since all strong paths are canceled through the D zeroes, each component of $\tilde{y}_{\alpha_i}[n]$ is the sum of the floor level of the (N-M) weak paths.

$$\begin{aligned} \sum_{n=0}^{L-1} \mid \tilde{y}_{\alpha_j}[n] \mid^2 &= \sum_{n=0}^{L-D-1} \left[\sum_{p=M+1}^{N} \frac{\mid A_p \mid^2}{L} \right] \\ &= \frac{L-D}{L} \sum_{p=M+1}^{N} \mid A_p \mid^2 \ . \end{aligned} \tag{5.73}$$

Assuming equal distribution of the total energy across the entire doppler channel, the mean-square floor of the ambiguity surface after preprocessing is given by

$$\begin{aligned} \tilde{M}_s^2 &= \frac{1}{L} \sum_{n=0}^{L-1} \mid \tilde{y}_{\alpha_j}[n] \mid^2 \\ &= \frac{L-D}{L^2} \sum_{p=M+1}^{N} \mid A_p \mid^2 \ . \end{aligned} \tag{5.74}$$

[6]Prior to preprocessing, assuming single path reception, the true doppler channel will consist of one peak and zeros everywhere else.

The evaluation of the mean-square floor in (5.74) does not require any knowledge of the partial crosscorrelation of m-sequences. Both the peaks of the weak paths and their sidelobes are incorporated in the total energy of the α_i^{th} doppler channel. In comparison, the mean-square floor in (5.70) is always less than the mean-square floor given in (5.74) due to the missing sidelobes in the calculation of (5.70). Specifically,

$$\hat{M}_s^2 \;=\; \tilde{M}_s^2 \left[\frac{L-D}{L}\right] \;. \tag{5.75}$$

A measure of the detectability of the p^{th} weak path is the weak signal-to-mutual floor (WSM) ratio given by

$$WSM \;\triangleq\; 10\ log\ \left[\frac{|\ \tilde{A}_{p,obs}\ |^2}{\tilde{M}_s^2}\right] \;, \tag{5.76}$$

For the special case of a single weak path (i.e. N=M+1),

$$\begin{aligned} WSM \;&=\; 10\ log\ \left[\frac{\left(1-\frac{D}{L}\right)^2}{\left(\frac{L-D}{L^2}\right)}\right] \\ &=\; 10\ log\ [L-D] \;, \end{aligned} \tag{5.77}$$

and for

$$\begin{aligned} &L = 511; \quad D = 1; \quad WSM = 27.1dB \\ &L = 511; \quad D = 20; \quad WSM = 26.9dB \\ &L = 511; \quad D = 200; \quad WSM = 24.9dB \\ &L = 511; \quad D = 500; \quad WSM = 10.4dB \end{aligned} \tag{5.78}$$

Therefore, the HCCO preprocessing will not significantly reduce the detection capability of weak paths compared to those path's own SNR.

5.2.4 Weak Path Corruption Under Noise

In practice, noise must be included in the above analysis. The performance of the preprocessing will deteriorate with increasing noise level in the reception. However, one of the primary requirement for preprocessing is the assumption that the weak signal-to-noise ratio must be sufficiently high. If this were not true, the process of eliminating the floor level associated with the strong paths would be meaningless.

In the presence of noise, the zeroing of the peaks will not only remove a portion of the weak paths but a few noise components as well. Assuming additive white gaussian noise (AWGN), the level of the noise components removed during the process of zeroing the peaks is determined by the mean-square floor of the noise components at the output stage of the preprocessing. Let $n_{\alpha_i}[d_p]$ be the noise output at the α_i^{th} doppler channel. Assuming uniform distribution of the noise energy across the entire doppler channel,

$$E[\mid n_{\alpha_i}[d_p] \mid^2] \;=\; G_n^2 \quad for\ all\ d_p\ , \tag{5.79}$$

where G_n is the standard deviation of the noise. After HCCO zeroing, the total noise energy remained in the α_i^{th} doppler channel is

$$\begin{aligned} E[\sum_{n=0}^{L-1} \mid \tilde{n}_{\alpha_i}[n] \mid^2] \;&=\; \sum_{n=0}^{L-D-1} G_n^2 \\ &=\; (L-D)G_n^2\ , \end{aligned} \tag{5.80}$$

and the mean-square floor of the noise floor after preprocessing is

$$\begin{aligned} \tilde{G}_n^2 \;&=\; \frac{1}{L}\sum_{n=0}^{L-1} \mid \tilde{n}_{\alpha_i}[n] \mid^2 \\ &=\; \frac{L-D}{L} G_n^2\ . \end{aligned} \tag{5.81}$$

With AWGN, the peak of the p^{th} weak path is further weakened.

$$\mid \tilde{A}_{p,obs} \mid^2 \approx \mid A_p \mid^2 \left(1 - \frac{D}{L}\right)^2 - \frac{L-D}{L^2} \sum_{\substack{j=M+1 \\ j \neq p}}^{N} \mid A_j \mid^2 - \tilde{G}_n^2 \,, \tag{5.82}$$

The signal+noise mean-square floor is

$$\tilde{M}_n^2 = \tilde{G}_n^2 + \frac{L-D}{L^2} \sum_{m=M+1}^{N} \mid A_p \mid^2 \,. \tag{5.83}$$

The weak signal-to-mutual floor measure of the p^{th} path becomes

$$WSM = 10\ log\left[\frac{\mid \tilde{A}_{p,obs} \mid^2}{\tilde{M}_n^2}\right] . \tag{5.84}$$

For the special case of a single weak path,

$$\begin{aligned} WSM &= 10\ log\left[\frac{\mid A_p \mid^2 \left(1 - \frac{D}{L}\right)^2 - \tilde{G}_n^2}{\tilde{G}_n^2 + \mid A_p \mid^2 \left(\frac{L-D}{L^2}\right)}\right] \\ &= 10\ log\left[\frac{\mid A_p \mid^2 \left(\frac{L-D}{L}\right)^2 - G_n^2 \left(\frac{L-D}{L}\right)}{G_n^2 \left(\frac{L-D}{L}\right) + \mid A_p \mid^2 \left(\frac{L-D}{L^2}\right)}\right] . \end{aligned} \tag{5.85}$$

If the signal-to-noise ratio prior to preprocessing is

$$S_r \triangleq \frac{\mid A_p \mid^2}{G_n^2}, \tag{5.86}$$

then, the WSM may be written as

$$WSM = 10\ log(S_r) + 10\ log\left[\frac{\left(\frac{L-D}{L}\right)^2 - \frac{1}{S_r}\left(\frac{L-D}{L}\right)}{\left(\frac{L-D}{L}\right) + S_r\left(\frac{L-D}{L^2}\right)}\right] . \tag{5.87}$$

Under high weak signal-to-noise ratio (i.e. $S_r \gg L$), the noise terms are negligible and

$$WSM \approx 10\ log\,[L-D]\,, \tag{5.88}$$

which is the noiseless WSM ratio in (5.77).

5.2.5 HCCO Preprocessing With the Lake Seneca Measurements

The data set taken at Lake Seneca in December, 1990 consisted of 12 hydrophone channels of data. The m-sequence signal used in the transmission contains 511 digits per period. The m-sequence law was 1175 (octal) which specifies the coefficient associated with the primitive polynomial in equation (A.9). There were 3 carrier cycles per digit and the modulation angle was 84.375 degrees. The carrier was 250 Hz and the sampling rate was 2 kHz. There was a little over 4 periods of the reception available for processing.

Only the first channel of the measured data is utilized for HCCO preprocessing. This is due to the relative location between the transducer and the first hydrophone (40 feet apart). The source is at a depth of 300 feet. The other 10 channels are at a distance of 51 feet from the surface and will most likely have strong surface return present. The last channel is a direct feed from the signal generator to the a/d converter.

The reception from the first channel contains a direct path at 0-doppler and a weak surface return also at 0-doppler. In order to simulate the effect of weak path corruption after HCCO preprocessing, it is assumed that there exist strong paths at an off-doppler channel. The purpose of the HCCO preprocessing is to remove the strong paths at this off-doppler channel in the arrival space by zeroing the peaks and impulse responses associated with the strong paths. To obtain the off-doppler response in the arrival space, the 0-doppler demodulated response in the data space is interpolated to the off-doppler channel of the strong paths. This is followed by a projection onto the arrival space where the assumed strong paths are zeroed. The zeroed response is then projected back onto the data space and interpolated to all doppler channels. Each of the doppler-interpolated response is projected onto its

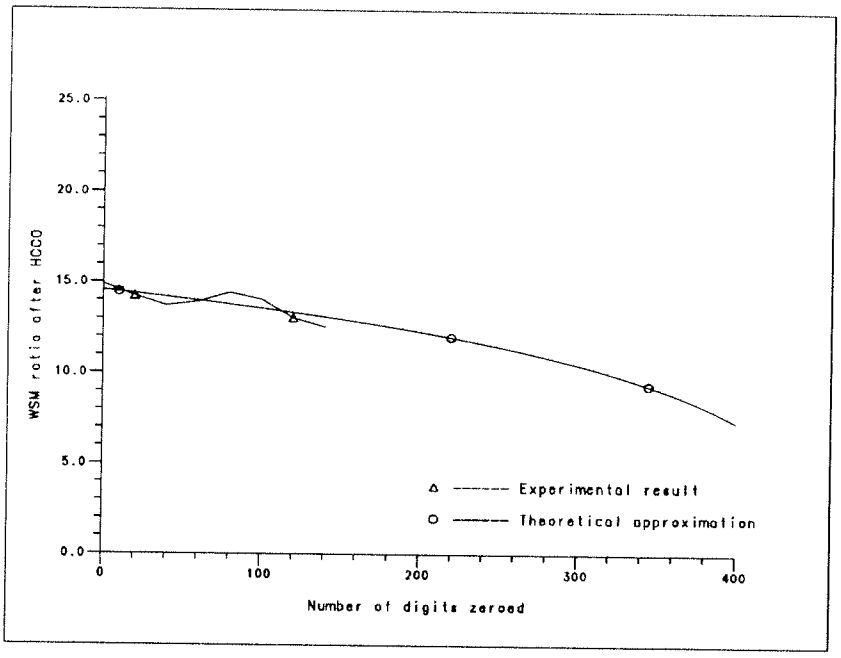

Figure 5.5: The signal-to-noise ratio of the weak path was 14.8dB prior to preprocessing. The difference between the true doppler of the weak path and the true doppler of the strong paths is $(e^{\alpha_p - \alpha_i} - 1) = 0.0006$.

arrival space. In combination, they form the residual ambiguity surface where weak paths may be detected. In order to measure the experimental result of the WSM ratio, the peak of the 0-doppler channel is used as the observed peak of the weak path (i.e. the direct path of the reception). The median of the residual ambiguity surface is used as the measurement of the floor level after strong path cancellation.

In figures (5.5) to (5.8), the theoretical approximation to (5.87) is plotted along with the results from the Lake Seneca measurement. Due to the presence of noise peaks, the WSM ratio for the experimental results were unreliable below 13dB.

5.2.6 Weak Path Corruption Within Blind-spots

Although the ambiguity surface of the m-sequence signal behaves much like the ambiguity surface of noise (i.e. one central peak and a flat floor level everywhere else), the ambiguity surface of the m-sequence differs from the noise ambiguity surface in

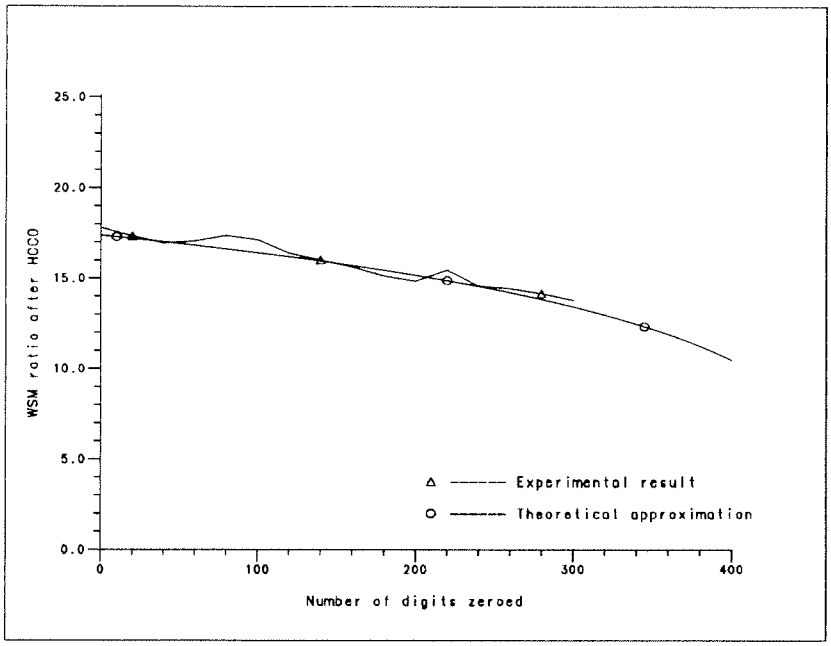

Figure 5.6: The signal-to-noise ratio of the weak path was 17.8dB prior to preprocessing. The difference between the true doppler of the weak path and the true doppler of the strong paths is $(e^{\alpha_p - \alpha_i} - 1) = 0.0006$.

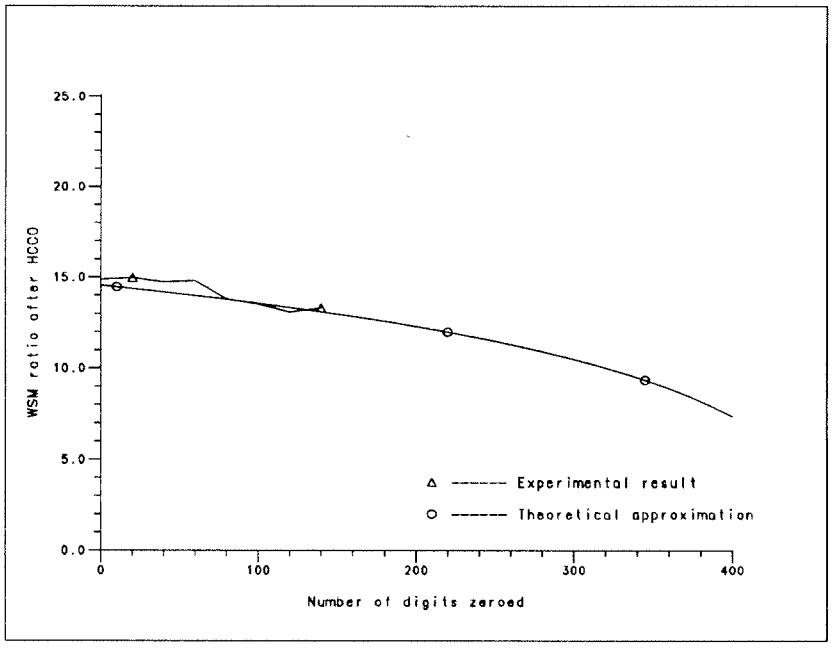

Figure 5.7: The signal-to-noise ratio of the weak path was 14.8dB prior to preprocessing. The difference between the true doppler of the weak path and the true doppler of the strong paths is $(e^{\alpha_p - \alpha_i} - 1) = 0.0026$.

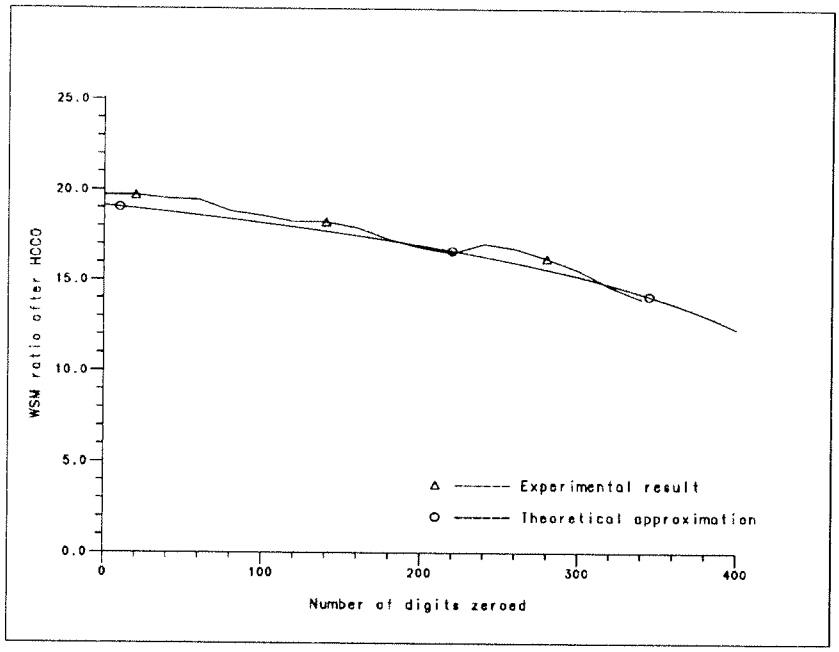

Figure 5.8: The signal-to-noise ratio of the weak path was 19.8dB prior to preprocessing. The difference between the true doppler of the weak path and the true doppler of the strong paths is $(e^{\alpha_p - \alpha_i} - 1) = 0.0026$.

that the m-sequence ambiguity surface has a sinc-like function along the doppler axis at the true travel time of the signal reception. If both the strong path and the weak path differ only in doppler, the cancellation of the strong path through HCCO preprocessing may severely degrade the detectability of the weak path. This is referred to as the "blind-spot" of the HCCO preproceesing. The term is originally used in MTI (Moving Target Indicator) to indicate the nulls occuring at multiples of the repetition frequency. Weak signals appearing at these repetition frequencies will be eliminated due to zeroing. For HCCO preprocessing, this is analogous to the reduction of the floor level of the strong path at the expense of removing the peaks of the weak path. For a single path reception, the noiseless ambiguity function evaluated at the true travel time is

$$A(e^{\alpha}, \tau \mid e^{\beta}, T_p', P_T) \mid_{\tau = T_p'} = P_T sinc(f_c(e^{\alpha - \beta} - 1)P_T) \ , \tag{5.89}$$

where P_T is the period in seconds, $f_c P_T$ is the number of carrier cycles per period, and one period processing is assumed. For multipath reception[7], the preprocessing affects the peak of the weak path in two ways. First, the magnitude-squared peak of the weak path is reduced by a factor of $\left(1-\frac{D}{L}\right)^2$ due to the zeroing of the general floor level as in equation (5.68). Then, the magnitude-squared peak is further reduced by a factor of $(1-sinc^2(f_c(e^{\alpha_i-\alpha_p}-1)P_T))$ which represents the partial elimination of the weak path due to the sinc-like structure of the ambiguity function. Combining the two effects, the magnitude-squared peak with AWGN is

$$\begin{aligned} \mid \tilde{A}_{p,obs} \mid^2 \;\approx\; & \mid A_p \mid^2 (1-sinc^2(f_c(e^{\alpha_i-\alpha_p}-1)P_T))\left(1-\frac{D}{L}\right)^2 \\ & -\frac{L-D}{L^2}\sum_{\substack{j=M+1 \\ j\neq p}}^{N} \mid A_j \mid^2 \; - \tilde{G}_n^2 \;, \end{aligned} \tag{5.90}$$

where α_i is the true doppler of the strong path and α_p is the true doppler of the weak path. The second term in (5.90) is the mutual interference among weak paths prior to HCCO preprocessing. Using the magnitude-squared peak in (5.90), the WSM ratio becomes

$$WSM \;=\; 10\;log\left[\frac{\mid \tilde{A}_{p,obs} \mid^2}{\tilde{G}_n^2+\frac{L-D}{L^2}\sum_{p=M+1}^{M} \mid A_p \mid^2}\right] \;. \tag{5.91}$$

For the case of a single weak path,

$$\begin{aligned} WSM \;&=\; 10\;log\left[\frac{\mid A_p \mid^2 (1-sinc^2(f_c(e^{\alpha_o-\alpha_p}-1)P_T))\left(1-\frac{D}{L}\right)^2-\tilde{G}_n^2}{\tilde{G}_n^2+\mid A_p \mid^2\left(\frac{L-M}{L^2}\right)}\right] \\ &=\; 10\;log\left[\frac{\mid A_p \mid^2 (1-sinc^2(f_c(e^{\alpha_o-\alpha}-1)P_T))\left(1-\frac{D}{L}\right)^2-G_n^2\left(\frac{L-D}{L}\right)}{G_n^2\left(\frac{L-D}{L}\right)+\mid A_p \mid^2\left(\frac{L-D}{L^2}\right)}\right] \\ &=\; 10\;log(S_r) \\ &\quad +\; 10\;log\left[\frac{(1-sinc^2(f_c(e^{\alpha_o-\alpha}-1)P_T))\left(\frac{L-D}{L}\right)^2-\frac{1}{S_r}\left(\frac{L-D}{L}\right)}{\left(\frac{L-D}{L}\right)+S_r\left(\frac{L-D}{L^2}\right)}\right] \;. \end{aligned} \tag{5.92}$$

[7]It is assumed that more than one strong path is present during the multipath reception; therefore, zeros must be placed at different regions of the ambiguity surface during preprocessing.

Recall that α_o corresponds to the doppler channel selected for HCCO preprocessing. It is also the true doppler of the strong paths. And under high signal-to-noise ratio,

$$WSM = 10\ log\left[(1 - sinc^2(f_c(e^{\alpha_o-\alpha} - 1)P_T))(L - D)\right] \quad (5.93)$$

$$= 10\ log\left[(1 - sinc^2((e^{\alpha_o-\alpha} - 1)QL))(L - D)\right]\ , \quad (5.94)$$

where Q is the number of cyles in a digit. Since WSM in (5.94) is a function of (1-sinc) squared, the strength of the i^{th} weak path will be significantly reduced if the true doppler of the strong paths and the i^{th} weak path differ in doppler by[8]

$$\mid e^{\alpha_o-\alpha_i} - 1 \mid < \frac{1}{QL}\ , \quad (5.95)$$

where $(e^{\alpha_i-\alpha_{i+1}} - 1)$ is referred to as the size of the doppler bin, and $\frac{1}{QL}$ corresponds to the width of the major lobe in the doppler axis of the ambiguity surface[9]. Another way to interpret (5.95) is that $QL \mid e^{\alpha_o-\alpha_i} - 1 \mid = 1$ corresponds to a one cylce difference between the period of the two doppler channels. Therefore, if two paths differ by more than one cycle, the affect of blind-spot is negligible.

Figures (5.9) and (5.10) provide a comparison between the experimental results and the theoretical WSM ratio given in (5.92). Again, the Lake Seneca measurement described in section 5.2.5 provides the basis for the experimental results. In this case, it is assumed that there exists a strong path which differ only in doppler from the weak path (i.e. the direct path). As in section 5.2.4, due to the presence of noise peaks, WSM ratio for the experimental results were unreliable below 13dB. In figures (5.9) and (5.10), the size of the doppler bin is $1/6QL$. The result show that the "blind spot" effect is significant only if the difference in doppler between the weak path and the strong path is less than ± 6 doppler bins or $\pm\frac{1}{QL}$.

[8]It is assumed that one of the strong paths and the i^{th} weak path have equal time-delay.

[9]If the doppler bins and the width of the major lobe are to be expressed in terms of frequency in Hz, multiply both sides of (5.95) by f_c. Hence, the size of the doppler bin in Hz is $f_c(e^{\alpha_o-\alpha_i} - 1)$, and the width of the major lobe is $\frac{1}{P_T}$.

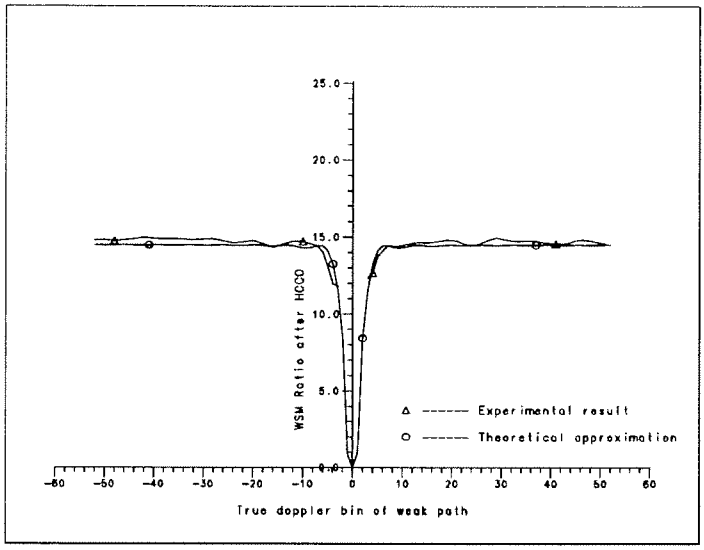

Figure 5.9: Removal of the strong path when the strong path and the weak path differ only in doppler. The signal-to-noise ratio of the weak path was 15.8dB prior to preprocessing.

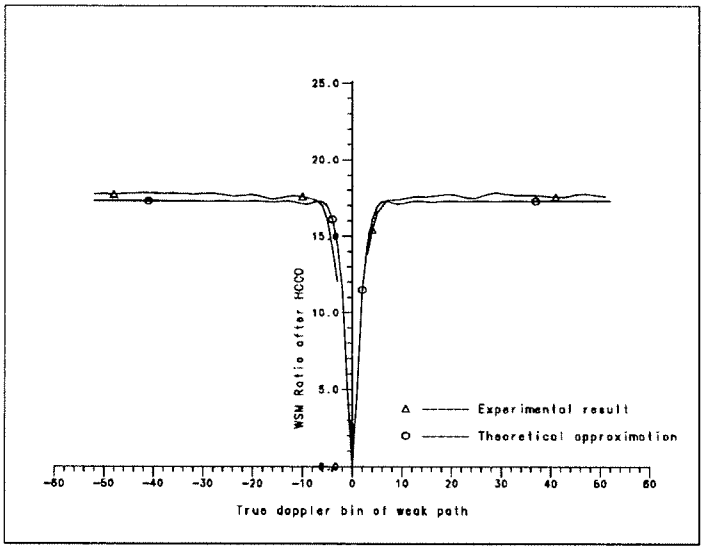

Figure 5.10: Removal of the strong path when the strong path and the weak path differ only in doppler. The signal-to-noise ratio of the weak path was 17.8dB prior to preprocessing.

5.2.7 Signal Processing of HCCO Preprocessing

In contrast to the weak signal detectability analyzed in previous sections, this section provides the reader with an in-depth knowledge of the signal processing aspects of HCCO preprocessing. The intent is to help the reader to understand *why* each of the steps in the signal processing is essential and *how* the reader may carry out these computations. A supplementary, step-by-step approach to HCCO preprocessing *without* the explanations is provided in Appendix B.

In order to avoid complicated notations, fixed-fixed bistatic sonar is assumed (i.e. all strong paths arrive at zero doppler; $\alpha_i = 0$). The procedure for detecting weak paths through HCCO preprocessing is split into three parts. Part A describes the process of sampling and demodulation. Part B implements the HCCO preprocessing, and part C calculates the ambiguity surface from the preprocessed demodulates.

Frequently, several periods of the signal reception are summed in order to improve the output signal-to-noise ratio. If X is the desired number of periods processed, at least X periods at the extreme dopplers must be sampled at the reception due to the broadband interpolation necessary for the calculation of the ambiguity surface; X+1 is the common practice and is usually more than sufficient.

The essential parameters for processing m-sequence signals are as follows.

L = Number of digits in a period of the m-sequence

Q = Number of cycles in a digit

QL = $f_c T_p$ = Number of cycles per period

m_r = Number of samples in a cycle

θ_L = period-matched angle

θ_T = transmission angle

b_m = ± 1 ; binary codes of the m-sequence

f_c = Center frequency for the signal transmission

$m_r f_c$ = Sampling rate

t_1 = time between samples, $1/m_r f_c$

X = Number of periods processed

$r(t)$ = continuous time reception

α_{min} = doppler index of interest with maximum time compression

α_{max} = doppler index of interest with minimum time compression

A) Sampling and Demodulation.

1) Sample the reception at zero doppler.

$$r[n] = r(nt_1) . \tag{5.96}$$

Since $m_r QL$ is the number of samples in a period, there should be $(X+1)m_r QL$ number of samples in $r[n]$.

2) Complex demodulate the sampled reception $r[n]$, forming $z[n]$.

$$\begin{aligned} z[n] &= r[n]e^{j2\pi f_o n t_1} \\ &= r[n]e^{j2\pi n/m_r} . \end{aligned} \tag{5.97}$$

3) Remove the $-2f_c$ component using a demodulate filter. A sinc-type LPF is obtained by averaging the demodulates over one cycle. A sinc-squared LPF is obtained by cascading the two sinc-type LPF in series. The sinc-squared LPF will perform better than the sinc-type LPF in rejecting the $-2f_c$ component since its sidelobes are lower.

$$z'[m] = \sum_{i=0}^{m_r-1} z[m-i] . \tag{5.98}$$

$$z''[m] \;=\; \sum_{i=0}^{m_r-1} z'[m-i]\;. \tag{5.99}$$

B) HCCO Preprocessing.

To implement the HCCO preprocessing, the demodulated samples are divided up into segments of one period each. Each segment of the demodulated samples is preprocessed individually. At the end of the preprocessing, the preprocessed segments are recombined to form a single, modified demodulated sequence.

1) Unlike the usual matched-filter receiver, the first step in the preprocessing is to remove only the m-sequences from the demodulated samples (i.e. divide the spectrum of the demodulates by $M(f)$ instead of $M(f)P(f)$). To remove the m-sequences and achieve *sharp* waveform responses, the Factor Inverse Filtering (FIF) from section 5.2.1 is applied. To implement FIF, each period (m_rQL samples) of the demodulated samples is divided up into m_rQ sequences[10]. m_rQ is the number of samples in a digit; hence, each of the m_rQ demultiplexed, demodulated sequences has length L. Each of these m_rQ sequences will be processed as if only one sample per digit were received. Let $z''_{q,r}[m]$, $q = 0, 1, 2, ..., m_rQ - 1$ be the q^{th} sequence of the r^{th} period of $z''[m]$ and is given by

$$z''_{q,r}[m] \;\triangleq\; z''[q + mQ + rm_rQL] \quad where \begin{cases} q = 0, 1, 2, ..., m_rQ - 1 \\ m = 0, 1, 2, ..., L - 1 \\ r = 0, 1, 2, .., X \end{cases} \tag{5.100}$$

After demultiplexing, the samples of each of the m_rQ sequences are spaced m_rQ apart. In order to obtain high peak responses after pulse compression, the reference m-sequence used in the cyclic crosscorrelation must utilize the same angle θ_T as in the transmission. Therefore, the output of the cyclic crosscorrelation[11] (the forward

[10]The crosscorrelation may be efficiently computed using Fast Hadamard Transform when the demodulated samples are demultiplexed into subsets of one sample per digit each.

[11]All cyclic crosscorrelation in this section is mod L.

projection) for each of the $m_r Q$ demultiplexed, demodulated sequences is

$$\begin{aligned} s_{q,r}[k] &= \sum_{m=0}^{L-1} z''_{q,r}[m] e^{-jb_{k+m}\theta_T} \quad k = 0, 1, 2, ..., L-1 \\ &= cos(\theta_T) \sum_{m=0}^{L-1} z''_{q,r}[m] - j\ sin(\theta_T) \sum_{m=0}^{L-1} z''_{q,r}[m] b_{k+m} \ . \end{aligned} \tag{5.101}$$

The first summation on the right of (5.101) requires only L summations for each of the $m_r Q$ sequences ($m_r QL$ additions in total). The second summation on the right of (5.101) involves only additions and subtractions. However, the second summation requires (L-1)L additions[12] for each of the $m_r Q$ sequences for a total of $m_r QL(L-1) + m_r QL = m_r QL^2$ additions. Due to the efficiency of Fast Hadamard Transform (FHT) the number of additions for both sums can be reduced to $(L+1) \cdot log_2(L+1)$ (see Appendix A) for each of the $m_r Q$ sequences for a total of $m_r Q(L+1) \cdot log_2(L+1)$.

2) In section 5.2.1, it is shown that when the transmission angle θ_T of the m-sequence is chosen as the period-matched angle (i.e. $\theta_T = \theta_L = tan^{-1}(\sqrt{L})$), the autocorrelation function will have zero off-peak values. Furthermore, the magnitude of the spectrum of the m-sequence $M(f)$ will be a constant so that dividing the demodulated reception $Z(f) = P(f)M(f)$ by $M(f)$ is the same as multiplying by $M^*(f)$ except for a constant. The FIF simply recovers the pulse factor $P(f)$. These are no longer true when the transmission angle is different from the period-matched angle. If FIF in (5.101) were implemented using a non-period-matched angle, the resultant output would not be the ideal pulse (i.e. one at the peak and zero everywhere else in the time domain). Instead, the peak will remain high, but the magnitude of the off-peak values will be a non-zero constant. The magnitude of this non-zero constant will depend on the angles θ_T and θ_L.

There are two primary reasons why the transmission angle is not the period-

[12]The time for computing an addition and a subtraction is approximately the same.

matched angle. First, it is a common practice to use an exalted carrier in the transmission. This is obtained by using a transmission angle in the range

$$\frac{\pi}{4} \leq \theta_T \leq \theta_L. \tag{5.102}$$

As an example, it may be shown that at $\theta_T = \frac{\pi}{4}$ half of the transmission power is in the carrier. Since the carrier is narrowband, it is easier to determine the presence of signal in the reception through FFT provided that the SNR is high enough. Additionally, any doppler-shift may be determined from the frequency-shift in the carrier; hence, the calculation of the ambiguity surface is not required. However, the carrier alone is insufficient for the purposes of sonar/radar since the carrier has very poor travel-time resolution. The second reason for not using the period-matched angle is that the signal generator used in experiments stores angles in discrete steps. Therefore, the angle used in the transmission may be slightly lower than the period-matched angle.

The purpose of this step is to remove the non-zero, off-peak values (the bias level) from the crosscorrelation output $s_{q,r}[k]$ in the arrival space to increase the resolution of the strong paths[13]. To understand the principle behind bias removal, let $\tilde{A}_+$ and $\tilde{A}_-$ be the phasors associated with the period-matched angle and let A_+ and A_- be the phasors associated with the transmission angle. The relationship among the phasors is diagrammed in figure 5.11.

In figure 5.11, if the phasor A_+ and A_- were

$$A_+ = e^{j\theta_T} \tag{5.103}$$

$$A_- = e^{-j\theta_T}, \tag{5.104}$$

[13]If the transmission angle is the same as the period-matched angle then this step may be skipped.

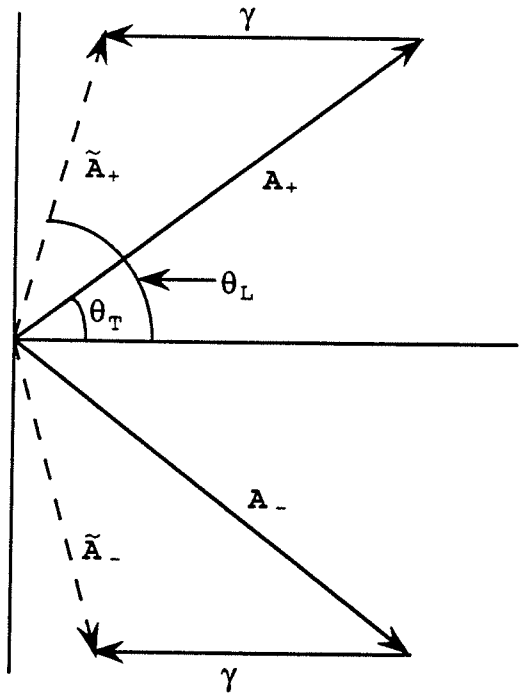

Figure 5.11: Phasor diagram: transmission angle vs. period-matched angle for the reference signal. The reference mapping constant γ re-directs A_+ an A_- to $\tilde{A}_+$ and $\tilde{A}_-$ respectively.

then

$$\tilde{A}_+ = \frac{sin(\theta_T)}{sin(\theta_L)} e^{j\theta_L} \tag{5.105}$$

$$\tilde{A}_- = \frac{sin(\theta_T)}{sin(\theta_L)} e^{-j\theta_L} , \tag{5.106}$$

provided that the reference mapping constant γ is real.

Consider the m-sequence $m[i] = e^{jb_i\theta_T}$ phase modulated at the transmission angle. $m[i]$ takes on value of either A_+ or A_- depending on the sign b_i. The autocorrelation of $m[i]$ is given by

$$\sum_{i=0}^{L-1} m[i]m^*[i+n] = C \qquad for\ n \neq 0\ (mod\ L) \tag{5.107}$$

$$\sum_{i=0}^{L-1} m[i]m^*[i+n] = L \qquad for\ n = 0\ (mod\ L) \tag{5.108}$$

where C is a complex constant which equals zero only if the transmission angle equals the period-matched angle. This suggests that when the transmission angle differs from the period-matched angle, the phasors A_+ and A_- may be re-directed to phasors with period-matched angle so that the constant C in (5.107) will equal zero. In other words, the autocorrelation of the re-directed phasors will take on all the properties associated with the period-matched angle. Specifically, if the reference mapping constant γ in figure 5.11 is subtracted from each of the m-sequence digits $m[i]$ used in the transmission, then the ideal autocorrelation results.

$$\sum_{i=0}^{L-1} (m[i]-\gamma)(m^*[i-n]-\gamma) = 0 \qquad for\ n \neq 0\ (mod\ L) \tag{5.109}$$

$$\sum_{i=0}^{L-1} (m[i]-\gamma)(m^*[i-n]-\gamma) = \frac{sin(\theta_T)}{sin(\theta_L)} L \qquad for\ n = 0\ (mod\ L) \tag{5.110}$$

In (5.109) and (5.110), both $(m[i]-\gamma)$ and $(m^*[i+n]-\gamma)$ are elements in the set $\{\tilde{A}_+, \tilde{A}_-\}$, the period-matched phasors.

The above method for bias level removal may be applied directly to the crosscorrelation in (5.101) with the exception that the data mapping constant δ_q subtracted

from $z''_{q,r}[m]$ is complex in general, and it must be properly scaled to take into account the M strong paths in $z''_{q,r}[m]$. As in (5.109), the zero off-peak level at the output of the crosscorrelation may be obtained when the mapping constants γ and δ_q are subtracted from sequences $m^*[n]$ and $z''_{q,r}[m]$, respectively.

$$\begin{aligned} \hat{s}_{q,r}[i] &= \sum_{n=0}^{L-1}(z''_{q,r}[n] - \delta_q)(m^*[n-i] - \gamma) \\ &= \sum_{n=0}^{L-1}(z''_{q,r}[n] - \delta_q)(e^{-jb_{n-i}\theta_T} - \gamma) \ . \end{aligned} \tag{5.111}$$

In (5.111), $\hat{s}_{q,r}[i]$ represents the crosscorrelation output with the bias level removed. Using the diagram in figure 5.11, the reference mapping constant γ is given by

$$\gamma = \frac{sin(\theta_L - \theta_T)}{sin(\theta_L)} \ , \tag{5.112}$$

To compute δ_q, consider the noiseless analytic model of the demultiplexed demodulates $z''_{q,r}[n]$ given by

$$z''_{q,r}[n] = z''_{s,q,r}[n] + z''_{w,q,r}[n] \ , \tag{5.113}$$

where $z''_{s,q,r}[n]$ and $z''_{w,q,r}[n]$ are the demultiplexed demodulates associated with the strong paths and weak paths respectively. Since all strong paths are assumed to arrive at zero doppler, each strong path may be modeled as a scaled, time-delayed, and phase-shifted version of the transmitted m-sequence.

$$z''_{q,r}[n] = \sum_{p=1}^{M} a_p e^{-j2\pi f_o S_p} m[n-k_p] + z''_{w,q,r}[n] \ . \tag{5.114}$$

Since the weak paths do not contribute significantly to the magnitude of $z''_{q,r}[n]$, it may be assumed that

$$\begin{aligned} z''_{q,r}[n] &\approx \sum_{p=1}^{M} a_p e^{-j2\pi f_o S_p} m[n-k_p] \\ &= \sum_{p=1}^{M} g_p e^{jb_{n-k_p}\theta_T} \ , \end{aligned} \tag{5.115}$$

where $m[n] = e^{jb_n\theta_T}$ and $g_p = a_p e^{-j2\pi f_o S_p}$. Substituting the noiseless demodulates $z''_{q,r}[n]$ in (5.115) into the equation for bias removal in (5.111) gives

$$\begin{aligned}\hat{s}_{q,r}[i] &\approx \sum_{n=0}^{L-1}(\sum_{p=1}^{M} g_p e^{jb_{n-k_p}\theta_T} - \delta_q)(e^{-jb_{n-i}\theta_T} - \gamma) \\ &= \sum_{p=1}^{M} g_p \sum_{n=0}^{L-1} e^{jb_{n-k_p}\theta_T} e^{-jb_{n-i}\theta_T} - \delta_q \sum_{n=0}^{L-1} e^{-jb_{n-i}\theta_T} \\ &\quad -\gamma \sum_{p=1}^{M} g_p \sum_{n=0}^{L-1} e^{jb_{n-k_p}\theta_T} + \gamma\delta_q L \ . \end{aligned} \tag{5.116}$$

For the noiseless model of the reception, the bias-removed output of the crosscorrelation $\hat{s}_{q,r}[i]$ will have zero off-peak level if

$$\hat{s}_{q,r}[k_p] = g_p \frac{sin(\theta_T)}{sin(\theta_L)} L \tag{5.117}$$

$$\hat{s}_{q,r}[i] = 0 \quad for\ i \neq k_1, k_2, ..., k_M \ . \tag{5.118}$$

The data mapping constant δ_q may be obtained by substituting the zero off-peak condition in (5.118) into (5.116).

$$\sum_{p=1}^{M} g_p \sum_{n=0}^{L-1} e^{j(b_{n-k_p}-b_{n-i})\theta_T} - \delta_q \sum_{n=0}^{L-1} e^{-jb_{n-i}\theta_T} - \gamma \sum_{p=1}^{M} g_p \sum_{n=0}^{L-1} e^{jb_{n-k_p}\theta_T} + \delta_q\gamma L = 0$$
$$for\ \ i \neq k_1, k_2, ..., k_M\ (mod\ L) \tag{5.119}$$

Using the property of m-sequences in [26], it is a straightforward analysis to show that $\sum_{n=0}^{L-1} e^{j(b_{n-k_p}-b_{n-i})\theta_T}$ is a constant regardless of the value of k_p as long as $i \neq k_1, k_2, ..., k_M\ (mod\ L)$. The same property may be used to show that $\sum_{n=0}^{L-1} e^{-jb_{n-i}\theta_T}$ and $\sum_{n=0}^{L-1} e^{jb_{n-k_p}\theta_T}$ are both constants regardless of i and k_p. In fact, these two sums are complex conjugates of one another. From these results, (5.119) may be simplified and reduced to

$$\sum_{p=1}^{M} g_p\phi_o - \delta_q\phi_1 - \gamma \sum_{p=1}^{M} g_p\phi_1^* + \delta_q\gamma L = 0 \ , \tag{5.120}$$

where

$$\phi_o = \sum_{n=0}^{L-1} e^{jb_n\theta_T} e^{-jb_{n-i}\theta_T} \quad i \neq 0\ (mod\ L) \tag{5.121}$$

$$\phi_1 = \sum_{n=0}^{L-1} e^{-jb_n\theta_T} \tag{5.122}$$

$$\phi_1^* = \sum_{n=0}^{L-1} e^{jb_n\theta_T} . \tag{5.123}$$

Solving for δ_q,

$$\delta_q = \left[\frac{\phi_o - \gamma\phi_1^*}{\phi_1 - \gamma L}\right] \sum_{p=1}^{M} g_p . \tag{5.124}$$

Multiplying both sides of (5.124) by $\sum_{n=0}^{L-1} e^{jb_{n-k_p}\theta_T} = \phi_1^*$ gives

$$\delta_q = \left[\frac{\phi_o - \gamma\phi_1^*}{\phi_1^*(\phi_1 - \gamma L)}\right] \sum_{n=0}^{L-1} z''_{q,r}[n] , \tag{5.125}$$

where

$$\sum_{n=0}^{L-1} z''_{q,r}[n] = \sum_{p=1}^{M} g_p \sum_{n=0}^{L-1} e^{jb_{n-k_p}\theta_T} . \tag{5.126}$$

Equation (5.125) states that the data mapping constant δ_q is proportional to the DC value of the demultiplexed demodulates $z''_{q,r}[n]$. The constant of proportionality is uniquely determined by the period L, the transmission angle θ_T and the period-matched angle θ_L.

Expanding the zero off-peak output in (5.111),

$$\begin{aligned} \hat{s}_{q,r}[i] &= \sum_{n=0}^{L-1} z''_{q,r}[n] e^{-jb_{n-i}\theta_T} - \gamma \sum_{n=0}^{L-1} z''q, r[n] - \delta_q\phi_1 + \delta_q\gamma L \\ &= s_{q,r}[i] - \text{bias level} , \end{aligned} \tag{5.127}$$

where

$$\text{bias level} = \gamma \sum_{n=0}^{L-1} z''_{q,r}[n] + \delta_q\phi_1 - \delta_q\gamma L . \tag{5.128}$$

The "bias level" in (5.128) is the component necessary to convert a non-zero, off-peak output $s_{q,r}[i]$ to one with zero, off-peak output $\hat{s}_{q,r}[i]$. As in the case of δ_q, the "bias level" in (5.128) is also proportional to the DC value of the demultiplexed

demodulates $z''_{q,r}[n]$. This method of removing the "bias" level has the advantage that the "bias" can be removed after the initial crosscorrelation in (5.101)[14].

3) With the "bias" level removed from each of the $m_r Q$ output sequences, the next step is to recombine the $m_r Q$ output sequences by multiplexing.

$$s_r[q+kQ] \;=\; \hat{s}_{q,r}[k] \quad where \begin{cases} q = 0,1,2,...,m_rQ-1 \\ m = 0,1,2,....,L-1 \\ r = 0,1,2,...,X \end{cases} \tag{5.129}$$

4) At this point the major peaks of the strong paths are well isolated from the weak paths. The energy of the strong paths are concentrated in very short intervals of time. Therefore, the strong paths can be readily removed by replacing the major peaks and their impulse responses with zeros. Let $\tilde{s}_r[n]$ denote the output sequence with strong paths remove. Ideally $\tilde{s}_r[n]$ will contain only weak paths.

5) The next step is to project $\tilde{s}_r[n]$ from the arrival space back to the data space (inverse projection). As in the forward projection, the inverse projection is also implemented using sharp sequences (i.e. one sample per digit). Therefore, it is necessary to demultiplex the modified output $\tilde{s}_r[n]$ as follows.

$$\tilde{s}_{q,r}[n] \;\triangleq\; \tilde{s}_r[q+nQ] \quad where \begin{cases} q = 0,1,2,...,m_rQ-1 \\ m = 0,1,2,....,L-1 \\ r = 0,1,2,...,X \end{cases} \tag{5.130}$$

In step 2), the transmission angle was used in the forward projection. For the inverse projection, the period-matched angle is used instead. The necessity for using the period-matched angle in the inverse projection is detailed in the following matrix

[14]Alternatively, one may use one value of δ for all q demodulates. δ may be obtained by taking the average over all δ_q (i.e. $\delta = 1/(m_rQ)\sum_{q=1}^{m_rQ}\delta_q$). This has the benefit of further reducing the affect of noise.

analysis. As in the previous model for the demultiplexed demodulates in (5.113), let

$$\boldsymbol{z}_{q,r} \;=\; \boldsymbol{z}_{s,q,r} + \boldsymbol{z}_{w,q,r} \;, \tag{5.131}$$

where $\boldsymbol{z}_{s,q,r}$ is the q^{th} vector of the multiplexed, demodulated sequence associated with the strong paths, and $\boldsymbol{z}_{w,q,r}$ is the q^{th} vector of the demultiplexed, demodulated sequence associated with the weak paths. In addition, let $\boldsymbol{M}_T$ denote the cyclic, m-sequence matrix with transmission angle θ_T, and let $\boldsymbol{M}_L$ denote the cyclic, m-sequence matrix with period-matched angle θ_L. Using the phasor diagram in figure 5.11, the relationship between $\boldsymbol{M}_T$ and $\boldsymbol{M}_L$ is given by

$$\boldsymbol{M}_L \;=\; \kappa(\boldsymbol{M}_T - \boldsymbol{\gamma}) \tag{5.132}$$

$$\boldsymbol{M}_L{}^H \;=\; \kappa(\boldsymbol{M}_T - \boldsymbol{\gamma})^H \tag{5.133}$$

where the entries of $\boldsymbol{\gamma}$ are all identically γ, and κ is a constant which reflects the differences between the magnitude of $\boldsymbol{M}_T$ and $\boldsymbol{M}_T - \boldsymbol{\gamma}$. In addition, from (5.45),

$$\frac{1}{L}\boldsymbol{M}_L^H\boldsymbol{M}_L \;=\; \frac{\kappa^2}{L}(\boldsymbol{M}_T - \boldsymbol{\gamma})^H(\boldsymbol{M}_T - \boldsymbol{\gamma}) \;=\; I \;. \tag{5.134}$$

The q^{th} forward projection with bias removal may be written as

$$\hat{\boldsymbol{s}}_{q,r} \;=\; (\boldsymbol{M}_T - \boldsymbol{\gamma})(\boldsymbol{z}_q - \boldsymbol{\delta}_q) \;. \tag{5.135}$$

Recall in (5.125) that δ_q is proportional to the DC value of the 0-doppler, demultiplexed demodulates $z''_{q,r}[n]$. Since the exalted carriers of the doppler-scaled weak paths are shifted away from DC, δ_q is the data mapping constant of only the strong paths. Therefore, the cyclic crosscorrelation in (5.135) becomes

$$\hat{\boldsymbol{s}}_{q,r} \;=\; (\boldsymbol{M}_T - \boldsymbol{\gamma})(\boldsymbol{z}_{d,q,r} - \boldsymbol{\delta}_q) + (\boldsymbol{M}_T - \boldsymbol{\gamma})\boldsymbol{z}_{w,q,r} \;. \tag{5.136}$$

After strong path are removed by zeroing, the output of the crosscorrelation contains only the weak paths so that

$$\begin{aligned} \tilde{\boldsymbol{s}}_{q,r} &= (\boldsymbol{M}_T - \gamma)\boldsymbol{z}_{w,q,r} \\ &= \frac{1}{\kappa}\boldsymbol{M}_L z_{w,q,r} \ . \end{aligned} \tag{5.137}$$

To recover $\boldsymbol{z}_{w,q,r}$ from $\tilde{\boldsymbol{s}}_{q,r}$, multiply both side of (5.137) by $\frac{\kappa}{L}\boldsymbol{M}_L^H$. Using the identity in (5.134), the modified demodulated sequence is

$$\begin{aligned} \tilde{\boldsymbol{z}}_{q,r} &= \frac{\kappa}{L}\boldsymbol{M}_L^H \tilde{\boldsymbol{s}}_{q,r} \\ &= \frac{1}{L}\boldsymbol{M}_L^H \boldsymbol{M}_L \boldsymbol{z}_{w,q,r} \\ &= \boldsymbol{z}_{w,q,r} \ . \end{aligned} \tag{5.138}$$

The significance of (5.138) is that the inverse projection is implemented using the m-sequence matrix $\boldsymbol{M}_L^H$ with period-matched angle. Futhermore, once the demodulates $\boldsymbol{z}_{w,q,r}$ has been correctly interpolated to the true doppler of the weak paths, the matrix utilized to project the weak paths $\boldsymbol{z}_{w,q,r}$ in the data space onto the arrival space is the m-sequence matrix with transmission angle $\boldsymbol{M}_T$. The weak paths in the arrival space will also require bias removal just as in the case of the strong paths.

The actual signal processing of (5.138) is given by

$$\begin{aligned} \tilde{z}_{q,r}[k] &= \frac{1}{L}\sum_{n=0}^{L-1} \tilde{s}_{q,r}[n] e^{jb_{k+n}\theta_L} \\ &= cos(\theta_L)\sum_{n=0}^{L-1} \tilde{s}_{q,r}[n] + j\ sin(\theta_L)\sum_{n=0}^{L-1} \tilde{s}_{q,r}[n] b_{k+n} \ . \end{aligned} \tag{5.139}$$

Again, the summation $\sum_{m=0}^{L-1} \tilde{s}_{q,r}[n] b_{k+n}$ may be efficiently computed using the Fast Hadamard Transform in Appendix A.

6) The next step is to multiplex the $m_r Q$ modified, demultiplexed demodulates $\tilde{z}_{q,r}[k]$ to form a single modified, demodulate sequence for the r^{th} period. This is required for interpolation.

Multiplexing $\tilde{z}_{q,r}[k]$, the modified, demodulated sequence is

$$\tilde{z}_r[q+kQ] \;=\; \tilde{z}_{q,r}[k] \quad where \quad \begin{cases} q = 0,1,2,...,m_rQ-1 \\ k = 0,1,2,....,L-1 \\ r = 0,1,2,...,X \end{cases} \tag{5.140}$$

7) Steps 1) $\longrightarrow$ 6) are repeated until all (X+1) one-period segments are preprocessed.

8) Recall that the sampled, demodulated sequence $z''[m]$ in Part A, step 3) is divided into single-period segments in order to utilize the efficiency of the Fast Hadamard Transform. Each of the single-period segments of the modified, demodulated sequence in (5.140) must be recombined to form a single, modified, demodulated sequence of $(X+1)(m_rQL)$ samples long. First, let $\boldsymbol{z}_r$ denote the vector of samples for the r^{th} period.

$$\boldsymbol{z}_r \;=\; [z_r[0], z_r[1], ..., z_r[m_rQL-1]]^T; \qquad r = 1,2,...,X+1 \tag{5.141}$$

Then the $X+1$ vectors are recombine to form a single vector.

$$\tilde{\boldsymbol{z}} \;=\; [\tilde{\boldsymbol{z}}_1, \tilde{\boldsymbol{z}}_2, ..., \tilde{\boldsymbol{z}}_{x+1}]\,. \tag{5.142}$$

The HCCO preprocessing is completed. The vector $\tilde{z}$ is a modified form of the demodulated sequence consisting of only weak paths.

C) Forming the Residual Ambiguity Surface For Weak Path Detection.

The formation of the residual ambiguity surface from $\tilde{\boldsymbol{z}}$ is a straightforwad application of the broadband receiver. To interpolate from 0-doppler to the α^{th} doppler channel, $\tilde{\boldsymbol{z}}$ is phase adjusted.

$$\hat{z}_\alpha[m] \;=\; \tilde{z}[m]e^{j2\pi(1-e^{-\alpha})m}\,. \tag{5.143}$$

The second step implements the time compression. Let

$$x[m] = me^{\alpha} \tag{5.144}$$

$$c[m] = \lfloor x[m] \rfloor \tag{5.145}$$

$$\lambda[m] = x[m] - c[m] \, . \tag{5.146}$$

Then the time-compressed samples are

$$\tilde{z}_{\alpha}[m] = (1 - \lambda[m])\hat{z}_{\alpha_i}[c[m]] + \lambda[m]\hat{z}_{\alpha_i}[c[m]+1] \, . \tag{5.147}$$

2)In order to improve the output signal-to-noise ratio, X periods are summed.

$$\tilde{z}_{\alpha,sum}[n] = \sum_{m=0}^{X-1} \tilde{z}_{\alpha}[n + mm_r QL] \tag{5.148}$$

3) Crosscorrelate the summed demodulates $\tilde{z}_{\alpha,sum}[n]$ with the transmitted m-sequence utilizing FHT in appendix A.

Let $\tilde{s}_{\alpha}[k]$ be the output of this cyclic crosscorrelation so that the residual ambiguity surface is simply the combined outputs of all doppler channels given by

$$A_{hcco}[k, e^{\alpha}] \mid_{e^{\alpha}=e^{\alpha_j}} = \tilde{s}_{\alpha_j}[k] \, , \tag{5.149}$$

where α_j is an element of $\{\alpha_{min}, ..., \alpha_{max}\}$. From this residual ambiguity surface, the presence of weak paths may be determined. A summary of the steps in parts A), B), and C) is provided in Appendix B.

5.2.8 Illustrative Results

To illustrate the effectiveness of HCCO preprocessing, simulation results are plotted in figures (5.12) and (5.13). In figure (5.12), the noiseles reception consists of a strong path and a weak path. The peak of the weak path is 23 dB below the peak of the strong path reception. For the 511 digit m-sequence, the signal floor (median

floor) associated with the strong path is 27dB below the peak of the strong path. Therefore, the weak path-to-mutual floor level (WSM) prior to HCCO preprocessing is 4dB and the weak path cannot be detected. However, after HCCO preprocessing, the WSM ratio is approximately 27dB and the weak path is clearly detected [figure (5.13)]. Since the simulation assumes a noiseless reception, each run in this simulation would have given the same result.

In order to simulate the reception of two paths with different dopplers, time-delays and magnitude, two separate sequences of the m-sequence signal are generated at 0-doppler with a non-zero time-delay between the two sequences. One of the two sequences is scaled in magnitude to serve as the weak path. The weak path is linear interpolated to an off-doppler channel so that the two sequences will differ in doppler. At this point the two sequences will differ in doppler, time-delay and magnitude. These two sequences are added together to simulate the demodulated response of a two-path reception at 0-doppler.

5.3 Other Considerations

When filtering (i.e. transducer, front-end, and demodulate filters) is introduced in the analysis for preprocessing, the main issue concerns the impulse response of the filters. Ideally, each major peak with its associated impulse response is replaced with zeros at the output stage of the preprocessing. The disadvantage of this approach is that the degree of weak path corruption depends on the number of zeros replaced. Therefore, the detectability of weak paths will largely depend on the tradeoff between weak signal corruption and floor level reduction of the strong paths. In most instances, the impulse response of the transducer is determined from experimental measurements; therefore, the performance of the preprocessing under filtering will

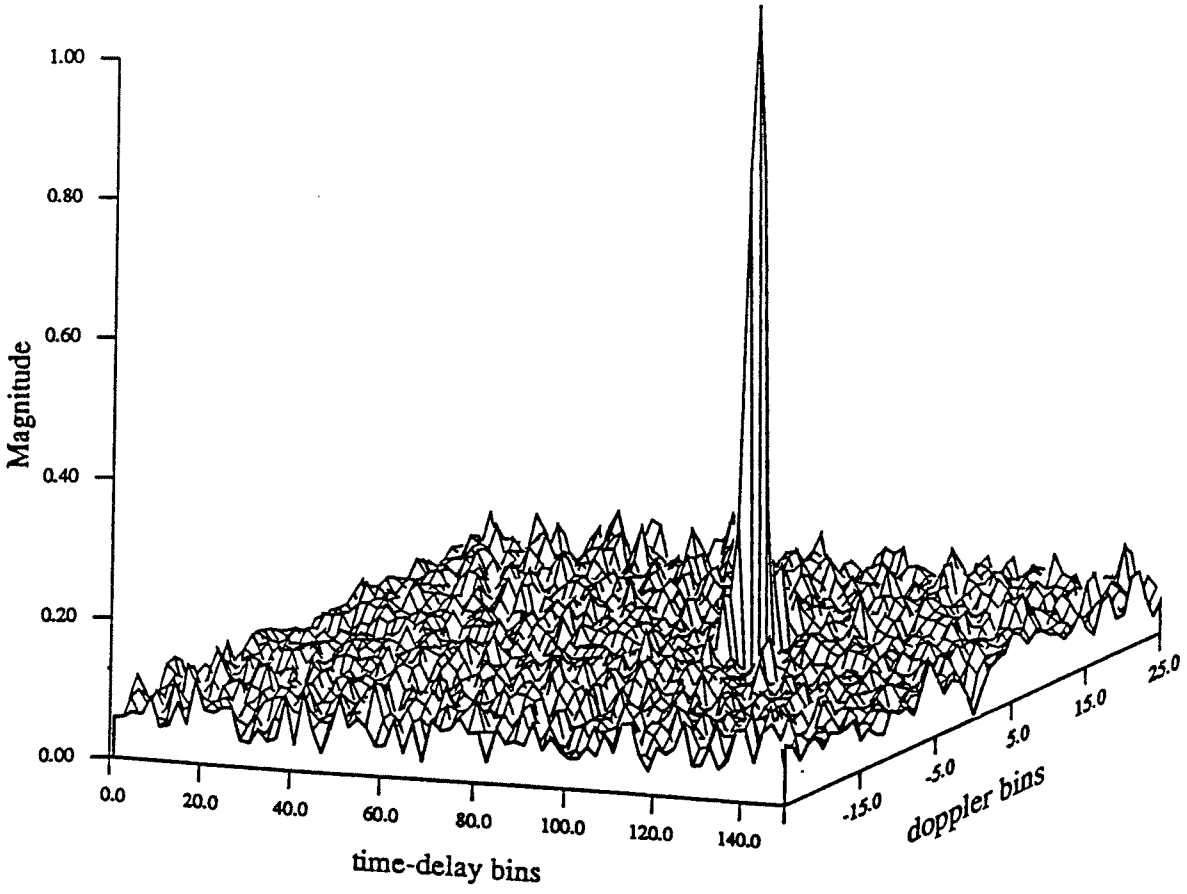

Figure 5.12: Ambiguity surface consisting of one strong path and one weak path.

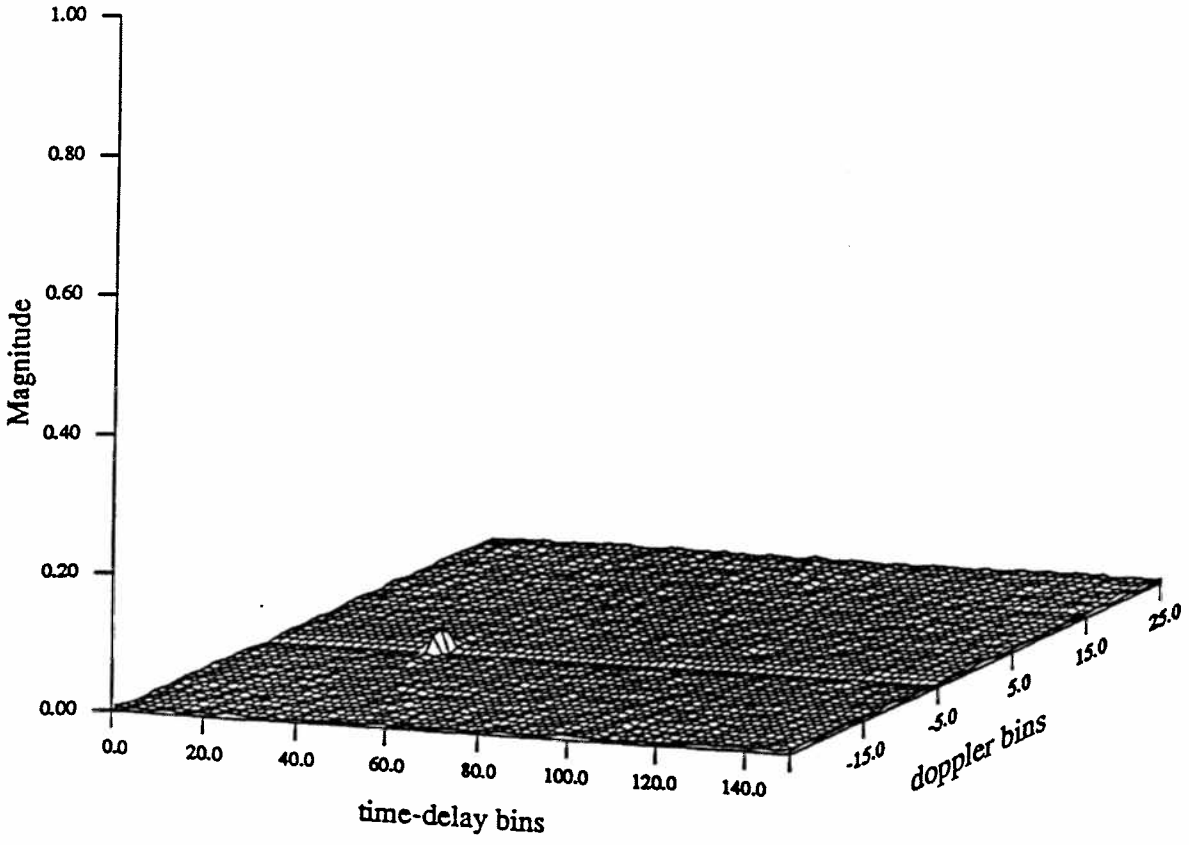

Figure 5.13: Strong path is removed through preprocessing. Weak path is clearly detected.

be evaluated along with experimental results.

In previous sections, it is assumed that all strong paths arrive at a single doppler channel. This is true in the case of a fixed-fixed bistatic sonar. In the case of a constant relative motion between the transducer and the receiver, HCCO preprocessing may require a slight modification. For example, in ocean acoustic tomography, each path would arrive at a slightly different doppler. This is known as the differential doppler and it is primarily due to the differences in sound speed at varying depths within the ocean. Since the preprocessing described in section (5.2) implements the *single-channel* elimination of the major peaks, the selected doppler channel (α_o) will be an "off-doppler" channel to most of the strong paths. Theoretically, at most one path will be "on-doppler" in any given doppler channel. On the other hand, if the differential doppler is small, preprocessing the strong paths at only one doppler channel may reduce the signal floor to a level that is much lower than the peaks of the weak paths.

If the doppler of the strong paths were significantly different, a variation of the HCCO preprocessing may be utilized. Assuming the true doppler for each and every strong path is known prior to preprocessing[15], the HCCO preprocessing may be repeated M times for M strong paths. Specifically, an HCCO preprocessing is implemented for each of the M doppler channels of the strong paths. At the output of each preprocessing, only the strong path corresponding to the selected doppler channel is eliminated through zeroing[16]. After M sequential repetitions, all M strong paths will be eliminated. Essentially, this method eliminates the major peak of each strong signal at its true doppler channel.

[15]The true doppler for each strong path may be obtained through the ambiguity surface of the reception without the preprocessing.

[16]For multiple period processing, all periods corresponding to the selected doppler channel must be preprocessed prior to the interpolation to the next doppler channel.

5.4 Constructing the Shift-Invariant Reference Ambiguity Surface

In Chapter IV the shift-invariant method for strong signal cancellation was discussed. This method has the adavantage that the strong paths may be eliminated by subtracting the shifted versions of the reference surface from the receiver ambiguity surface. Therefore, only one reference surface was required for storage. The simple, yet impractical way of constructing the reference surface discussed in chapter IV requires a reception consisting of only one-path. In the case of m-sequence signaling, a better approach is to utilize a variation of the HCCO preprocessing to create a reference surface from a multipath reception.

The construction of a reference ambiguity surface utilizing the HCCO preprocessing is quite simple. Instead of zeroing the peaks of the strong paths at the output of the crosscorrelation, one would retain the peak pulse associated with a *single* strong path and zero the rest of the output. In other words, the single, strong path becomes the desired signal and the rest of the paths are the interference. After zeroing, the residue would consist of only a single strong path. To create the reference ambiguity surface from the single path, the steps outlined in section 5.2 for weak path detection is carried out without further modification.

Suppose $\tilde{y}_{s,\alpha_i}[n]$ is the cleansed output containing a single strong path. The corresponding modified, demodulated sequence is

$$\tilde{z}_{s,\alpha_i}[n] \;=\; \tilde{y}_{s,\alpha_i}[n] \otimes m^*[n] \;. \tag{5.150}$$

Using the set of equations for interpolation from (5.54) and (5.55), $\tilde{z}_{s,\alpha_j}[n]$ for $\alpha_{min} \leq \alpha_j \leq \alpha_{max}$ can be computed from $\tilde{z}_{s,\alpha_i}[n]$. In combination, the modified, demodulated sequences for all doppler channels forms the reference demodulate surface $D_{r,b}[n, e^{\alpha}]$

discussed in section 4.4.1 for block processing.

For sliding processing (section 4.3), each of the modified, demodulated sequences is crosscorrelated with the m-sequence itself to form the output

$$\tilde{y}_{s,\alpha_j}[n] \;=\; \tilde{z}_{s,\alpha_j}[n] \otimes m[n] \;. \tag{5.151}$$

The combination of these outputs forms the reference ambiguity surface $A_{r,s}[n, e^{\alpha}]$.

CHAPTER VI

Noise Peaks

In previous chapters, it is assumed that the weak signal-to-noise ratio is large enough to detect the weak path's presence once the interference from strong paths are eliminated. If the reception can have at most one arrival and the arrival time is known a priori, then the problem may be set up as a simple binary detection problem utilizing the likelihood ratio test. The probability of false alarm P_F and the probability of detection P_D may be calculated given the median noise level and the signal-to-noise ratio (SNR). Unfortunately, in a doppler-scaled, multipath reception, the time-delay, doppler and the number of path arrivals are unknown. Under this circumstance, the problem of joint detection and estimation requires a generalized likelihood ratio test. This corresponds to setting a threshold on the envelope of the ambiguity surface. When a peak pulse is greater than this threshold, a path is assumed to be detected, and the parameters associated with the signal is determined by its location in the ambiguity surface. In the binary detection problem the threshold is determined by the median noise level in the reception. However, the noise level alone is insufficient in the case of a generalized likelihood ratio test.

Consider the case of a single-period reception. To arrive at the probability of false alarm one must calculate the probability that the highest peak of the noise

within the period exceeds the threshold. This would be followed by calculating the probability that the second highest peak of the noise exceeds the threshold and so forth. Furthermore, the probability of detection would depend on the signal-to-noise *peak* ratio (SNPR) as opposed to the SNR. Therefore, in the case of doppler-scaled, multipath reception, the problem of joint detection and estimation is closely tied to the level of noise peak within the reception.

In section 6.1, the noise peak of a single doppler channel is described. In the case of a single doppler channel, the noise-only reception may be modeled as an i.i.d. random sequence. The distribution of the noise peak is the distribution of the peak of this random sequence; hence, P_F may be approximated using the distribution of this peak. Alternatively, P_F may be modeled as a problem in level crossing. This is an accurate model when the threshold level is set high enough such that P_F is much smaller than one. Under this assumption, the crossing rate may be described by the Poisson distribution.

Section 6.2 describes the noise peak of the entire ambiguity surface. Since the ambiguity surface is a linear interpolation of the single doppler channel, it is of interest to determine the relationship between the noise peak of the ambiguity surface and the noise peak of a single doppler channel. Specifically, the problem is to determine the relative magnitude between the noise peak of the entire ambiguity surface and the noise peak of the single doppler channel. This provides a simple generalization of P_F from a single doppler channel to an ambiguity surface.

Finally, in section 6.3, the detectability of path arrivals is determined by the SNPR. The SNPR may be easily derived using the distribution of the noise peak in sections 6.1 and 6.2.

6.1 Noise Peak of Single Doppler Channel

6.1.1 Distribution of Noise Peak Under I.I.D. Assumption

The power spectral density of white gaussian noise $\Psi(f)$ may be approximated by a constant value, say $\frac{1}{2}N_o$ from -W to W and is zero everywhere else. W may represent the bandwidth of the match filter receiver. Since $\Psi(f) = \frac{1}{2}N_o rect(f/2W)$, the correlation function of the noise is

$$\psi(\tau) = N_o W sinc(2W\tau), \tag{6.1}$$

which equals zero when τ is a multiple of $\frac{1}{2W}$ except at $\tau = 0$. At $\tau = 0$, $\psi(\tau)$ has the value N_oW, which is the total noise power. Hence, samples of noise spaced in time by multiples of $1/2W$ are statistically independent zero-mean, gaussian random variables. For a single path reception with period T_p, the number of i.i.d. complex gaussian variables is

$$N_p = 2WT_p \tag{6.2}$$

The magnitude-squared noise reception may be modeled as

$$r_k = \mid x_k + jy_k \mid^2 , \tag{6.3}$$

where x_k and y_k are independent gaussian random variables with equal variance. Since the magnitude-squared output of the reception is of interest, the N_p random variables $r_k's$ are independent, exponentially distributed random variables given by

$$F_R(r) = 1 - e^{-\frac{r}{2\sigma^2}}, \tag{6.4}$$

where $\sigma^2 = R_x(0) = N_oW$ is the variance of the gaussian random variables. In practice, it is more efficient to compute the median level of the noise rather than the noise variance. It may be shown that the median value of the exponential distribution

(i.e. x_m s.t. $F_R(r_m) = 0.5$) is linearly proportional to the noise variance (i.e. $r_m = 2ln(2)\sigma^2$). Therefore, SNR and the signal-to-noise (median) ratio (SNR_m) are closely related.

The distribution of the peak of N_p independent random variables is given by the products of the individual distribution. Since they are also identically distributed, the maximum s of N_p i.i.d. random variables has the distribution

$$\begin{aligned} F_S(s) &= F_{R_1}(s)F_{R_2}(s) \cdots F_{R_{N_p}}(s) \\ &= \left[1 - e^{-\frac{s}{2\sigma^2}}\right]^{N_p} . \end{aligned} \tag{6.5}$$

Setting $F_S(s_m) = 0.5$, the median value of the peak is given by

$$s_m = -2\sigma^2 ln\left(1 - e^{\frac{-ln(2)}{N}}\right) . \tag{6.6}$$

Although the distribution of noise peak for exponential distribution in (6.5) is meaningful, the extensions to multiple doppler channels is somewhat limited.

Asymtotic Distribution of Extremes

The study of classical extreme value theory is concerned with distributional properties of the maximum of n i.i.d. random variables

$$s_n = max(r_1, r_2, ..., r_n) \tag{6.7}$$

as n becomes large. In central limit theory, one obtains an asymptotic normal distribution for the sum of many i.i.d. random variables regardless of their common original distribution function. A similar situation holds in extreme value theory. The classical extreme value states that if for some sequences of normalizing constants $a_n > 0$, b_n, $a_n(s_n - b_n)$ has a nondegenerate limiting distribution function $G(x)$, then G must have one of just three possible general families of distribution.

Furthermore, it is not necessary to know the detailed nature of F to know which limiting form of distribution it belongs to. In fact, this is determined by the behavior of the tail of $F_R(r)$ for large r [25].

The extreme value theory which is referred to as the Extremal Types Theorem was discovered first by Fisher and Tippett [15] and later proved in complete generality by Gnedenko [18]. The three Extreme Value Distributions are

$$Type\ I: \quad G(x) = exp(-e^{-x}), \qquad -\infty < x < \infty \tag{6.8}$$

$$Type\ II: \quad G(x) = \begin{cases} 0 & x \leq 0 \\ exp(-x^{-\alpha}) & \alpha > 0 \quad x > 0 \end{cases} \tag{6.9}$$

$$Type\ III: \quad G(x) = \begin{cases} exp(-(-x)^{\alpha}) & \alpha > 0 \quad x \leq 0 \\ 1 & x > 0 \end{cases} \tag{6.10}$$

For the special case of an exponential distribution in (6.4), the sequences a_n and b_n may be obtained using Theorem 1.5.1 in [25]. Briefly, the theorem states that for a sequence of real numbers u_n, if

$$n(1 - F_R(u_n)) \rightarrow \mu \qquad as\ n \rightarrow \infty \tag{6.11}$$

then

$$P[s_n \leq u_n] \rightarrow e^{-\mu} \qquad as\ n \rightarrow \infty. \tag{6.12}$$

For the exponential distribution, one may choose u_n to be

$$u_n = -2\sigma^2 ln\left(\frac{\mu}{n}\right) \tag{6.13}$$

such that $1 - F_R(u_n) = \frac{\mu}{n}$ holds. Then by (6.12)

$$P[s_n \leq -2\sigma^2 ln(\mu) + 2\sigma^2 ln(n)] \rightarrow e^{-\mu}\ . \tag{6.14}$$

Now, let $\mu = e^{-x}$ and (6.14) becomes

$$P[s_n \leq 2\sigma^2 x + 2\sigma^2 ln(n)] \rightarrow exp(-e^{-x}) , \tag{6.15}$$

which is the Type I form of the Extreme Value Distributions with

$$a_n = \frac{1}{2\sigma^2} \tag{6.16}$$

$$b_n = 2\sigma^2 ln(n) . \tag{6.17}$$

Rearranging variables, it may be shown that

$$P[s_n \leq x'] \rightarrow exp(-e^{-(2\sigma^2)^{-1}(x'-2\sigma^2 ln(n))}) . \tag{6.18}$$

Therefore, the distribution of the noise peak for N_p i.i.d. random variables may be approximated by

$$F_S(x') \approx exp(-e^{-(2\sigma^2)^{-1}(x'-2\sigma^2 ln(N_p))}) \tag{6.19}$$

for large N_p.

Simulation results of independent exponential random variables with $\sigma^2 = 1$ are plotted in figures (6.1) and (6.2). The points are plotted on double exponential probability paper. The linear approximation is used to determine the parameters a_n and b_n (i.e. $-ln(ln(-F_S(x'))) = a_n(x' - b_n)$ where $n = N_p$). Each point in figure (6.1) represent the maximum of 511 independent random variables, and a total of 150 maxima are plotted to approximate the probability distribution. As expected, a_n and b_n obtained from figure (6.1) agrees with the analytical results in (6.16) and (6.17).

In figure (6.2), the number of independent variables is still 511; however, three interpolated samples are added between every two independent variables. This is achieved by zero-padding the frequency domain of the independent variables. The

reason for finding maximum of interpolated sequences is twofold. As mentioned previously, for single period reception, samples that are spaced $1/2W$ apart are uncorrelated. However, the maximum of these N_p uncorrelated samples do not reflect the maximum of the period in continuous time. This is the practical consequence of discrete measurement of a continuous signal. The interpolation represents a better approximation to a continuous waveform. Second, the interpolation is an essential part of the doppler-scaling discussed in section 6.2. In figure (6.2), the maximum of (4x512) samples are plotted. The value of a_n does not vary significantly with interpolation; however, b_n increased from 12.3 to 14.3, which corresponds to an increase in the median level of about 0.7dB. As a comparison, the median of the individual exponential random variable is 1.4 dB while the median of the maximum of 511 i.i.d. exponential random variables is 11.1 dB.

The advantage of analyzing the peak distributions using the Extreme Value Distributions stems from the fact that the limiting distribution of the peak has the same form regardless of the actual distribution of the individual samples $F_R(r)$. As in the case of the interpolation in figure (6.2), the peak distribution is well approximated by the Type I Extreme Value Distribution given the appropriate values of a_n and b_n. On the other hand, the product of N_p distributions in (6.5) does not accurately reflect the peak distribution under interpolation.

6.1.2 Probability of False Alarm For High Threshold Level

Instead of analyzing the peak distribution of noise within a period of the reception, an alternate approach is to consider the number of *upcrossings* of a high threshold by a random noise process $r(t)$. Each threshold crossings may be regarded as points (i.e."time instants") at which the noise process exceeds a certain threshold

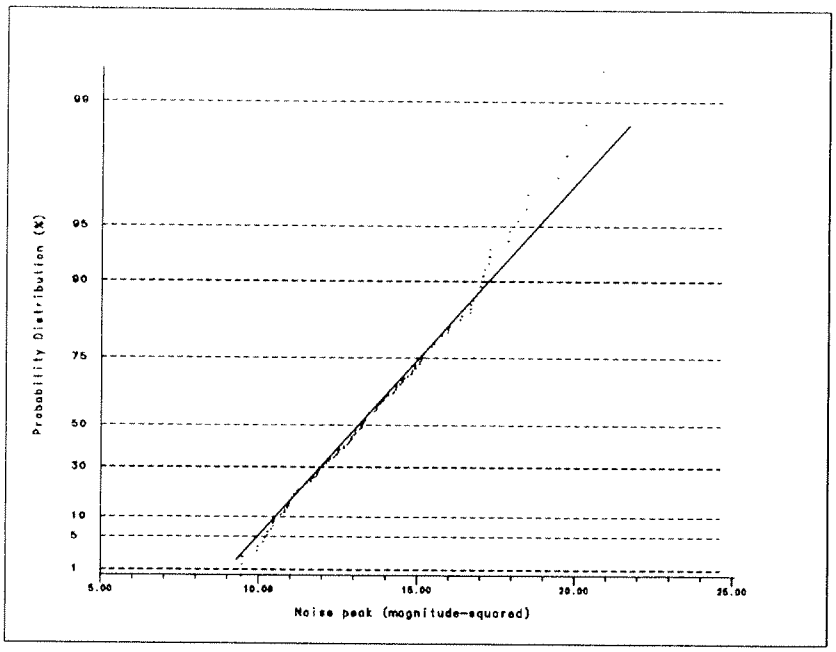

Figure 6.1: Distribution of the maximum of n=511 i.i.d. exponential random variables. The results are plotted on double exponential probability paper. ($a_n = 0.46$, $b_n = 12.3$)

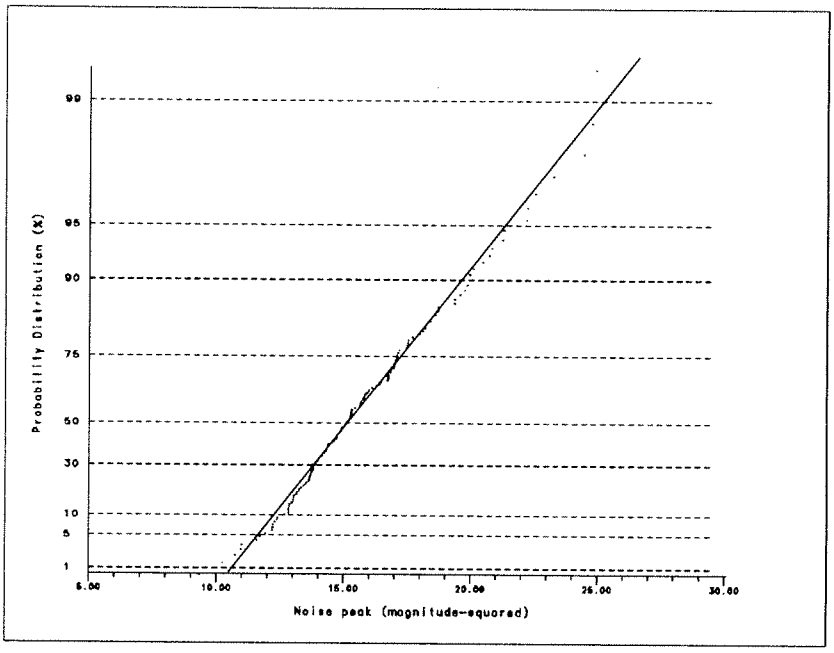

Figure 6.2: Distribution of the maximum of 2048 interpolated samples of n=512 i.i.d. exponential random variables. The results are plotted on double exponential probability paper. ($a_n = 0.42$, $b_n = 14.3$)

level u. These times of exceedances are stochastic in nature and may be viewed as a point process. It is possible to show that the point process of upcrossings of a level takes on an increasingly Poisson character as the threshold level becomes higher [25]. This is intuitively satisfying since threshold crossings at very high level are very rare events so that they can be considered statistically independent. The number of times n the noise process crosses the threshold u from below within an interval T may be approximated by the Poisson distribution

$$P_n(T) = \frac{(\lambda T)^n}{n!} e^{-\lambda T} . \tag{6.20}$$

For very high threshold level, the probability of false detection may be approximated by the probability that the noise process crosses the threshold at least once during the interval and is given by

$$\begin{aligned} Q_o &= 1 - e^{-\lambda T} \\ &\approx P_F . \end{aligned} \tag{6.21}$$

For very high threshold, λT, the expected value of the number of crossings within T, is kept small. And for $\lambda T << 1$,

$$Q_o \approx \lambda T . \tag{6.22}$$

In order to calculate Q_o in (6.22), the false alarm rate λ may be obtained using Rice's formula [32] given by

$$\lambda(u) = \int_0^\infty \dot{r} p(u, \dot{r}) d\dot{r} , \tag{6.23}$$

where $\dot{r} = dr/dt$ is the rate of change of the noise process $r(t)$ and $p(r, \dot{r})$ is the joint probability density function of $r(t)$ and $\dot{r}(t)$. A brief derivation of the formula may be found in Helstrom [21] and Papoulis [30].

For the special case of exponentially distributed noise process $r(t)$ given by

$$r(t) = \mid x(t) + jy(t) \mid^2, \tag{6.24}$$

where $x(t)$ and $y(t)$ are independent Gaussian processes with mean zero, it may be shown that at any time t, $r(t)$ and its first derivative $\dot{r}(t)$

$$\dot{r}(t) = 2x(t)\dot{x}(t) + 2y(t)\dot{y}(t) \tag{6.25}$$

is orthogonal (i.e. $R_{rr}(\tau)$ even implies $R_{r\dot{r}}(0) = 0$). Since the $r(t)$ and $\dot{r}(t)$ are jointly Gaussian [30], the two processes are independent at any time t. Therefore, using conditional probabilities, a modified form of Rice's formula is

$$\lambda(u) = \int_0^\infty \dot{r}p(\dot{r}/u)p(u)d\dot{n} \ . \tag{6.26}$$

The conditional probability density function is

$$\begin{aligned} p(\dot{r}/u) &= (2\pi R_{\dot{r}\dot{r}}(0))^{-\frac{1}{2}} exp\left[-\frac{\dot{r}^2}{2R_{\dot{r}\dot{r}}(0)}\right] \\ &= (8u\pi R_{\dot{x}\dot{x}}(0))^{-\frac{1}{2}} exp\left[-\frac{\dot{r}^2}{8uR_{\dot{x}\dot{x}}(0)}\right] \ , \end{aligned} \tag{6.27}$$

where

$$R_{\dot{r}\dot{r}}(0) = 4uR_{\dot{x}\dot{x}}(0) \ , \tag{6.28}$$

and the variance of the in-phase and quadrature components in (6.24) are assumed to be the same. The probability density function $p(u)$ is

$$p(u) = \frac{1}{2R_x(0)} exp\left[-\frac{u}{2R_x(0)}\right] \ , \tag{6.29}$$

where $R_x(0)$ is the variance of $x(t)$. Substituting the conditional probability in (6.27) and $p(u)$ in (6.29) into Rice's formula in (6.26),

$$\begin{aligned} \lambda(u) &= p(u)\left[\frac{2uR_{\dot{x}\dot{x}}(0)}{\pi}\right]^{\frac{1}{2}} \\ &= \left[\frac{uR_{\dot{x}\dot{x}}(0)}{2\pi R_x^2(0)}\right]^{\frac{1}{2}} exp\left[-\frac{u}{2R_x(0)}\right] \ . \end{aligned} \tag{6.30}$$

Using the approximation for the probability of false alarm in (6.22),

$$Q_o = TW_e \left[\frac{u}{2\pi R_x(0)}\right]^{\frac{1}{2}} exp\left[-\frac{u}{2R_x(0)}\right] , \tag{6.31}$$

where W_e is the r.m.s. bandwidth of the gaussian process $x(t)$ defined in [21] as

$$\begin{aligned} W_e &= \left[\frac{R_{\dot{x}\dot{x}}(0)}{R_{xx}(0)}\right]^{\frac{1}{2}} \\ &= \left[\frac{\int_{-\infty}^{\infty} f^2 S_x(f)df}{\int_{-\infty}^{\infty} S_x(f)df}\right]^{\frac{1}{2}} \end{aligned} \tag{6.32}$$

and $S_x(w)$ is the power spectral density of $x(t)$.

For the special case of m-sequence processing, the noise power spectral density at the output of the receiver is

$$S_x(w) = \frac{N_o}{2} sinc^2(T_d f) \quad for \quad -f_c \leq f \leq f_c . \tag{6.33}$$

and the r.m.s. bandwidth is given by

$$W_e = \frac{\sqrt{Q}}{\pi T_d} , \tag{6.34}$$

where Q is the number of cycles in a digit. Substituting (6.34) into the probability of false alarm in (6.31),

$$Q_o = \frac{\sqrt{Q}L}{\pi}\left[\frac{u}{2\pi}\right]^{\frac{1}{2}} exp\left[-\frac{u}{2}\right] , \tag{6.35}$$

In figure (6.3), the probability of false alarm in (6.35) is plotted against the probability of false alarm calculated using the peak distribution function (i.e. $P_F = 1 - F_S(u)$) in section 6.1.1. Note that for small P_F, the two approximations are essentially the same. For the Poisson distribution, the P_F is only valid when the crossing rate is small. When P_F is approximated using the extreme distribution, it is assumed that at most one sample may cross the threshold within one period (i.e. the 2nd, 3rd ...

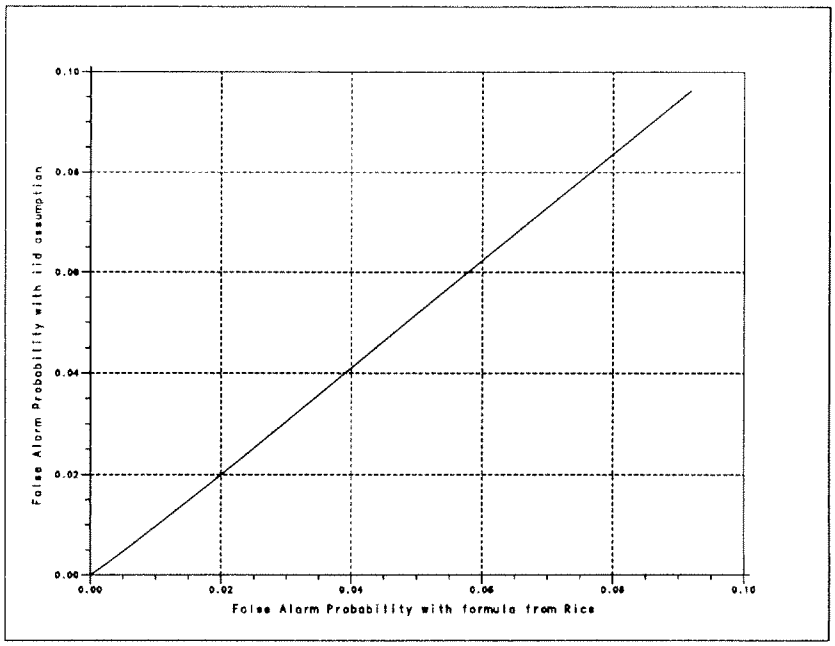

Figure 6.3: The probability of false alarm using the distribution of noise peak vs.the probability of false alarm using Rice's Formula.

n^{th} largest peaks are insignificant under high threshold). Hence, at higher threshold, both approximations are invalid. Although both methods lead to similar result in approximating P_F, the peak distribution function of section 6.1.1 plays a more important role in determining the signal detectability described in section 6.3.

6.2 Noise Peak of Ambiguity Surface

In section 6.1, the extreme value distribution was discussed as a means of evaluating the probability of false alarm. This sections discusses the noise peaks of ambiguity surface by extending the results given in the previous section. The primary goal of this section is to compare the extremes of the ambiguity surface with the extremes of the single-doppler channel. The ratio of the two extremes would indicate how much larger the peak surface noise is relative to peak noise of a single doppler channel.

At first, one may arrive at a distribution function for the noise peak by assum-

ing i.i.d. samples for the entire ambiguity surface (i.e. all doppler channels are independent). Although this would simplify the analysis of noise peaks, it does not accurately reflect the presence of "coupling" among doppler channels.

For a single-channel processor, the ambiguity surface is obtained by interpolating the output of the sampled, demodulated reception. Therefore, the "off-doppler" noise samples are simply interpolated versions of the noise samples from the 0-doppler channel[1]. For a fixed noise sequence at the 0-doppler channel, the noise sequence at "off doppler" channels are deterministic. It may be thought that due to the deterministic nature of the sequence at "off doppler" channels, one may derive a deterministic upper bound for the noise peak for the ambiguity surface. In particular, given the magnitude of the noise peak at 0-doppler, the question is whether or not there exits an upper bound on the magnitude of the noise peak for the entire surface. One upper bound for the noise peak is given by the total noise energy within the doppler channel. However, this upper bound does not provide any meaningful description of the noise peak. Unfortunately, a tighter upper bound does not exist in general. The ambiguity surface of a single-path reception may be described as a sum of the signal ambiguity function and the noise ambiguity function or cross-ambiguity function. Specifically,

$$A(\tau, e^{\alpha}) \;=\; A_s(\tau, e^{\alpha}) + A_n(\tau, e^{\alpha}) \;, \tag{6.36}$$

where the signal ambiguity function is

$$A_s(\tau, e^{\alpha}) \;=\; \int_0^{P_T} m(e^{\alpha-\beta}(t-\tau))m^*(t)dt \;. \tag{6.37}$$

and the cross-ambiguity function of the noise is

$$A_n(\tau, e^{\alpha}) \;=\; \int_0^{P_T} n(e^{\alpha}(t-\tau))m^*(t)dt \;. \tag{6.38}$$

[1]The output of the single-channel processor is assumed to be fixed at 0-doppler output.

Due to the deterministic nature of the signal ambiguity function, properties of the signal ambiguity function may be pre-determined. However, the cross-ambiguity function is random; hence, it is impossible to derive a tigher *energy* upper bound other than the total noise energy within any doppler channel. In other words, the properties of the ambiguity function applies to the signal and not the noise. Any attempt to describe the noise peak must be based on stochastic analysis; hence, a stochastic upper bound would be more appropriate.

6.2.1 Noise Peak With Independent Doppler Channels

A simple extension from the noise peak of a single-doppler channel to the noise peak of the ambiguity surface is to assume independent doppler channels. This assumption is briefly discussed by Helstrom in [21]. The number of independent doppler channels within the ambiguity surface may be approximated by the correlation between doppler channels. If M_p independent channels are assumed, then the noise peak of the ambiguity surface is the same as the noise peak of a single-doppler channel with M_p periods. Consider the special case of m-sequence signaling with AWGN, the *narrowband* noise outputs at two doppler channels f_i and f_j are given by

$$n_i(\tau) = \int n_w(t)m^*(t-\tau)e^{j2\pi f_i t}dt \tag{6.39}$$

$$n_j(\tau) = \int n_w(t)m^*(t-\tau)e^{j2\pi f_j t}dt \ , \tag{6.40}$$

where $n_w(t)$ is the AWGN with noise power $N_o/2$. The cross spectral density of the noise is

$$S_{ij}(f) = S(f-f_i)S^*(f-f_j)S_w(f) \ , \tag{6.41}$$

where $S_w(f) = N_o/2$ is the power spectral density of the noise and $S(f)$ is the signal spectrum given in [7] by

$$\begin{aligned} S(f) &= P(f)M(f) \\ &= (-1)^{f_o T_d} A T_d e^{-j\pi f T_d} sinc((f_o - f)T_d) \sum_{n=1}^{L} e^{jb_n\theta} e^{-j2\pi f T_d n} , \end{aligned} \tag{6.42}$$

and T_d, b_k, θ, L are the m-sequence parameters defined in appendix B. The correlation $C_{ij}(0)$ between $n_i(\tau)$ and $n_j(\tau)$ at zero delay may be calculated by

$$\begin{aligned} C_{ij}(0) &= E[n_i(\tau)n_j^*(\tau)] \\ &= \int S_{ij}(f)df \\ &= \frac{N_o}{2} \sum_{k=1}^{L} e^{-j2\pi f_d T_d k} \int P(f - f_d)P^*(f)df \\ &= C_M(f_d)C_P(f_d) , \end{aligned} \tag{6.43}$$

where

$$\begin{aligned} C_M(f_d) &= \frac{N_o}{2} \sum_{k=1}^{L} e^{-j2\pi f_d T_d k} \\ &= \frac{N_o}{2} \frac{sin(\pi T_d L f_d)}{(\pi T_d f_d)} e^{-j(L-1)\pi T_d f_d} , \end{aligned} \tag{6.44}$$

$$\begin{aligned} C_P(f_d) &= \int P(f - f_d)P^*(f)df \\ &= (AT_d)^2 \int sinc[T_d(f - f_d)]sinc[T_d f_d]df \\ &= (\pi T_d^2 f_d)^{-1} cos(\pi T_d f_d) , \end{aligned} \tag{6.45}$$

and

$$f_d = f_i - f_j . \tag{6.46}$$

Both $C_M(f_d)$ and $C_P(f_d)$ are functions of the difference in frequency shifts. However, $C_M(f_d)$ is usually much narrower than $C_P(f_d)$ so that the first zero of $C_{ij}(0)$ is the same as the first zero of $C_M(f_d)$. The first zero of $C_M(f_d)$ would determine the

minimum frequency shift $f_d = F_o$ required for two doppler channels to be considered independent. Therefore, if the ambiguity surface has a doppler spread of $(f_{max} - f_{min})$, the total number of independent doppler channels is

$$M_p = \frac{f_{max} - f_{min}}{F_o} . \tag{6.47}$$

The P_F may be determined by the distribution of the maximum in (6.5) with N_p replaced by $M_p N_p$ or with Rice's Formula in (6.31) with T replaced by $M_p T$. In some cases (i.e. high threshold), the independent-channel assumption may be justified; however, under lower threshold, the approximation may be inappropriate. Furthermore, it is assumed that the number of independent channels for narrowband processing is the same as the number of independent channels for broadband processing. To get a more precise form of the peak noise distribution, the extreme value distribution in section 6.1.1 may be utilized.

6.2.2 Distribution of Noise Peak Using Extreme Value Distribution

In section 6.1.1, the Type I extreme value distribution for the exponentially distributed random variables is introduced. It is shown that the parameter a_n is a function of the variance σ^2, while b_n increases logarithmically with increasing number of independent samples. In the case of the ambiguity surface, the samples are still exponentially distributed; however, the samples from different doppler channels may be highly correlated. As mentioned previously, the extreme value distribution is a limiting form of distribution which require very little knowledge of the sample distribution. In fact, if the correlation function $E[r_i r_{i+n}]$ decays to zero at a sufficient rate, the Type I extreme value distribution will hold for dependent sequences [25].

Using the Type I extreme value approximation, the distribution of the noise peak

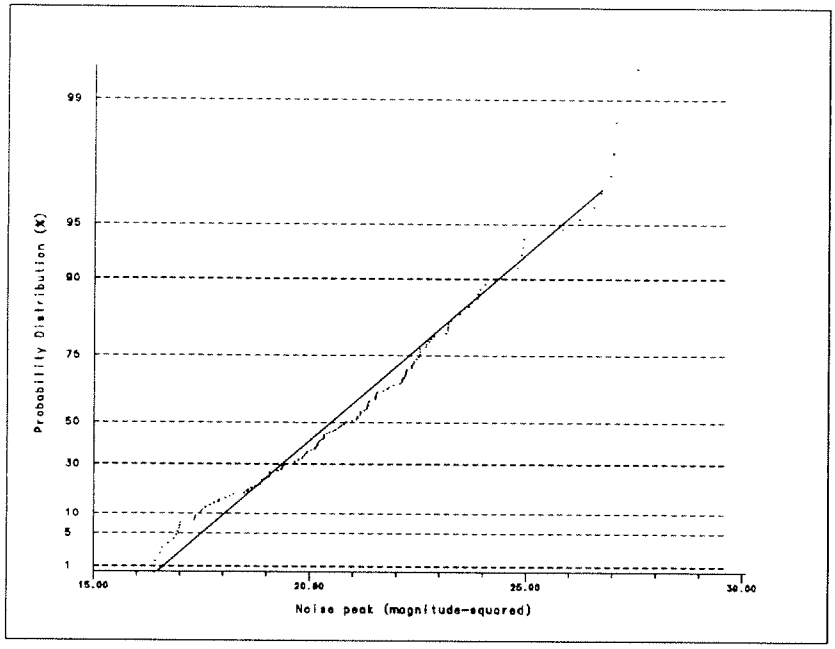

Figure 6.4: Distribution of the noise peak of the ambiguity surface (511 digits, 52 doppler bins; 1 doppler bin=0.58 knots). The results are plotted on double exponential probability paper. ($a_a = 0.49$, $b_a = 19.74$)

for the ambiguity surface may be approximated by

$$F_a(x_a) \approx exp(-e^{a_a(x_a - b_a)}) \tag{6.48}$$

for some constants $a_a > 0$, b_a depending on the length of the period and the number of doppler channels in the ambiguity surface. In figure (6.4), the noise peaks of 150 ambiguity surfaces under m-sequence signaling are plotted on double exponential paper. The straight line in the figure is the distribution function for a double exponential distribution. The P_F may be readily calculated from this double exponential distribution. The normalized parameters $2a_a\sigma^2$ and $b_a/2\sigma^2$ for varying surface size are plotted in figures (6.5) and (6.6) respectively. Since the parameter $2a_a\sigma^2$ remains relatively constant, the double exponential approximation will only vary with b_a for different surface sizes.

In order to compare the noise peak of a single doppler channel versus the noise

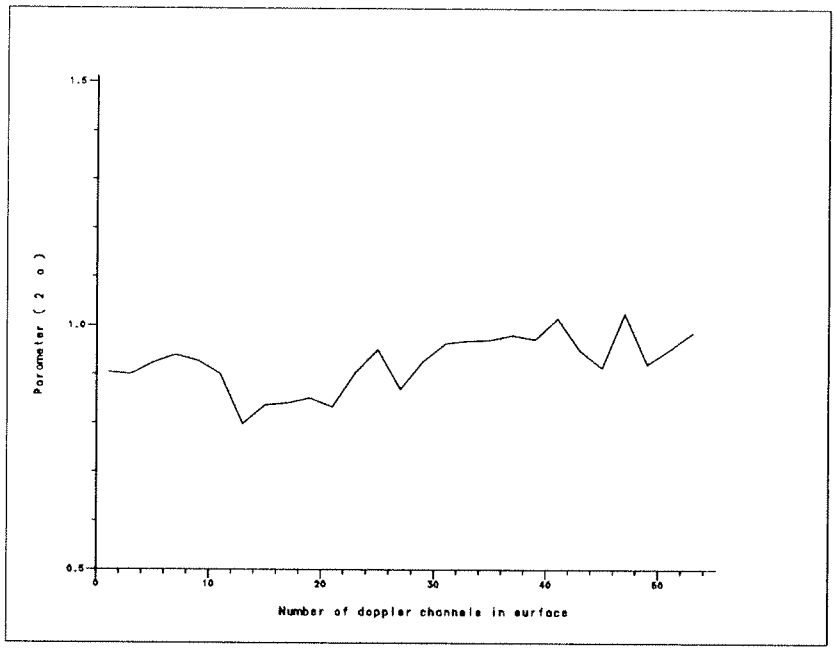

Figure 6.5: A plot of the normalized parameter $2a_a\sigma^2$ for different size of the ambiguity surface. A doppler channel is equivalent to 0.58 knots.

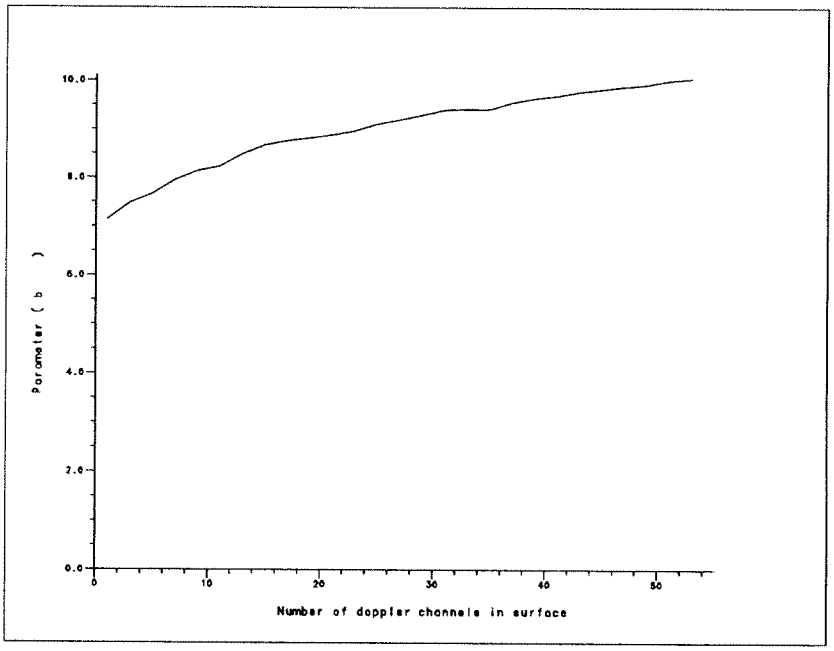

Figure 6.6: A plot of the normalized parameter $b_a/2\sigma^2$ for different size of the ambiguity surface. A doppler channel is equivalent to 0.58 knots.

peak of the ambiguity surface, one may evaluate the differences between their median levels. Specifically, let

$$\begin{aligned} F_s(x_s) &= exp(-e^{-a_s(x_s-b_s)}) \\ &\approx exp(-e^{-(2\sigma^2)^{-1}(x_s-2\sigma^2 ln(N))}) \end{aligned} \tag{6.49}$$

be the distribution of the noise peak for a single doppler channel. Additionally, let $x_{s,m}$ be the median level of the peak of a single doppler channel when $F_s(x_{s,m}) = 1/2$, and $x_{a,m}$ be the median level of the surface peak when $F_a(x_{a,m}) = 1/2$. Evaluating (6.48) and (6.49) at 1/2 give

$$(2\sigma^2)^{-1}(x_{s,m} - 2\sigma^2 ln(N)) = 0.37 \tag{6.50}$$

$$a_a(x_{a,m} - b_a) = 0.37\ , \tag{6.51}$$

and the difference between the median levels is

$$x_{a,m}(dB) - x_{s,m}(dB) = 10log(0.37a_a^{-1} + b_a) - [10log(0.37 + ln(N)) + 10log(2\sigma^2)]\ . \tag{6.52}$$

Since a_a does not vary significantly with increasing surface size, let $a_a \approx a_s$ and the difference in (6.52) becomes

$$x_{a,m}(dB) - x_{s,m}(dB) = 10log(0.37 + b'_a) - 10log(0.37 + ln(N))\ , \tag{6.53}$$

where $b'_a = \frac{b_a}{2\sigma^2}$. For the special case of m-sequences with $N = 511$ independent samples, b'_a varies from 7.1 to 10.0 for surface sizes ranging from ± 0.58 knots to ± 15 knots. This corresponds to a difference in the median level from 0.5dB to 2.0dB; a small but significant increase in the median level.

Although the limiting distribution function provides an adequate approximation to the distribution of the noise peak, the parameters a_a and b_a need to be evaluated

on a case by case basis. Each type of ambiguity surface will have its own set of parameters. Therefore, the distribution of the noise peak cannot be generalized for all types of signals.

6.3 Signal-to-Noise Peak Ratio

In sections 6.1 and 6.2, different methods for calculated the P_F was introduced. This section describes the likelihood of signal detection with additive noise. Usually, signal detectability is analyzed using the P_D which is a function of both the P_F and the SNR. In the simple case of a single arrival, the P_D may be approximated by the method described in Hestrom (pp.309-312)[21]. Specifically, he plotted the SNR versus the time-bandwidth product by first using the equation for P_F in (6.31) to calculate the threshold level u and then applying the result of P_D for the case of unknown phase (i.e. known time-delay, unknown phase) to determine the value of the SNR attaining the specified value of P_D. However, in a multipath reception the number of arrivals is unknown and the P_D is difficult to evaluate. Instead the detectability of arrivals at reasonable P_F is determined by the signal-to-noise peak ratio (SNPR). In contrast to the SNR, the SNPR will indicate the strength of the signal relative to the threshold u determined by the statistics of the noise peak.

As described in the beginning of chapter VI, the median noise level is a good approximation of the noise variance. Similarly, the variance of the noise peak may be approximated by the median of the noise peak. Although the median noise level for the ambiguity surface can be readily calculated, the median of the noise peak will be approximated using the Type I extreme value distribution described in section 6.2.2. The SNPR may be defined as

$$SNPR \triangleq 10log\left[\frac{A^2}{x_{a,m}}\right], \tag{6.54}$$

where $x_{a,m}$ is the median value of the noise peak and A is the magnitude of the signal. Using the approximation in section 6.2.2,

$$SNPR = 10log\left[\frac{A^2}{2\sigma^2(0.37+b'_a)}\right] . \tag{6.55}$$

As mentioned above, the median noise level m_n can be readily calculated by taking the median value of the ambiguity surface. Since $m_n = 2ln(2)\sigma^2$ is the magnitude-squared median level of a single noise variable, the SNPR may be written as

$$\begin{aligned} SNPR &= 10log\left[\frac{ln(2)A^2}{m_n(0.37+b'_a)}\right] \\ &= SNR - NP , \end{aligned} \tag{6.56}$$

where

$$NP = 10log\left[\frac{0.37+b'_a}{ln(2)}\right] . \tag{6.57}$$

Therefore, NP represents the decrease in detectability of the signal arrival due to noise peaks. For the case of m-sequences, NP ranges from 10.3dB to 11.8dB for surface sizes of ± 0.58 knots to ± 15.0 knots. This range of NP suggests that NP is largely due to the noise peak of the single doppler channel. Extensions to multiple doppler channels does not increase the level of NP significantly. Although the level of NP may be large for long periods, signal detectability will ultimately depend on SNR. For m-sequences, the SNR will depend on two factors; the length of the m-sequence L and the number of periods M that is averaged coherently. Specifically, the SNR for m-sequences is given by

$$SNR = 10log\left[\frac{MA_m^2L}{m_n}\right] , \tag{6.58}$$

where A_m is the magnitude of the signal prior to pulse compression.

CHAPTER VII

Summary and Conclusion

This dissertation is concerned with the detection of weak, broadband signals in the presence of strong signal interference. The basic philosophy adopted in this dissertation is to approximate the time-delay by a linear, time-varying model so that the presence of a path arrival is indicated by the peak pulse of a 2-D receiver surface known as the broadband ambiguity surface. Due to the presence of the floor level (i.e. 2-D sidelobes) associated with strong paths, the peaks of the weak paths are undetected. To detect the weak paths, the floor level of the strong paths must be removed. Accordingly, this dissertation discussed two computationally efficient method for strong path cancellation under broadband processing: (1) The Shift-Invariant Method for Strong Path Cancellation and (2) the Hyperslice Cancellation by Coordinate Zeroing (HCCO) preprocessing.

Chapter II presented some of the basic mathematical relationships, terminology and concepts in narrowband, radar/sonar resolution. For single parameter resolution, it is shown that travel time resolution is inversely proportional to the bandwidth while the resolution in doppler is inversely proportional to the signal duration. For the combined resolution, the ambiguity function is the appropriate tool for analyzing radar/sonar signals. It is shown that resolution in the 2-D ambiguity surface can only

be reduced at the expense of increasing floor level. This is due to the property that the volume of the ambiguity surface is a constant regardless of the type of signal transmitted.

Chapter III discussed some of the fundamental differences between narrowband and broadband processing of radar/sonar signals. For narrowband signals, the received signal is simply modeled as doppler-*shifted* signal. Consequently, matched-filters for individual doppler channels are simply doppler-*shifted* versions of one another. For broadband signals, the received signal is not only doppler-shifted but time-scaled as well. This time-scaling of the baseband signal introduces additional complexities in a broadband receiver. Depending on the type of receiver utilized, either the matched-filters or the received signal must be rescaled in time. Chapter III introduced two different broadband receivers. The first receiver, processing using transmitter time scaling (PUTTS), rescales the matched-filters to compensate for the doppler-scale of the received signal. For single-period processing, the linear crosscorrelation between the matched-filters and the received signal may be efficiently computed via FFT. The second method, processing using receiver time scaling (PURTS), is utilized when multiple-period processing and cyclic crosscorrelation are desired. In this case, the matched-filter is fixed while the received signal is rescaled in time. Since the matched-filter is fixed, it is easier to obtain a computationally efficient scheme to implement the crosscorrelation. For m-sequence signaling, the cyclic crosscorrelation is implemented using the Fast Hadamard Transform discussed in Appendix A.

The Shift-Invariant Method for Strong Path Cancellation (SIMSPC) in chapter IV is a computationally efficient means for strong path cancellation. The primary goal is to construct a shift-invariant reference surface such that the strong signal and its floor level may be canceled by subtracting a shifted version of the reference

surface from the receiver surface. The shift-invariance in doppler is achieved by moving the doppler factor into the exponent. The shift-invariance in time-delay is more complicated. For the case of a sliding processing receiver (i.e. receiver utilizing linear crosscorrelation), the shift-invariance in time-delay is accomplished by appropriate remapping of the time-delay variable. However, for a block processing receiver (i.e. receiver utilizing cyclic crosscorrelation), this is no longer true. Instead, a reference surface constructed from two periods of the demodulate surface is stored in memory. It is shown that the envelope of the demodulate surface is shift-invariant in both doppler and time-delay. Simulation result indicate that the signal floor level may be lowered by 30-40 dB.

In chapter V, the HCCO preprocessing is introduced. Instead of subtracting the entire floor level, the strong paths are removed at a single doppler channel. For m-sequences, the matched-filter output of the strong paths are compressed into very narrow pulses. If weak paths are present in the reception but at a different doppler, the energy of the weak paths would be uniformly distributed across the entire period of the matched filter output. The basic principle of HCCO preprocessing is to eliminate the strong paths by zeroing the peaks associated with the strong paths before processing for the entire ambiguity surface. The zeroing of these peaks does introduce distortion to the weak paths as well. However, numerical analysis of m-sequences indicate that even when half of the period is zeroed, the weak signal-to-mutual floor ratio remains relatively high at 25 dB for L=511 digits.

The problem of noise peaks is discussed in chapter VI. Within the ambiguity surface, noise peaks maybe falsely identified as path arrivals. For the single doppler channel, the P_F may be approximated by the distribution of the noise peak. Under the i.i.d. assumption, the distribution of the noise peak may be readily computed.

However, for multiple-channel surface, the doppler channels are highly correlated and the i.i.d. assumption is invalid. It is shown that the extreme value distribution may be utilized as an approximation to the noise peak when the noise samples are correlated. For doppler channels of interest, simulation result indicate that the noise peak of the entire ambiguity surface is only 2 dB above the noise peak of the single doppler channel.

Throughout this dissertation it is assumed that the search parameters for the received signal consist of a constant time delay and a doppler factor. In the case of SIMSPC, the modelling and the remapping of the search parameters are essential to the shift-invariant property of the broadband ambiguity surface. In the case of HCCO preprocessing, the remapping of the doppler and time-delay variable are not required. However, HCCO preprocessing does rely on signals having "good" autocorrelation property. Furthermore, the characteristics of the inverse projection is critical to the degree of floor reduction. The advantage of SIMSPC over HCCO preprocessing is that SIMSPC will work with any type of signal as long as a reference surface can be constructed. On the other hand, when the time-delay is more accurately modeled with the addition of a third term (i.e. the second derivative of $\tau(t)$), the HCCO preprocessing will be superior to SIMSPC since HCCO preprocessing eliminates the strong signal at one doppler channel. In future studies, the tradeoffs between SIMSPC and HCCO preprocessing may be further analyzed. The tradeoffs will most likely depend on the type of signal transmitted and the model of its reception. Additionally, it may be possible to extend HCCO preprocessing to signals without "good" autocorrelation property. For instance, it may be possible to transform the matched-filter output to a domain where energy of the weak and strong is further isolated. Finally, in this dissertation it is assumed that only one

sensor is utilized in the receiver. Future studies may investigate the possibility of utilizing beamforming with multiple sensors in conjunction with the methods for weak signal detection.

APPENDICES

APPENDIX A

Efficient Computation of M-sequence Correlation Through Fast Hadamard Transform

This appendix describes an efficient means of m-sequence cross-correlation through Fast Hadamard Transform (FHT). It is also known as the "Hadamard processing" for m-sequence signals. The problem with the direct method of computation is that the cyclic cross-correlation requires L^2 additions where L is the period of the m-sequence (i.e. $L = 2^k - 1$). The output of the cyclic cross-correlation may be written in matrix form as

$$\boldsymbol{Y}_{\alpha_o} = \boldsymbol{M}_{2^k-1}\boldsymbol{z}_{\alpha_o} , \tag{A.1}$$

where where $\boldsymbol{z}_{\alpha_o}$ is a $2^k - 1$ vector composed of the demodulated sequences of the α_o^{th} doppler channel and is given by

$$\boldsymbol{z}_{\alpha_o} = [z_{\alpha_o}[0], z_{\alpha_o}[1], \cdots, z_{\alpha_o}[2^k - 1]]^T . \tag{A.2}$$

The computation in (A.1) can be drastically reduced by exploiting the equivalence between the m-sequence matrix and the Walsh-Hadamard matrices [4], [19]. Due to the special form of the Fast Hadamard matrix, the matrix multiplication may be implemented through a "butterfly" similar to those of Fast Fourier Transform. In fact, the matrix multiplication requires only $(L+1) \cdot log_2(L+1)$ additions. In

[11] and [9], the equivalence between m-sequence matrix and the Walsh-Hadamard matrices has been reorganized to provide a step by step approach to implementing the m-sequence correlation through FHT.

A.1 Fast Hadamard Transform

As in the case for the Discrete Fourier Transform, the Hadamard Transform may be described in terms of a matrix multiplication. The matrix used in the transformation is known as the Walsh-Hadamard matrix which has only ± 1 as its elements. The Walsh-Hadamard matrix may be specified recursively by

$$\begin{aligned} \boldsymbol{H}_1 &= [1] \\ \boldsymbol{H}_i &= \begin{bmatrix} \boldsymbol{H}_{i-1} & \boldsymbol{H}_{i-1} \\ \boldsymbol{H}_{i-1} & -\boldsymbol{H}_{i-1} \end{bmatrix}, \end{aligned} \tag{A.3}$$

and these matrices exist only for orders of 2^k.

$$\boldsymbol{H}_4 = \begin{bmatrix} 1 & 1 & 1 & 1 \\ 1 & -1 & 1 & -1 \\ 1 & 1 & -1 & -1 \\ 1 & -1 & -1 & 1 \end{bmatrix}. \tag{A.4}$$

The associated butterfly for the 4^{th} order Walsh-Hadamard matrix is provided in figure (A.1).

In order to establish an equivalence between the Walsh-Hadamard matrix with the m-sequence matrix, it is convenient to express the Walsh-Hadamard matrix over GF(2)[1].

[1]The equivalence between the Walsh-Hadamard matrix and the m-sequence matrix is easily shown over GF(2). However, the implementation of the cross-correlation through FHT is over the reals.

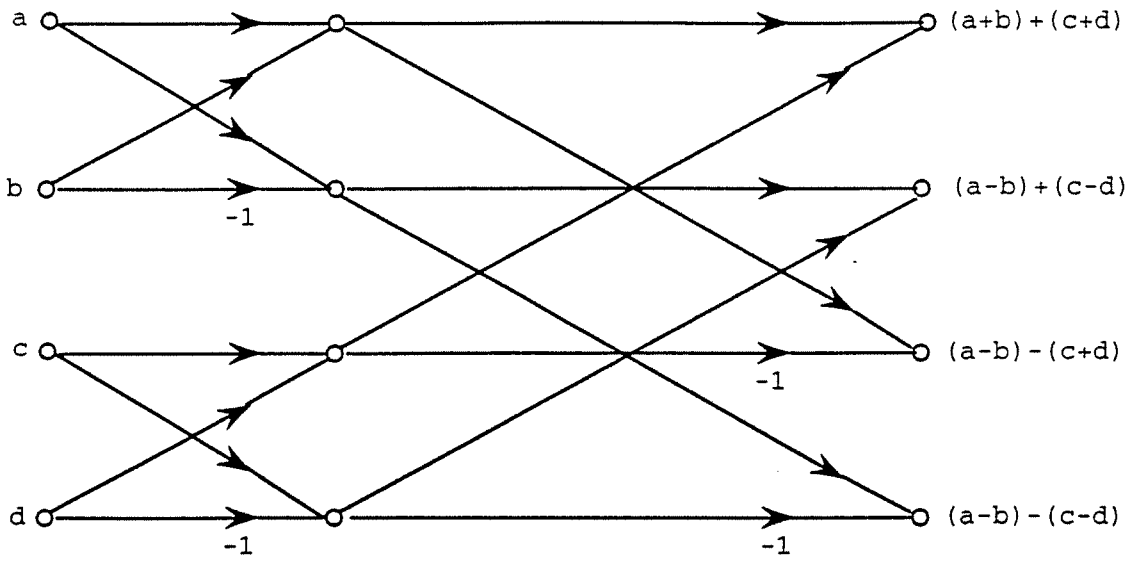

Figure A.1: 4-point butterfly for the FHT. Their are a total of two stages and each stage requires four additions.

The correspondence between ± 1 and GF(2) is as follows:

$$\begin{array}{ccc} GF(2) & & Reals \\ 0 & \Longleftrightarrow & +1 \\ 1 & \Longleftrightarrow & -1\,. \end{array} \tag{A.5}$$

To prevent any further confusion, the Walsh-Hadamard matrix over GF(2) will be denoted as $\tilde{\boldsymbol{H}}_i$. It can be easily shown that the Walsh-Hadamard matrix over GF(2) may be factored as [23]

$$\boldsymbol{H}_i = \boldsymbol{B}\boldsymbol{B}^T\,, \tag{A.6}$$

where

$$\boldsymbol{B}_i \;=\; [0 \;\; 1 \;\; 2 \;\; 3 \;\; \cdots \;\; i-1]^T\,. \tag{A.7}$$

and the elements of $\boldsymbol{B}$ in (A.7) denotes the corresponding binary representation. For

the example above,

$$\tilde{\boldsymbol{H}}_4 = \boldsymbol{B}\boldsymbol{B}^T = \begin{bmatrix} 0 & 0 \\ 0 & 1 \\ 1 & 0 \\ 1 & 1 \end{bmatrix} \begin{bmatrix} 0 & 0 & 1 & 1 \\ 0 & 1 & 0 & 1 \end{bmatrix}$$

$$= \begin{bmatrix} 0 & 0 & 0 & 0 \\ 0 & 1 & 0 & 1 \\ 0 & 0 & 1 & 1 \\ 0 & 1 & 1 & 0 \end{bmatrix} . \tag{A.8}$$

The matrices $\boldsymbol{B}$ and $\boldsymbol{B}^T$ will play a central role in establishing the equivalence between the Walsh-Hadamard matrix and the m-sequence matrix.

A.2 The M-Sequence Matrix for Cross-Correlation

To construct a period of the m-sequence of length $L = 2^k - 1$, one needs a primitive polynomial h(x) of degree k. The primitive polynomial may be expressed as

$$h(x) = x^k + \sum_{j=0}^{k-1} c_j x^j . \tag{A.9}$$

Once the primitive polynomial is specified, the m-sequence may be recursively computed over GF(2) by

$$m_{l+k} = \sum_{j=0}^{k-1} c_j m_{l+j} . \tag{A.10}$$

The m-sequence matrix used in the crosscorrelation is a L x L square matrix. Each row of the m-sequence matrix is a period of the m-sequence and each successive row is simply the successive cyclic shift of the previous row. Again, the m-sequence matrix over the reals ± 1 will be denoted by $\boldsymbol{M}_i$ while the m-sequence over GF(2)

will be denoted by $\tilde{\boldsymbol{M}}_i$. For the simple case of k=2, the characteristic polynomial is [26]

$$h(x) = x^2 + x + 1 \,, \tag{A.11}$$

and one form of the m-sequence matrix associated with this characteristic polynomial is

$$\tilde{\boldsymbol{M}}_3 = \begin{bmatrix} 0 & 1 & 1 \\ 1 & 0 & 1 \\ 1 & 1 & 0 \end{bmatrix} . \tag{A.12}$$

One of the special structure of the m-sequence matrix is that any row of the matrix may be obtained from the k previous rows of the matrix. Specifically, if $m_{i,j} \quad i,j = 0,1,...,2^k-1$ are the elements of the m-sequence matrix, then using the recursion given in (A.10) the elements of the p^{th} row may be obtained from rows $p-k$ to $p-1$.

$$m_{p,j} = \sum_{n=0}^{k-1} c_n m_{(p-k+n),j} \ \ (mod\ 2) \qquad for \ \ j = 0,1,2,..,L-1 \tag{A.13}$$

It is not difficult to conclude from (A.13) that $\tilde{\boldsymbol{M}}_{2^k-1}$ can be constructed from linear combinations of k successive rows of $\tilde{\boldsymbol{M}}_{2^k-1}$ (i.e. since $(k+1)^{th}$ row of $\tilde{\boldsymbol{M}}_{2^k-1}$ is a mod 2 combination of the first k rows of $\tilde{\boldsymbol{M}}_{2^k-1}$, the $(k+2)^{th}$ row is also a mod 2 combination of the first k rows, and so forth). Due to this property, $\tilde{\boldsymbol{M}}_{2^k-1}$ may be factored as

$$\tilde{\boldsymbol{M}}_{2^k-1} = \boldsymbol{W}\boldsymbol{S} \,, \tag{A.14}$$

where $\boldsymbol{S}$ is a binary matrix of size k x 2^k-1 which is formed by the k successive rows of the matrix $\tilde{\boldsymbol{M}}_{2^k-1}$. $\boldsymbol{W}$ is a weight matrix of size 2^k-1 x k with elements determined by the recursive relation in (A.10). For the above example when $2^k-1=3$,

$$\boldsymbol{S} = \begin{bmatrix} 0 & 1 & 1 \\ 1 & 0 & 1 \end{bmatrix} . \tag{A.15}$$

To construct the matrix $\boldsymbol{W}$, observe that the first k rows must form a k x k identity matrix. The remaining rows of $\boldsymbol{W}$ will be constructed using the recursion

$$w_{p,j} = \sum_{n=0}^{k-1} c_n w_{(p-k+n),j} \ (mod\ 2) \qquad for\ \ p > k\ ; \quad j = 0,1,2,..,2^k - 2 \qquad \text{(A.16)}$$

where $w_{p,j}$ are elements of the matrix $\boldsymbol{W}$. Hence, for k=2,

$$\boldsymbol{W} = \begin{bmatrix} 1 & 0 \\ 0 & 1 \\ 1 & 1 \end{bmatrix} . \qquad \text{(A.17)}$$

As a consequence of this factorization, it is now possible to analyze the equivalence between the m-sequence matrix and the Walsh-Hadamard matrix.

A.3 The Equivalence Between Walsh-Hadamard Matrix and the M-sequence Matrix

The benefit of factorizing $\tilde{\boldsymbol{M}}_{2^k-1}$ and $\tilde{\boldsymbol{H}}_{2^k}$ is that their equivalence may be obtained through the equivalence of their factors. Before this equivalence can be established, $\tilde{\boldsymbol{M}}_{2^k-1}$ must be slightly modified since $\tilde{\boldsymbol{M}}_{2^k-1}$ is a $2^k - 1\ x\ 2^k - 1$ matrix and $\tilde{\boldsymbol{H}}_{2^k}$ is a $2^k\ x\ 2^k$ matrix. This is accomplished by bodering the matrix $\boldsymbol{W}$ with a row of zero on top and a column of zeros on the left of $\boldsymbol{S}$. Specifically, let

$$\hat{\boldsymbol{W}} \triangleq \begin{bmatrix} \mathbf{o} \\ \boldsymbol{W} \end{bmatrix} \qquad \text{(A.18)}$$

$$\hat{\boldsymbol{S}} \triangleq \begin{bmatrix} \mathbf{o} & \boldsymbol{S} \end{bmatrix} \qquad \text{(A.19)}$$

The modified m-sequence matrix may be defined as

$$\hat{\tilde{\boldsymbol{M}}}_{2^k} \triangleq \hat{\boldsymbol{W}}\hat{\boldsymbol{S}}\ , \qquad \text{(A.20)}$$

which has a row of zero on top and a column of zero on the left. The equivalence between $\hat{\tilde{\boldsymbol{M}}}_{2^k}$ and $\tilde{\boldsymbol{H}}_{2^k}$ can be established by comparing $\hat{\boldsymbol{W}}$ with $\boldsymbol{B}$ and $\hat{\boldsymbol{S}}$ with $\boldsymbol{B}^T$.

Since $\hat{\boldsymbol{W}}$ is simply a row permutation of $\boldsymbol{B}$, the two matrices are related by

$$\hat{\boldsymbol{W}} = \boldsymbol{P}_w \boldsymbol{B} , \tag{A.21}$$

where $\boldsymbol{P}_w$ is the permutation matrix. This permutation matrix may be constructed as follows. Recall that the rows of $\boldsymbol{B}$ given in (A.7) is listed in increasing numberical order. Suppose the numerical representation for the i^{th} row of $\hat{\boldsymbol{W}}$ is N_i, then one simply needs to place a '1' at the $(N_i + 1)^{th}$ column of the i^{th} row of $\hat{\boldsymbol{P}}_w$ with zeros everywhere else on the i^{th} row. For the above example,

$$\boldsymbol{P}_w = \begin{bmatrix} 1 & 0 & 0 & 0 \\ 0 & 0 & 1 & 0 \\ 0 & 1 & 0 & 0 \\ 0 & 0 & 0 & 1 \end{bmatrix} . \tag{A.22}$$

In (A.22), the location of the '1' for the second row is placed at the third column since the numerical value of the second row of $\hat{\boldsymbol{W}}$ is 2 or [1 0] in binary (i.e. $N_2 = 2$).

Similarly, $\hat{\boldsymbol{S}}$ is a column permutation of $\boldsymbol{B}^T$; hence

$$\hat{\boldsymbol{S}} = \boldsymbol{B}^T \boldsymbol{P}_s , \tag{A.23}$$

where $\boldsymbol{P}_s$ is a column permutation matrix for $\hat{\boldsymbol{S}}$. To construct $\boldsymbol{P}_s$, note that the numerical value of the j^{th} column of $\hat{\boldsymbol{S}}$ denoted as N_j determines the location of the '1' in the j^{th} column of $\boldsymbol{P}_s$. Specifically, the '1' is placed at the $(N_j + 1)^{th}$ row of the j^{th} column of $\boldsymbol{P}_s$ with zero everywhere else on the j^{th} column. And for the case above,

$$\boldsymbol{P}_s = \begin{bmatrix} 1 & 0 & 0 & 0 \\ 0 & 1 & 0 & 0 \\ 0 & 0 & 1 & 0 \\ 0 & 0 & 0 & 1 \end{bmatrix} , \tag{A.24}$$

which turns out to be the identity matrix. Using (A.21) and (A.23), the modified m-sequence matrix may be expressed as

$$\hat{\tilde{\boldsymbol{M}}}_{2^k} = \boldsymbol{P}_w \boldsymbol{B}\boldsymbol{B}^T \boldsymbol{P}_s \, . \tag{A.25}$$

The original m-sequence matrix $\tilde{\boldsymbol{M}}_{2^k-1}$ may be reduced to its original size by

$$\begin{aligned} \tilde{\boldsymbol{M}}_{2^k-1} &= \boldsymbol{V}_L \hat{\tilde{\boldsymbol{M}}}_{2^k} \boldsymbol{V}_T \\ &= \boldsymbol{V}_L \boldsymbol{P}_w \boldsymbol{B}\boldsymbol{B}^T \boldsymbol{P}_s \boldsymbol{V}_T \\ &= \boldsymbol{V}_L \boldsymbol{P}_w \tilde{\boldsymbol{H}}_{2^k} \boldsymbol{P}_s \boldsymbol{V}_T \, , \end{aligned} \tag{A.26}$$

where

$$\boldsymbol{V}_L = \begin{bmatrix} \mathbf{o} & \boldsymbol{I}_{2^k-1} \end{bmatrix} \tag{A.27}$$

$$\boldsymbol{V}_T = \begin{bmatrix} \mathbf{o} \\ \boldsymbol{I}_{2^k-1} \end{bmatrix} , \tag{A.28}$$

and $\boldsymbol{I}_{2^k-1}$ is the identity matrix of size $(2^k - 1)$ x $(2^k - 1)$. For k=2,

$$\boldsymbol{V}_L = \begin{bmatrix} 0 & 1 & 0 & 0 \\ 0 & 0 & 1 & 0 \\ 0 & 0 & 0 & 1 \end{bmatrix} \tag{A.29}$$

$$\boldsymbol{V}_T = \begin{bmatrix} 0 & 0 & 0 \\ 1 & 0 & 0 \\ 0 & 1 & 0 \\ 0 & 0 & 1 \end{bmatrix} , \tag{A.30}$$

Recall that the equivalence above is constructed under GF(2), whereas the implementation for the crosscorrelation is performed under the reals[2]. Fortunately, the

[2]The reason for constructing the equivalence under GF(2) is due to the fact that $\boldsymbol{H}_{2^k}$ and $\boldsymbol{M}_{2^k-1}$ cannnot be factored into any desirable form over the reals.

matrices $\boldsymbol{P}_w$ and $\boldsymbol{P}_s$ are permutation matrices; hence, the zeroes and ones of $\hat{\boldsymbol{H}}_{2^k}$ and $\tilde{\boldsymbol{M}}_{2^k-1}$ may be replaced by ± 1 without any further modification. Therefore, the output of the crosscorrelation utilizing FHT may be written as

$$\begin{aligned} \boldsymbol{Y}_{\alpha_o} &= \boldsymbol{M}_{2^k-1}\boldsymbol{z}_{\alpha_o} \\ &= \boldsymbol{V}_L\boldsymbol{P}_w\boldsymbol{H}_{2^k}\boldsymbol{P}_s\boldsymbol{V}_T\boldsymbol{z}_{\alpha_o} , \end{aligned} \tag{A.31}$$

The purpose of $\boldsymbol{V}_T$ is to increase the size of the data vector $\boldsymbol{z}_{\alpha_o}$ by appending a zero at the top of this vector. In contrast, the purpose of $\boldsymbol{V}_L$ is to reduce the size of the processed 2^k vector to a vector of size 2^k-1. Both $\boldsymbol{V}_T$ and $\boldsymbol{V}_L$ do not require any computations. The permutation matrix $\boldsymbol{P}_s$ scrambles the data vector through index reordering and the computation involved is negligible in comparision to the process of interpolation and the computation of the butterfly during FHT. Likewise, the permutation matrix $\boldsymbol{P}_w$ descrambles the output vector from FHT and the number of computation is also negligible. The only significant computation involves the process of computing the butterfly in the FHT. Each stage of the butterfly requires 2^k additions. Since there are k stages in the butterfly, the total number of additions required for the computation of the butterfly is $k2^k$.

APPENDIX B

A Summary of the Signal Processing Aspects of HCCO Preprocessing

L = Number of digits in a period of the m-sequence

Q = Number of cycles in a digit

QL = $f_c T_p$ = Number of cycles per period

m_r = Number of samples in a cycle

θ_L = period-matched angle

θ_T = transmission angle

b_m = ± 1 ; binary codes of the m-sequence

f_c = Center frequency for the signal transmission

$m_r f_c$ = Sampling rate

t_1 = time between samples, $1/m_r f_c$

X = Number of periods processed

$r(t)$ = continuous time reception

α_{min} = doppler index of interest with maximum time compression

α_{max} = doppler index of interest with minimum time compression

A) Sampling and Demodulation.

1) Sample the reception at zero doppler.

$$r[n] \;=\; r(nt_1)\;, \tag{B.1}$$

where $t_1 = \frac{1}{m_r f_o}$.

2) Complex demodulate the sampled reception.

$$z[n] \;=\; r[n]e^{j2\pi f_o n t_1}\;. \tag{B.2}$$

3) Remove the $-2f_c$ component using a sinc-squared filter.

$$\begin{aligned} z'[m] &= \sum_{i=0}^{m_r-1} z[m-i] \\ z''[m] &= \sum_{i=0}^{m_r-1} z'[m-i]\;. \end{aligned} \tag{B.3}$$

B) HCCO Preprocessing.

1) Implement the forward projection using Factor Inverse Filtering (FIF):

a) Demultiplex the demodulated sequence for one period of the demodulated sequence.

$$z''_{q,r}[m] \;\triangleq\; z''[q+mQ+rm_rQL] \quad where \begin{cases} q = 0,1,2,...,m_rQ-1 \\ m = 0,1,2,....,L-1 \\ r = 0,1,2,..,X \end{cases} \tag{B.4}$$

b) Calculate the FIF for each of the m_rQ demultiplexed demodulates using FHT in appendix A.

$$\begin{aligned} s_{q,r}[k] &= \sum_{m=0}^{L-1} z''_{q,r}[m]e^{-jb_{k+m}\theta_T}(mod\ L) \quad k = 0,1,2,...,L-1 \\ &= cos(\theta_T)\sum_{m=0}^{L-1} z''_{q,r}[m] - j\ sin(\theta_T)\sum_{m=0}^{L-1} z''_{q,r}[m]b_{k+m}\;. \end{aligned} \tag{B.5}$$

c) If the transmission angle differs from the period-matched angle, remove the "bias" level from each of the $m_r Q$ demultiplexed outputs.

$$\hat{s}_{q,r}[k] \;=\; s_{q,r}[k] \;-\; \text{bias level}\;, \tag{B.6}$$

where

$$\text{bias level} \;=\; \gamma \sum_{n=0}^{L-1} z''_{q,r}[n] + \delta_q \phi_1 - \delta_q \gamma L\;, \tag{B.7}$$

and

$$\delta_q \;=\; \left[\frac{\phi_o - \gamma\phi_1^*}{\phi_1^*(\phi_1 - \gamma L)}\right] \sum_{n=0}^{L-1} z''_{q,r}[n] \tag{B.8}$$

$$\gamma \;=\; \frac{sin(\theta_L - \theta_T)}{sin(\theta_L)} \tag{B.9}$$

$$\phi_o \;=\; \sum_{n=0}^{L-1} e^{jb_n\theta_T} e^{-jb_{n-i}\theta_T} \quad i \neq 0 \;(mod\; L) \tag{B.10}$$

$$\phi_1 \;=\; \sum_{n=0}^{L-1} e^{-jb_n\theta_T} \tag{B.11}$$

$$\phi_1^* \;=\; \sum_{n=0}^{L-1} e^{jb_n\theta_T}\;. \tag{B.12}$$

d) Multiplex the $m_r Q$ output sequences to form a single output sequence.

$$s_r[q + km_rQ] \;=\; \hat{s}_{q,r}[k] \quad where \begin{cases} q = 0, 1, 2, ..., m_rQ - 1 \\ k = 0, 1, 2, ..., L - 1 \\ r = 0, 1, 2, ..., X \end{cases} \tag{B.13}$$

2) For each strong path, remove its peak and its transducer response. This is accomplished by zeroing the output sequence $s_r[k]$ at the peaks and transducer responses. Denote this modified output by $\tilde{s}_r[k]$.

3) Implement the inverse projection to obtain the modified, demodulated sequence.

a) Demultiplex the modified, output sequence.

$$\tilde{s}_{q,r}[k] \triangleq \tilde{s}_r[q + km_rQ] \quad where \begin{cases} q = 0, 1, 2, ..., m_rQ - 1 \\ k = 0, 1, 2, ..., L - 1 \\ r = 0, 1, 2, ..., X \end{cases} \tag{B.14}$$

b) Implement the FIF for each of the m_rQ segments via FHT.

$$\begin{aligned} \tilde{z}_{q,r}[k] &= \frac{1}{L} \sum_{n=0}^{L-1} \tilde{s}_{q,r}[n] e^{jb_{k+n}\theta_L} \ \ (mod\ L) \\ &= cos(\theta_L) \sum_{n=0}^{L-1} \tilde{s}_{q,r}[n] + j\ sin(\theta_L) \sum_{n=0}^{L-1} \tilde{s}_{q,r}[n] b_{k+n} \ . \end{aligned} \tag{B.15}$$

c) Multiplex the modified, demodulate sequence.

$$\tilde{z}_r[q + km_rQ] = \tilde{z}_{q,r}[k] \quad where \begin{cases} q = 0, 1, 2, ..., m_rQ - 1 \\ k = 0, 1, 2, ..., L - 1 \\ r = 1, 2, .., X + 1 \end{cases} \tag{B.16}$$

4) Repeat steps 1)$\longrightarrow$3) for each of the remaining periods.

5) Form a single modified, demodulated sequence from all preprocessed periods.

$$\tilde{\boldsymbol{z}} = [\tilde{\boldsymbol{z}}_1, \tilde{\boldsymbol{z}}_2, ..., \tilde{\boldsymbol{z}}_{x+1}] \ , \tag{B.17}$$

where

$$\tilde{\boldsymbol{z}_r} = [z_r[0], z_r[1], ..., z_r[m_rQL - 1]]^T; \quad r = 1, 2, ..., X + 1 \ . \tag{B.18}$$

C) Generation of the Ambiguity Surface.

1) Interpolate the modified, demodulated sequence to all doppler channels.

a) Properly demodulate for the α^{th} doppler channel.

$$\hat{z}_\alpha[m] = \tilde{z}[m] e^{j2\pi(1-e^{-\alpha})m} \ . \tag{B.19}$$

b) Time compress for the α^{th} doppler channel.

$$\tilde{z}_\alpha[m] = (1-\lambda[m])\hat{z}_\alpha[c[m]] + \lambda[m]\hat{z}_\alpha[c[m]+1] , \qquad (B.20)$$

where

$$x[m] = me^\alpha \qquad (B.21)$$

$$c[m] = \lfloor x[m] \rfloor \qquad (B.22)$$

$$\lambda[m] = x[m] - c[m] . \qquad (B.23)$$

c) Repeat a) and b) for each doppler channel from α_{min} to α_{max}.

2) For each interpolated sequence, sum over X periods to achieve higher SNR.

$$\tilde{z}_{\alpha,sum}[m] = \sum_{r=0}^{X-1} \tilde{z}_\alpha[m + rm_rQL] \qquad (B.24)$$

3) For each doppler channel, immplement the crosscorrelation using Factor Inverse Filtering (FIF):

a) Demultiplex the demodulated sequence for the single-period, modified demodulated sequence of the α^{th} doppler channel.

$$\tilde{z}_{q,\alpha}[m] \triangleq \tilde{z}_{\alpha,sum}[q+mm_rQ] \quad where \begin{cases} q = 0,1,2,...,m_rQ-1 \\ m = 0,1,2,....,L-1 \end{cases} \qquad (B.25)$$

b) Calculate the FIF for each of the m_rQ sequences using FHT in appendix A.

$$\tilde{s}_{q,\alpha}[k] = \sum_{m=0}^{L-1} \tilde{z}_{q,\alpha}[m] e^{-jb_{k+m}\theta_T} (mod\ L) \quad k = 0,1,2,...,L-1$$

$$= cos(\theta_T) \sum_{m=0}^{L-1} \tilde{z}_{q,\alpha}[m] - j\ sin(\theta_T) \sum_{m=0}^{L-1} \tilde{z}_{q,\alpha}[m] b_{k+m} . \qquad (B.26)$$

c) Remove the "bias" level for each of the $m_r Q$ modified, output sequences.

$$\hat{\tilde{s}}_{q,\alpha}[k] = \tilde{s}_{q,\alpha}[k] - \gamma \sum_{m=0}^{L-1} \tilde{z}_{q,\alpha}[m] - \delta_q \sum_{m=0}^{L-1} e^{-jb_{k+m}\theta_T} + \gamma\delta_q L \ \ (mod\ L)\ , \tag{B.27}$$

where

$$\delta_q = \left[\frac{\phi_o - \gamma\phi_1^*}{\phi_1^*(\phi_1 - \gamma L)}\right] \sum_{n=0}^{L-1} \tilde{z}''_{q,r}[n]\ , \tag{B.28}$$

and γ, ϕ_o, ϕ_1 are as defined in (B.9), (B.10) and (B.11) respectively.

d) Multiplex the $m_r Q$ modified, output sequences to form a single output sequence.

$$\tilde{s}_\alpha[q + km_rQ] = \hat{\tilde{s}}_{q,\alpha}[k] \quad where \begin{cases} q = 0, 1, 2, ..., m_rQ - 1 \\ k = 0, 1, 2, ..., L - 1 \end{cases} \tag{B.29}$$

e) Repeat a)$\longrightarrow$d) for all doppler channels from α_{min} to α_{max}.

3) Form the ambiguity surface using crosscorrelation outputs of all doppler channels.

$$A_{hcco}[k, e^\alpha]\ |_{e^\alpha = e^{\alpha_o}} = \tilde{s}_{\alpha_o}[k]\ , \tag{B.30}$$

where α_o is an element of $\{\alpha_{min}, ..., \alpha_{max}\}$.

APPENDIX C

Cost For Storing Reference Surfaces Without Time Shift-Invariance

In a large-scale tomography, storing reference surfaces for strong signal cancellation is very costly. To get an idea of this cost, examples are given below which calculates the number of pixels required for each reference surface. The following is a list of parameters in a typical m-sequence transmission:

L = number of digits in a period = 1023 digits

f_c = center frequency = 250 Hz

Q = number of cycles in a digit = 4

α' = search variable for doppler

α'_{max} = maximum of α' = $3.43x10^{-2}$ (+10 knots)

α'_{min} = minimum of α' = $-3.43x10^{-2}$(−10 knots)

T_p = signal period = 16.368 seconds .

To calculate the number of pixels required for each reference ambiguity surface, one must compute the number of time-delay bins and doppler bins required to capture the essential features of an ambiguity surface. At a sampling rate of $4f_c$, the total

number of time-delay bins in a period is

$$M_t \;=\; 4f_cT_p \;=\; 16368\ . \tag{C.1}$$

It is often easier to determine the step size of doppler bins through single frequency analysis[7]. In a single frequency transmission, the crosscorrelation between two sinewaves is zero if they differ by ± 1 cycle in a period. Now, f_cT_p is the total number of cycles in a period for a zero doppler sinewave whereas the total number of cycles in a period for a doppler-shifted sine wave is $(1-\alpha')f_cT_p$. Therefore, a one-cyle difference between these two sinewaves will result if $\alpha' = 1/f_cT_p$. If $1/f_cT_p$ were chosen as the doppler step size, the details of the ambiguity surface would be missing. In practice, one chooses a doppler step size that is one-fourth of $1/f_cT_p$ (i.e. $1/4f_cT_p$). Therefore, the total number of doppler bins is given by

$$M_d \;=\; (\alpha'_{max} - \alpha'_{min})4f_cT_p \;\approx\; 113\ . \tag{C.2}$$

The total number of pixels in a reference surface is $M_tM_d = 1.85x10^6$. At 8 bytes/pixel, one reference surface requires 14.8 megabytes of storage space. Without time shift-invariance, one reference surface is required for each possible time-delay bin. Therefore, 16368 reference surfaces at 14.8 megabytes each corresponds to 242.2 gigabytes of memory. At a rate of \$1000/gigabyte, the storage space will cost approximately \$250,000. Furthermore, if the number of digits in a period of the m-sequence were increased to 2047, the number of time-delay and doppler bins for each reference surface would increase to 32752 and 225, respectively. This would require a total memory of 1932 gigabytes which is approximately equivalent to \$2 million.

APPENDIX D

Simulating the Shift-Invariant Property of the M-Sequence Receiver Ambiguity Surface

The m-sequence law used in the simulation is 45 (octal) which specifies the coefficient associated with the primitive polynomial $x^5 + x^2 + 1$. Four periods of the 31 digit m-sequence are jointly processed. The search variable for doppler covers ± 10 knots which is evenly divided into 37 doppler bins. These 37 doppler bins also corresponds to a four-cycle difference between the analysis interval with the maximum doppler compression and the analysis interval with the minimum doppler compression. Specifically, the difference between the maximum and the minimum search variable for doppler is approximately $4/f_c T_A$ where T_A is the analysis interval equal to four periods. A detailed discussion on the structure of the m-sequence ambiguity surface is provided in appendix E. The following is a list of pertinent parameters associated with the m-sequence simulation.

L = Number of digits in a period of the m-sequence = 31

N_r = Total number of periods in the analysis interval = 4

Q = Number of cycles in a digit = 4

QL = $f_c T_p$ = Number of cycles per period = 124

m_r = Number of samples in a cycle = 4

m_rQ = Number of samples per digit = 16

N_T = Total number of samples in N_r periods = $(m_rQ)(N_rL)$

θ = period-matched angle = 79.82 *degrees*

b_k = ± 1 ; binary codes of the m-sequence

f_o = Center frequency for the signal transmission = 250 Hz

m_rf_o = Sampling rate = 1 kHz

t_1 = time between samples, $1/m_rf_o$

$e^{\alpha_{min}}$ = doppler index of interest with maximum time compression = 1.00361

$e^{\alpha_{max}}$ = doppler index of interest with minimum time compression = 0.99641

N_x = extra digits sampled at 0-doppler necessary for interpolation = 2

D.1 The Single-Path Receiver Ambiguity Surface

The noiseless, single-path reception is modeled as a 0-doppler, zero time-delay reception. The sampled reception is given by

$$\begin{aligned} r[n] &= m\left[\lfloor\frac{n}{m_rQ}\rfloor\right] e^{j2\pi f_o n t_1} \\ &= m\left[\lfloor\frac{n}{m_rQ}\rfloor\right] e^{j2\pi n/m_r}, \qquad 0 \le n \le (m_rQ)(N_rL-1+N_x) \end{aligned} \tag{D.1}$$

where $\lfloor x \rfloor$ is the greatest integer less than or equal to x, and

$$m[k] = e^{jb_k\theta}, \qquad k = 0, 1, ..., N_rL-1+N_x \tag{D.2}$$

are the period-matched, m-sequence digits. In (D.1), $r[n]$ consists of samples from the 4-period m-sequence signal. Specifically, there are 16 samples per digit of the m-sequence. The extra digits N_x is included to compensate for the time compression

during linear doppler interpolation. The 0-doppler, demodulated reception is

$$z[n] \;=\; r[n]e^{-j2\pi n/m_r} \;. \tag{D.3}$$

The steps for linear doppler interpolation were explained in more detail in section 3.4.2 and are repeated here in a more compact form. To interpolate the demodulated reception to the α_i^{th} doppler channel, the phase of $z[n]$ is adjusted so that

$$z'_{\alpha_i}[n] \;=\; z[n]e^{j2\pi n/m_r}e^{-j2\pi e^{\alpha_i} n/m_r} \;. \tag{D.4}$$

The linear interpolated version of $z'_{\alpha_i}[n]$ is

$$z_{\alpha_i}[n] \;=\; (1-\lambda[n])z'_{\alpha_i}[c[n]] + \lambda[n]z'_{\alpha_i}[c[n]+1] \;, \tag{D.5}$$

where

$$x[n] \;=\; ne^{\alpha_i} \tag{D.6}$$

$$c[n] \;=\; \lfloor x[n] \rfloor \tag{D.7}$$

$$\lambda[n] \;=\; x[n] - c[n] \;. \tag{D.8}$$

Each of the interpolated doppler channels $z_{\alpha_i}[n]$ will have the same number of samples. For a 4-period analysis, each doppler channel will have $N_T = (m_r Q)(N_r L)$ samples. In this simulation, the four periods are concatenated and not averaged prior to crosscorrelation. The receiver output for the α_i^{th} doppler channel is given by the (mod N_T) cyclic crosscorrelation

$$y_{\alpha_i}[k] \;=\; \sum_{n=0}^{N_T-1} z_{\alpha_i}[n]m_d^*[n-k] \qquad 0 \le k \le N_T - 1 \;. \tag{D.9}$$

where $m_d[n]$ are samples of the m-sequence given by

$$m_d[n] \;=\; m\left[\left\lfloor \frac{n}{m_r Q} \right\rfloor\right] \qquad 0 \le n \le N_T - 1 \;. \tag{D.10}$$

The combined receiver outputs from all doppler channels forms the receiver ambiguity surface $A(k, e^{\alpha_i} \mid 0, 1, 1)$ where

$$A(k, e^{\alpha_i} \mid 0, 1, 1) \;=\; y_{\alpha_i}[k] \quad \forall \;\; e^{\alpha_{min}} \leq e^{\alpha_i} \leq e^{\alpha_{max}} \; . \tag{D.11}$$

D.2 Reference Ambiguity Surface for Doppler Invariance

The first type of reference surface desired is a reference surface which only differ in doppler from the 0-doppler, single-path surface in section D.1. To obtain the noiseless, reference surface, let the single-path reference signal be modeled as

$$\begin{aligned} r_r[n] &= m\left[\lfloor \frac{n}{m_r Q} \rfloor\right] e^{j2\pi f_o e^{\beta_j} n t_1} \\ &= m\left[\lfloor \frac{n}{m_r Q} \rfloor\right] e^{j2\pi e^{\beta_j} n/m_r}, \quad 0 \leq n \leq (m_r Q)(N_r L - 1 + N_x) \end{aligned} \tag{D.12}$$

where e^{β_j} is the true doppler of the reference surface. To obtain the reference ambiguity surface from $r_r[n]$, substitute $r_r[n]$ for $r[n]$ in (D.3) and continue through to the end of section D.1. The resultant reference ambiguity surface becomes $A_r(k, e^{\alpha_i} \mid 0, e^{\beta_j}, 1) \;\; for \;\; e^{\alpha_{min}-\beta_j} \leq e^{\alpha_i} \leq e^{\alpha_{max}+\beta_j}$. In essense, once the signal reception is properly modeled, the processing is identical regardless of its true doppler. To simulate the SIMSPC, subtract the doppler shifted version of the reference ambiguity surface from the receiver ambiguity surface

$$A_{residue}(k, e^{\alpha_i}) \;=\; A(k, e^{\alpha_i} \mid 0, 1, 1) - A_r(k, e^{\alpha_i - \beta_j} \mid 0, e^{\beta_j}, 1) \; . \tag{D.13}$$

In figures (4.3) and (4.4) the "shift in doppler" in the x-axis represents the specific value of e^{β_j} chosen for the reference surface. The "improvement in dB" in the y-axis is the m.s.e. and median-squared level of the residue $A_{residue}(k, e^{\alpha_i})$. The two curves in (4.3) reflect the changes in performance under different sampling rate.

D.3 Reference Ambiguity Surface for Time-Delay Invariance

The second type of reference surface desired is a reference surface which only differ in time-delay from the 0-doppler, single-path surface in section D.1. To obtain the time-shifted, 0-doppler reference surface, let the single-path reference signal be modeled as

$$\begin{aligned} r_r[n] &= m\left[\lfloor\frac{n}{m_r Q}\rfloor\right] e^{j2\pi f_o(n-T_j)t_1} \\ &= m\left[\lfloor\frac{n}{m_r Q}\rfloor\right] e^{j2\pi(n-T_j)/m_r}, \quad 0 \le n \le (m_r Q)(N_r L - 1 + N_x) \end{aligned} \tag{D.14}$$

Again, the processing steps (i.e. demodulation, interpolation, crosscorrelation) are the same as those in section D.1. The resultant reference ambiguity surface is denoted as $A_r(k, e^{\alpha_i} \mid T_j, 1, 1)$ for $T_j \le k \le N_T + T_j$. An example of the reference ambiguity surface is depicted in figure D.1. To simulate the SIMSPC, subtract the time-shifted, phase-adjusted version of the reference ambiguity surface from the receiver ambiguity surface given by

$$A_{residue}(k, e^{\alpha_i}) = A(k, e^{\alpha_i} \mid 0, 1, 1) - e^{-j2\pi T_j/m_r} A_r(k - T_j, e^{\alpha_i} \mid T_j, 1, 1)\ . \tag{D.15}$$

In figures (4.5) and (4.8) the "shift in time-delay" in the x-axis represents the particular value of T_j chosen for the reference surface. The "improvement in dB" in the y-axis is the m.s.e. and median-squared level of the residue $A_{residue}(k, e^{\alpha_i})$.

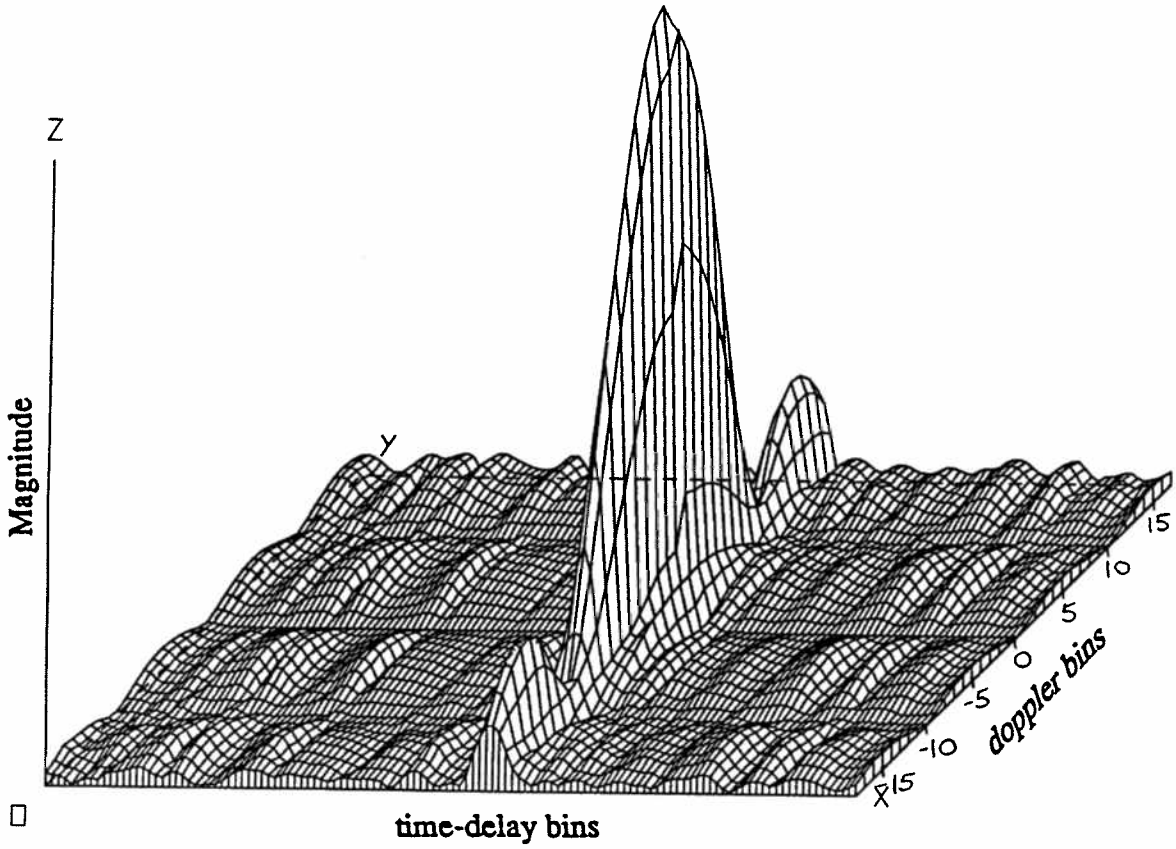

Figure D.1: Normalized magnitude of a 0-doppler, single-path, reference ambiguity surface for m-sequences; one doppler bin is equivalent to 0.58 knots. The time-delay bins are spaced 1/2 cycles apart. The demodulated sequence is filtered by a third-order Butterworth filter.

APPENDIX E

Structure of the M-Sequence Ambiguity Surface

One of the main differences between the ambiguity surface of the m-sequence and the thumbtack-like ambiguity surface of random noise is the presence of a sinc-shaped pulse in the doppler axis of the m-sequence ambiguity surface (see figure D.1). In addition to the sinc-shaped pulse, figure D.1 also indicate the presence of nulls along the time-delay axis at multiples of ± 10 doppler bins (i.e. multiples of $1/(f_o N T_p)$ where NT_p is the analysis interval). The first feature, the sinc-shaped pulse, is a property of all m-sequences regardless of the number of periods processed. The second feature, the nulls along the time-delay axis, is present only if multiple-period crosscorrelation is implemented. These features are detailed in the following analysis.

E.1 Single-Period Crosscorrelation

In continuous time, the ambiguity surface for a 0-doppler, m-sequence signal is given by

$$A_1(\tau, e^{\alpha} \mid 0, 1, 1) \;=\; \int_0^{T_p} m(e^{\alpha} t) m^*(t-\tau) e^{-j2\pi f_o (e^{\alpha}-1)t} dt \;, \qquad \text{(E.1)}$$

where T_p is the period of the m-sequence signal and the subscript 1 denote a single-period crosscorrelation. For small doppler differences, it may be assumed that

$m(e^{\alpha}t) \approx m(t)$ so that the ambiguity surface in (E.1) evaluated at $\tau = 0$ becomes

$$\begin{aligned} A_1(\tau, e^{\alpha} \mid 0,1,1) \mid_{\tau=0} &\approx \int_0^{T_p} e^{-j2\pi f_o(e^{\alpha}-1)t} dt \\ &= T_p sinc(f_o(e^{\alpha}-1)T_p) e^{-j\pi f_o(e^{\alpha}-1)T_p} . \end{aligned} \tag{E.2}$$

Therefore, at zero delay, the magnitude of the ambiguity function is approximately sinc-like in the doppler axis. From (E.2) the zeros of the sinc-shaped pulse is at multiples of $1/(f_o T_p)$.

$$e^{\alpha} - 1 = \frac{n}{f_o T_p} \quad for \quad n = \pm 1, \pm 2, ... \tag{E.3}$$

The first zero (i.e. $e^{\alpha_o} - 1 = 1/(f_o T_p)$) corresponds to a one-cycle difference between the period of the 0-doppler channel and the period of the α_o^{th} doppler channel.

E.2 Multiple-Period Crosscorrelation

The ambiguity surface for the multiple-period crosscorrelation may be written as

$$A_N(\tau, e^{\alpha} \mid 0,1,1) = \int_0^{NT_p} m(e^{\alpha}t) m^*(t-\tau) e^{-j2\pi f_o(e^{\alpha}-1)t} dt , \tag{E.4}$$

where N is the number of periods processed. Again, assuming no doppler-scaling for the baseband signal, then

$$A_N(\tau, e^{\alpha} \mid 0,1,1) \approx \sum_{k=0}^{N-1} e^{-j2\pi f_o(e^{\alpha}-1)kT_p} \int_0^{T_p} m(t) m^*(t-\tau) e^{-j2\pi f_o(e^{\alpha}-1)t} dt . \tag{E.5}$$

Using the fact that

$$\begin{aligned} \sum_{k=0}^{N-1} e^{-j2\pi f_o(e^{\alpha}-1)kT_p} &= \frac{1 - e^{-j2\pi f_o(e^{\alpha}-1)T_p N}}{1 - e^{-j2\pi f_o(e^{\alpha}-1)T_p}} \\ &= \frac{sin(\pi f_o(e^{\alpha}-1)T_p N)}{sin(\pi f_o(e^{\alpha}-1)T_p)} e^{-j\pi(N-1)f_o(e^{\alpha}-1)T_p} , \end{aligned} \tag{E.6}$$

the ambiguity surface in (E.5) becomes

$$\begin{aligned} A_N(\tau, e^{\alpha} \mid 0,1,1) \approx & \frac{sin(\pi f_o(e^{\alpha}-1)T_p N)}{sin(\pi f_o(e^{\alpha}-1)T_p)} e^{-j\pi(N-1)f_o(e^{\alpha}-1)T_p} \\ & \cdot \int_0^{T_p} m(t) m^*(t-\tau) e^{-j2\pi f_o(e^{\alpha}-1)t} dt . \end{aligned} \tag{E.7}$$

The magnitude of the N-period, ambiguity surface is related to the magnitude of the single-period, ambiguity surface by

$$\mid A_N(\tau, e^{\alpha} \mid 0,1,1) \mid = \left| \frac{sin(\pi f_o(e^{\alpha}-1)T_pN)}{sin(\pi f_o(e^{\alpha}-1)T_p)} \right| \mid A_1(\tau, e^{\alpha} \mid 0,1,1) \mid \ . \qquad \text{(E.8)}$$

The factor $sin(\pi f_o(e^{\alpha}-1)T_pN)/sin(\pi f_o(e^{\alpha}-1)T_p)$ is a comb filter which peaks up at every $e^{\alpha}-1 = n/(f_oT_p), \quad n = 0, \pm 1, \pm 2, ...$ and has N-1 zeroes between any two peaks. The zeros are located at every $e^{\alpha}-1 = n/(f_oNT_p), \quad n = \pm 1, \pm 2, ...$ Therefore, the four-period crosscorrelation in figure D.1 contains nulls along the time-delay axis at multiples of $1/(f_oNT_p)$. The first zero at $e^{\alpha_o}-1 = 1/(f_oNT_p)$ corresponds to a one-cycle difference between the analysis interval of the 0-doppler channel and the anaylsis interval of the α_o^{th} doppler channel. The most significant difference between the zeros described in this section and the zeros described in the previous section is that the zeros in this section is valid for all time-delay τ whereas the zeros described in the previous section is true only at $\tau = 0$.

BIBLIOGRAPHY

BIBLIOGRAPHY

[1] M. Ares. Radar waveforms for suppression of extended clutter. *IEEE Trans. Aerospace Electronics and Systems*, 3:138–141, Jan., 1967.

[2] Louis Auslander and Izidor Gertner. *Wide-Band Ambiguity Function and ax+b Group.* Springer-Verlag, New York, 1990.

[3] Raymond S. Berkowitz, editor. *Modern Radar.* Wiley, New York, 1965.

[4] E. R. Berlekamp. *Algebraic Coding Theory.* McGraw-Hill, New York, 1968.

[5] T. G. Birdsall and Jr. K. Metzger. Factor inverse matched filtering. *J. Acoust. Soc. Am.*, 79:91–, 1986.

[6] T.G. Birdsall. Private communication.

[7] T.G. Birdsall and Jr. K.Metzger. M-sequence signal tutorial. April, 1988.

[8] Richard E. Blahut. *Fast Algorithms For Digital Signal Processing.* Addison-Wesley, Reading, Mass., 1987.

[9] Jeffrey Borish and James B. Angell. An efficient algorithm for measuring the impulse response using pseudorandom noise. *J. Audio Eng. Soc.*, 31:478–487, July/August, 1983.

[10] Leon Cohen. Seminar on time-frequency distributions. March, 1988.

[11] Martin Cohn and Abraham Lempel. On fast m-sequence transforms. *IEEE Trans. Information Theory*, pages 135–137, Jan. 1977.

[12] D.E.Vakman. *Sophisticated Signals and the Uncertainty Principle in Radar.* Springer-Verlag, New York, 1968.

[13] J. V. Difranco and W. L. Rubin. *Radar Detection.* Prentice-Hall, Englewood Cliffs, N.J., 1968.

[14] A. Farina and A. Protopapa. New results on linear prediction for clutter cancellation. *IEEE Trans. Aerospace Electronics and Systems*, 24:275–286, May 1988.

[15] R. A. Fisher and L. H. C. Tippet. Limiting forms of the frequency distribution of the largest or smallest member of a sample. *Proc. Cambridge Phil. Soc.*, 24:180–190, 1928.

[16] D. Gabor. *Theory of Communication, J. IEE*, 93, Part III:429–457, Nov. 1946.

[17] Ronald L. Gassner and George R. Cooper. Note on a generalized ambiguity function. *IEEE Trans. Information Theory*, IT-13:126, Jan. 1967.

[18] B. V. Gnedenko. Sur la distribution limite du terme maximum d'une serie aleatoire. *Ann. Math.*, 44:423–453, 1943.

[19] P. Delsarte J. M. Goethals and F. J. MacWilliams. On generalized reed-muller codes and their relatives. *Information and Control*, 16:403–442, 1970.

[20] Simon Haykin. *Communication Systems, 2nd Edition.* John Wiley & Sons, New York, 1983.

[21] Carl W. Helstrom. *Statistical Theory of Signal Detection, 2nd Edition.* Pergamon Press, 1968.

[22] K. W. Henderson. Comment on computation of the fast walsh-fourier transform. *IEEE Transactions on Computers*, 19:850, 1970.

[23] E.J. Kelly and R.P. Wishner. Matched-filter theory for high velocity, accelerating targets. *IEEE Trans. on Military Electronics*, 9:56–69, Jan., 1965.

[24] F.F. Kretschmer. Mti weightings. *IEEE Trans. Aerospace Electronics and Systems*, 10:153–155, Jan., 1974.

[25] Holger Rootzen M. R. Leadbetter, Georg Lindgren. *Extremes and Related Properties of Random Sequences and Processes.* Springer-Verlag, New York, 1983.

[26] F. Jessie MacWilliams and Neil J. A. Sloane. Pseudo-random sequences and arrays. *Proceedings of the IEEE*, 64:1715–1728, 1976.

[27] R. Manasse. The use of pulse coding to discriminate against clutter. *MIT Lincoln Lab., Group Rept. 312-12(Rev.1)*, June, 1961.

[28] R.L. Mitchell and A.W. Rihaczek. Clutter suppression properties of wieghted pulse trains. *IEEE Trans. Aerospace Electronics and Systems*, 1968.

[29] T. Murakami and R.S. Johnson. Clutter suppression by use of weighted pulse trains. *RCA rev.*, 32:402–428, Sept., 1971.

[30] Athanasios Papoulis. *Probability, Random Variables, and Stochastic Processes.* McGraw-Hill Inc., New York, 1984.

[31] Robert J. Purdy and George R. Cooper. A note on the volume of generalized ambiguity functions. *IEEE Trans. Information Theory*, IT-14:153–154, Jan. 1968.

[32] S.O. Rice. The mathematical analysis of random noise. *Bell Sys. Tech. J.*, 23:282–332, 1944.

[33] A. W. Rihaczek. *Principles of High-Resolution Radar.* McGraw-Hill, New York, 1969.

[34] A. W. Rihaczek. Optimum filters for signal detection in clutter. *IEEE Transactions on Aerospace and Electronic Systems*, AES-1:297–299, December, 1965.

[35] A. W. Rihaczek. Radar signal design for target resolution. *IEEE Proceedings*, pages 116–128, Feb., 1965.

[36] A. W. Rihaczek. Doppler-tolerant signal waveforms. *IEEE Proceedings*, 54:849–857, June, 1966.

[37] W. McC. Siebert. A radar detection philosophy. *IRE Trans.*, (No. PGIT-3):68–89, 1956.

[38] A.I. Sinsky and C.P. Wang. Standardization of the definition of the radar ambiguity function. *IEEE Trans. on Aerospace and Electronic Systems*, pages 532–533, 1974.

[39] M. I. Skolnik, editor. *Radar Handbook.* McGraw-Hill, New York, 1970.

[40] Merrill I. Skolnik. *Introduction to Radar Systems.* McGraw-Hill, New York, 1980.

[41] Samir S. Soliman and Robert A. Scholtz. Spread ambiguity functions. *IEEE Trans. Information Theory*, IT-34:343–347, Mar., 1988.

[42] Charles A. Stutt. A note on invariant relations for ambiguity and distance functions. *IEEE Trans. Information Theory*, IT-5:164–167, Dec., 1959.

[43] Charles A. Stutt. Some results on real-part/imaginary-part and magnitude-phase relations in ambiguity functions. *IEEE Trans. Information Theory*, IT-10:321–327, Oct., 1964.

[44] David A. Swick. Wideband ambiguity function of pseudo-random sequences: An open problem. *IEEE Trans. Information Theory*, IT-14:602–603, July, 1968.

[45] H. Harold Szu and J. A. Blodgett. *Wigner Distribution and Ambiguity Function.* American Institute of Physics, New York, 1981.

[46] H. L. Van Trees. *Detction Estimation, and Modulation Theory, Part III.* Wiley, New York, 1971.

[47] Robert J. Urick. *Principles of Underwater Sound.* McGraw-Hill, New York, 1975.

[48] Harry Urkowitz. Filters for detection of small radar signals in clutter. *Journal of Applied Physics*, 24:1024–1031, August, 1953.

[49] P. M. Woodward. *Probability and Information Theory, with Applications to Radar.* McGraw-Hill, New York, 1953.

[50] M. Zakai. A class of definition of 'duration' (or 'uncertainty') and the associated uncertainty relations. *Information and Control*, 3:101–115, 1960.

[51] Rodger E. Ziemer and Roger L. Peterson. *Digital Communications and Spread Spectrum Systems.* Macmillan Publishing Company, New York, 1985.